การแพร่ของไอโซเมอร์เพนเทนในซิลิกาไลต์-1 โดยการจำลองแบบพลวัตเชิงโมเลกุล

นายอาทร ลอยสรวงสิน

DIFFUSION OF PENTANE ISOMERS IN SILICALITE–1 BY MOLECULAR DYNAMIC SIMULATION

Mr. Arthorn Loisruangsin

A Dissertation Submitted in Partial Fulfillment of the Requirements

for the Degree of Doctor of Philosophy Program in Chemistry
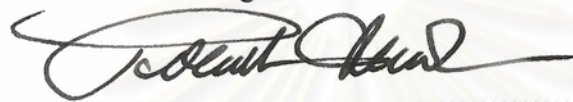
Department of Chemistry

Faculty of Science

Chulalongkorn University

Academic Year 2006

Thesis Title   DIFFUSION OF PENTANE ISOMERS IN SILICALITE-1 BY
                    MOLECULAR DYNAMIC SIMULATION

By   Mr. Arthorn Loisruangsin

Field of Study   Chemistry

Thesis Advisor   Professor Supot Hannongbua, Ph. D.

Thesis Co-advisor   Privatdozent Siegfried Fritzsche, Dr. rer. nat. habil.

Accepted by the Faculty of Science, Chulalongkorn University in Partial Fulfillment of
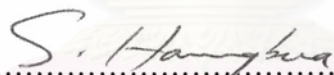the Requirements for the Doctoral Degree

…………………………………………………….. Dean of the Faculty of Science
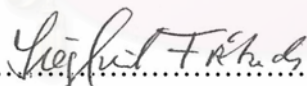(Professor Piamsak Menasveta, Ph. D.)

THESIS COMMITTEE

…………………………………………….. Chairman
(Associate Professor Sirirat Kokpol, Ph. D.)

……………………………………….……… Thesis Advisor
(Professor Supot Hannongbua, Ph. D.)

……………………………………………….. Thesis Co-advisor
(Privatdozent Siegfried Fritzsche, Dr. rer. nat. habil.)

…………………………………………….….. Member
(Associate Professor Vudhichai Parasuk, Ph. D.)

…………………………………………………….. Member
(Associate Professor Tawan Sooknoi, Ph. D.)

…………………………………………………….. Member
(Assistant Professor Teerakiat Kerdchareon, Ph. D.)

อาทร ลอยสรวงสิน: การแพร่ของไอโซเมอร์เพนเทนในซิลิกาไลต์-1 โดยการจำลองแบบพลวัตเชิงโมเลกุล. (DIFFUSION OF PENTANE ISOMERS IN SILICALITE-1 BY MOLECULAR DYNAMIC SIMULATION) อ. ที่ปรึกษา: ศ. ดร. สุพจน์ หารหนองบัว, อ.ที่ปรึกษาร่วม: ดร. ซิกฟริด ฟริซเซอร์ 116 หน้า.

การคำนวณเชิงเคมีควอนตัมที่ระดับทฤษฎีการรบกวนอันดับสองโมลเลอร์และเพลส์เสต (MP2) นำมาใช้หาอันตรกิริยาระหว่างนอร์มัลเพนเทน/นอร์มัลเพนเทน และระหว่างนอร์มัลเพนเทน/ซิลิกาไลต์-1 จำนวนนับร้อยโครงแบบ โครงสร้างผลึกของซิลิกาไลต์-1 แทนด้วยวงแหวนประกอบด้วยของที-อะตอม ขนาด 10 อะตอม โดยที่องค์ประกอบทางเคมีเป็น O[10]Si[10]H[20] นำพลังงานและพิกัดของอะตอมที่เกี่ยวข้องของโครงแบบเหล่านี้มาฟิตเข้ากับฟังก์ชันเชิงวิเคราะห์ ทำการฟิตหลายครั้งเพื่อให้ได้ฟังก์ชันที่ดีที่สุดซึ่งจำลองค่าความร้อนการดูดซับและค่าสัมประสิทธิ์การแพร่จากการทดลองได้ ในฟังก์ชันแบบสุดท้ายใช้การคำนวณระดับ MP2/6-31+G(d,p) และใส่ค่าคงที่การปะทะในศักย์ซึ่งฟิตด้วยข้อมูลแอบอินิซิโอ ด้วยวิธีการซึ่งพัฒนาใหม่นี้ อัตราส่วนของคู่อะตอมในศักย์คู่เชิงโมเลกุลจะถูกแบ่งส่วนอย่างดี ฟังก์ชันที่ได้รับสำหรับอนุกรมการจำลองแบบพลวัตเชิงโมเลกุลโดยการแปรอุณหภูมิและจำนวนของนอร์มัลเพนเทนที่ใส่เข้าไป แปรผลข้อมูลเชิงโครงสร้างที่ได้ในรูปของการกระจายที่อยู่ซึ่งการเปลี่ยนแปลงของการกระจายนี้บรรยายว่าเป็นการแข่งขันระหว่างสนามศักย์โดยซีโอไลต์ และการเคลื่อนไหวเชิงโมเลกุล สนามศักย์มีอิทธิพลเหนือการเคลื่อนไหวที่อุณหภูมิต่ำ และลดลงเมื่ออุณหภูมิเพิ่มขึ้น นอกจากนี้ ค่าความร้อนการดูดซับโดยประมาณจากฟังก์ชันใหม่นี้เท่ากับ 52.28 กิโลจูลต่อโมลซึ่งน้อยกว่าค่าการทดลอง 9.39 เปอร์เซ็นต์ และการเปลี่ยนแปลงค่าสัมประสิทธิ์การแพร่เป็นฟังก์ชันของอุณหภูมิซึ่งมีความพ้องกับค่าที่วัดได้จากการทดลอง

ภาควิชา.........เคมี................................. ลายมือชื่อนิสิต..อาทร ลอยสรวงสิน..............
สาขาวิชา.......เคมี................................. ลายมือชื่ออาจารย์ที่ปรึกษา.........................
ปีการศึกษา.....2549................................. ลายมือชื่ออาจารย์ทีปรึกษาร่วม..................

4373858623   : MAJOR CHEMISTRY

KEY WORD: *ab initio* fitted potential / simulation / pentane / silicalite-1 / diffusion

ARTHORN LOISRUANGSIN: DIFFUSION OF PENTANE ISOMERS IN SILICALITE-1 BY MOLECULAR DYNAMIC SIMULATION. THESIS ADVISOR: PROF.: SUPOT HANNONGBUA, DR. THESIS CO-ADVISOR: SIEGFRIED FRITZSCHE, DR. 116 pp.

Quantum chemical calculations at the second order Møller-Plesset Perturbation (MP2) levels were performed to evaluate *n*-pentane/*n*-pentane and n-pentane/silicalite-1 interactions where several hundred configurations of the pair were generated. The silicalite-1 crystal structure was represented by a 10-T ring, in which the chemical compositions is O[10]Si[10]H[20]. The energies and corresponding coordinates of these configurations were fitted to analytical functions. Several attempts were made to get the best functions which reproduce the experimental heat of adsorption (Q_{st}) as well as the self-diffusion coefficient (D_s). In the final form, the MP2/6-31+G(d,p) was applied and the collision constants were introduced into the ab initio fitted potential. With this newly developed approach, ratio of the atomic pairs in the molecular pair potential was nicely partitioned. The obtained function was applied for a series of molecular dynamic simulations by varying temperatures and loadings of *n*-pentane. The obtained structural data was interpreted in terms of residence distributions where their changes were, then, described by a competition between potential fields exerted by zeolite and molecular movement. The potential fields dominate the molecular movement at low temperature and decreases when the temperature increases. In addition, the extrapolated Q_{st} from the newly developed function of 52.28 kJ/mol is 9.39% lower than that of the experiment and change of the D_s as a function of temperatures is in good agreement with that observed experimentally.

Department.......Chemistry...................Student's signature... Arthorn Loisruangsin.....

Field of study.....Chemistry..................Advisor's signature......................

Academic year...2006.......................Co-advisor's signature...................

ACKNOWLEDGMENTS

TABLE OF CONTENTS

LIST OF TABLES

LIST OF FIGURES

CHAPTER I

INTRODUCTION

Some background information that is necessary for understanding the relevance of the study conducted in this dissertation, including the scope of this dissertation were given in this chapter.

1.1 Research Rationale

Zeolites are molecular sieves that are of importance for many refinery and petrochemical processes such as the separation of linear and branch alkanes, the conversion of linear to branch hydrocarbon and so on [1]. The performance of these molecular sieves in such processes depends critically on the match between sieve topology and the shape and size of the adsorbate [2]. ZSM-5, a kind of zeolite whose pore sizes are of the same order of magnitude as those of the adsorbing hydrocarbons, demonstrates selective adsorptions on its cavity. Diffusion and adsorption of molecules in the pores of zeolites are fundamental attributes of many industrial separation and also catalytic processes [3, 4, 5, 6]. To the best of our knowledge, many hydrocarbon/zeolite potentials based on the force-field parametrization are available [7, 8, 9, 10]. These models are different in details, *e.g.*, some are all-atom representation, some includes three-body interactions. Despite the potentials being expressed as functions of energies which depend on atomic coordinates, they all were parametrized through experimental data, mostly adsorption data, which are macroscopic property. Within different approaches and different experimental data, different parameter sets have been published. An alternative approach for developing the function that represents interaction between pair of molecules is to obtain the potential function from the *ab initio* energy points. An advantage of this approach is that the function is directly fitted to molecular interaction, *i.e.*, the energy obtained from the function is one-to-one correspondence with the *ab initio* data.

There are several successful cases for the *ab initio* fitted functions [11, 12, 13, 14, 15] in which the structural properties were in good agreement with the experimental data. Complication arises when dealing when intermolecular pair interactions are divided into atomic pair interactions based on mathematical algorithm because ratio contribution of atomic pairs to the molecular pair is actually unknown. The unknown ratio does not exhibit a problem in dealing with structural properties, but can lead to serious discrepancy when thermodynamic, perhaps also, dynamic properties are concerned [14, 16, 17]. Beside the development of the guest/host and guest/guest potential functions using the energy data calculated from the *ab initio* calculation, aim of this study extends also to figure out the optimal ratio of the atomic pairs in the molecular pair potential.

1.2 Zeolite

Zeolites [3, 18, 19] are minerals with a nano to microporous structure. The term was originally coined in the 18th century by a Swedish mineralogist named Axel Fredrik Cronstedt [3] who observed, upon rapidly heating a natural mineral, that the stones began to dance as the water evaporated. Using the Greek words which mean stone that boils. He called this material zeolite.

More than 150 zeolite types have been synthesized and 48 naturally occurring zeolites are known. Zeolites [18, 20] are basically hydrated aluminosilicate of the alkali or alkali earth metals such as Na, K, Ca, Mg. These metals are rather loosely held as cations and can readily be exchanged for others in a contact solution. Some common mineral zeolites are: analcime, chabazite, heulandite, natrolite, phillipsite, and stilbite.

Natural zeolites form where volcanic rocks and ash layers react with alkaline groundwater. Zeolites also crystallized in post-depositional environments over periods ranging from thousands to millions of years in shallow marine basins. Naturally occurring zeolites are rarely pure and are contaminated to varying degrees by other minerals, metals, quartz or other zeolites. For this reason, naturally occurring zeolites are excluded from many important commercial applications where uniformity and purity are essential.

Zeolites are the aluminosilicate members of the family of microporous solids known as molecular sieves. The term molecular sieve refers to a particular property of these materials, *i.e.* the ability to selectively sort molecules based primarily on a size exclusion process. This is due to a very regular pore structure of molecular dimensions. The maximum size of the molecular or ionic species that can enter the pores of a zeolite is controlled by the diameters of the tunnels. These are conventionally defined by the ring size of the aperture, where, for example, the term 8-T ring refers to a closed loop that is built from 8 T atoms where T stands for tetrahedral. These rings are not always perfectly flat and symmetrical due to a variety of effects, including strain induced by the bonding between units that are needed to produce the overall structure, or coordination of some of the oxygen atoms of the rings to cations within the structure. Therefore, the pore openings for all rings of one size are not identical.

1.3 MFI-type Zeolites

MFI-type zeolites are the 10-T ring systems and consist of bidirectional straight and sinusoidal channels connected via intersections. Figure 1.1a shows an electron micrograph of the MFI type zeolite.
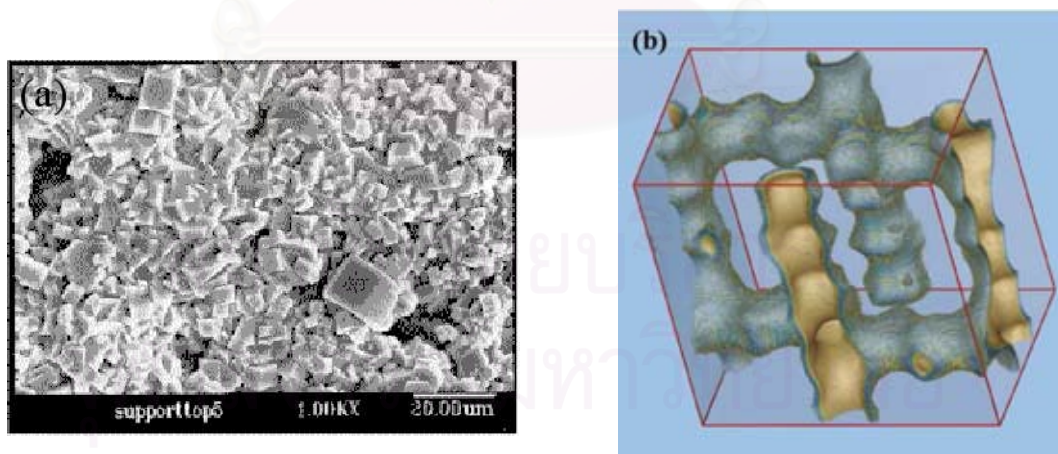
Figure 1.1 MFI zeolite: (a) Electron micrograph and (b) schematic view representing the channels in the unit cell [10].

The size of straight and sinusoidal channel openings are approximately 5.3 Å x 5.6 Å and 5.1 Å x 5.5 Å, respectively [21]. A unit cell of the zeolite has a dimension of 20.07 Å x 19.98 Å x 13.42 Å. This contains 2 straight channels and 4 sinusoidal channels with 4 intersections between them. The length of the straight channels is equal to 19.8 Å, while the sinusoidal channels are of 6.65 Å in size and the diameter of the intersections is 5.4 Å [22].

Silicalite–1 is an all-silica zeolite. HZSM-5 zeolite is an iso-structural framework, in which some of the Si atoms are substituted with Al. HZSM-5 can possess acidic properties because substituted Al atoms are provided electrical neutrality by the protons. Both Silicalite–1 and HZSM-5 belong to the most applied synthetic zeolites. They are broadly used in the petroleum and petrochemical industries as catalysts for fluid catalytic cracking (FCC), xylene isomerization, conversion of methanol to gasoline, and as selective sorbents [23, 24, 25]. These zeolites have uniform pores with out large supercages or bottlenecks, which is an important factor for the shape selective catalyst as well as for their very low coke forming abilities as acidic catalysts.

Silicalite–1 provides numerous possibilities for the hydrocarbon separation and it is the most studied membrane material [3]. Recently, a lot of theoretical studies have been conducted on the application of silicalite–1 in the selective separation of mixtures of C5-C6 alkanes isomers [26, 27, 28, 29] which are the products of the hydroisomerization process, mentioned above. The separation possibilities is based on the specific adsorption and related micropore diffusion properties of silicalite–1 toward alkanes.

1.4   Situation on the Diffusion of Hydrocarbon in Zeolite

The diffusion of hydrocarbon molecules within the pores of a zeolite is currently of significant interest. This is because zeolites are widely used as selective adsorbents in separation/adsorption processes and as heterogeneous catalysts in the oil-processing and chemical industry. The catalytic properties of zeolites, such as shape selectivity and effectiveness, are closely related to the molecular mobility of the reactants and products within the inner voids of the zeolite. Given the molecular dimensions of the pores (4-8 Å) a small variation in the shape and/or geometry of the molecule usually leads to large differences in diffusion. These

differences may in turn contribute significantly to the shape-selective effects often observed in zeolite catalysis. Therefore, to allow a better understanding of the phenomena of diffusion at a molecular level, detailed examinations are very helpful.

Several experimental methods are available to study translation mobility in zeolites including uptake methods, chromatographic techniques, membrane techniques and pulsed field gradient nuclear magnetic resonance (PFG-NMR). Each of these methods has its own particular merits.

Alternatively, theoretical methods provide an approximative description of reality, excellently suited for investigating the absorptive/diffusive processes on a microscopic scale. They can provide accurate data at a microscopic level under catalytic process condition. Molecular simulation techniques, especially Monte Carlo (MC) and molecular dynamic (MD) simulations, [30, 31] have become a powerful tool to investigate various diffusive guests in zeolites. In most cases, the thermodynamic results are in good agreement with those obtained from experimental techniques [3, 4, 32, 33, 34, 35, 36].

1.5 Scope of the Dissertation

Several attempts have been made to study the adsorption and diffusion of hydrocarbons in silicalite–1 by means of both theoretical [37, 38, 39, 40, 41, 42] and experimental [43, 44, 45, 46] investigations. Some simulations of linear and also branched hydrocarbons and even of mixtures of them in silicalite–1 are reported in the literature [9, 10, 37, 47, 48, 49]. These simulations have been done with empirical potentials that were fitted to reproduce thermodynamic properties. Especially, in Reference [9, 10], Dubbeldam *et al.* proposed potential parameter set which was mainly fitted to adsorption isotherms. They claimed that their potential parameters not only yield a superior description of the experimental data that formed the basis for the fitting procedure, but also yield an excellent description of reference systems which were not included in the calibration set. They also proposed that parameter set should be universally applicable for all alkanes/zeolites system. Generally those force field parameters were generated to reproduce thermodynamic properties which

were statistical average values. As a result, different parameter sets have been published. Despite these differences, most studies claim a good agreement with experimental data.

As mentioned in the last paragraph of Section 1.1, an alternative approach to deal with the potential function is to fit the functional form to an *ab initio* data and the main problem of this type of function is due to the ratio of the atomic pairs to the *ab initio* molecular pair potential. Therefore, scope of this work was set up to

(i) Develop the *ab initio* fitted n-pentane/silicalite–1 and n-pentane/n-pentane intermolecular potentials.

(ii) Repeat the process employing the developed potential using MD simulations and investigate the structural, dynamic and thermodynamic properties of the system until the optimal ratio of the atomic pairs was yielded validated by the experimental properties.

(iii) Apply the newly validated function to study molecular properties of the n-pentane/silicalite–1 system by varying n-pentane concentrations and temperatures.

CHAPTER II

THEORY

2.1 Computational Quantum Mechanics

2.1.1 Introduction

Quantum mechanics (QM) is a science dealing with the behavior of matter and waves on the scale of atoms and subatomic particles. It was accepted by physics community because it can accurately predict physical behavior of the systems where Newtonian mechanics fails. Two equivalent formulations of QM were derived by Schrödinger and Heisenberg. The Schrödinger form was presented here since it is the basis for nearly all computational chemistry methods. The Schrödinger equation is

$$\left\{ -\frac{\hbar^2}{2m}\left(\frac{\partial^2}{\partial x^2} + \frac{\partial^2}{\partial y^2} + \frac{\partial^2}{\partial z^2}\right) + \quad \right\} \Psi(r,t) = i\hbar\frac{\partial \Psi(r,t)}{\partial t} \qquad [2.1]$$

Equation 2.1 is the time dependent form and refers to a single particle of mass m which is moving through space (given by a position vector $r = x\mathrm{i}+y\mathrm{j}+z\mathrm{k}$) and time t under the influence of an external field   (which might be the electrostatic potential due to the nuclei of a molecule). $\hbar$ is Plank's constant divided by 2π and i is the square root of -1. Ψ is the wave function which characterizes the particle's motion. Various properties can be derived from this equation. When the external potential   is independent of time, the wave function can be written as the product of a spatial part and a time part: $\Psi(r,t) = \psi(r)T(t)$ which enables the time-dependent Schrödinger to be written in the time-independent form:

$$\Psi(r) = E\Psi(r) \qquad [2.2]$$

Here, E is the energy of the particle and   is the Hamiltonian operator:

$$= \frac{\hbar^2}{2m}\nabla^2 + \qquad\qquad [2.3]$$

where

$$\nabla^2 = \frac{\partial^2}{\partial x^2} + \frac{\partial^2}{\partial y^2} + \frac{\partial^2}{\partial z^2} \qquad\qquad [2.4]$$

Equation 2.2 falls into the category of equations known as partial differential eigenvalue equations in which an operator acts on a function (the eigenfunction) and returns the function multiplied by a scalar (eigenvalue). $\Psi(r)$ and E are, thus, the eigenfunction and the eigenvalue, respectively.

2.1.2   The Born-Oppenheimer Approximation

The Born-Oppenheimer approximation is central to quantum chemistry. This approximation simplifies the problem by decoupling the motion of the electrons from the motion of the nuclei. The approximation states that masses of the nuclei are 1836 times heavier than that of the electrons. This means that the electrons can adjust almost instantaneously to any changes in the positions of the nuclei. Under the Born-Oppenheimer approximation, the total wave function for the molecule $\Psi_{\text{total}}(\{r_i\}, \{R_A\})$, which depends on coordinates of electrons $\{r_i\}$ and nuclei $\{R_A\}$, can be written as

$$\Psi_{\text{total}}(\{r_i\}, \{R_A\}) = \Psi_{\text{electrons}}(\{r_i\}; \{R_A\})\Psi_{\text{nuclei}}(\{R_A\}) \qquad\qquad [2.5]$$

The electronic wave function $\Psi_{\text{electrons}}$, thus, depends only on the positions of the nuclei and not on their momenta. When this approximation is used, the motions of electrons

are independent; the nuclei are considered to be fixed. Schrödinger equation is solved for electrons alone for each arrangement of the nuclei. The nuclear repulsion can separately be calculated and added to the electronic energy to obtain the total energy of the configuration.

2.1.3 Slater Determinants

A many-electron wave function termed a *Hartree product* which is a simple product of spin orbital wave function of each electron reads:

$$\Psi(1, 2, \cdots, N) = \chi_i(1)\chi_j(2)\cdots\chi_k(N) \qquad [2.6]$$

$\chi_i(1)$ is a spin orbital which depends on the space and spin coordinates of the electron labeled '1'. Hartree product does not satisfy the antisymmetry principle because exchange any two electrons in any two spin orbitals forms a new wave function rather than the negative of the original wave function; however, the appropriate linear combination of these Hartree products from exchanging any two electrons can form the wave function for a system that satisfied the antisymmetry principle. Such linear combination can be written as a determinant called the *Slater determinant*, for N-electron system:

$$\Psi = \frac{1}{\sqrt{N!}} \begin{vmatrix} \chi_i(1) & \chi_j(1) & \cdots & \chi_k(1) \\ \chi_i(2) & \chi_j(2) & \cdots & \chi_k(2) \\ \vdots & \vdots & & \vdots \\ \chi_i(N) & \chi_j(N) & \cdots & \chi_k(N) \end{vmatrix} \qquad [2.7]$$

The factor $1/\sqrt{N!}$ is a normalize factor. Exchanging any two rows of a determinant corresponds to exchanging two electrons. This changes the sign of the determinant and leads to the antisymmetry property. If any two rows of a determinant are identical, then the determinant vanishes. This can be considered as an illustration of the Pauli principle, which states that no two electrons can have the same set of quantum numbers.

For any considerable system, the Slater determinant is inconvenient to write out. A common used shorthand notation is to write only the terms along the diagonal of the matrix as a single-row determinant:

$$\begin{vmatrix} \chi_1(1) & \chi_2(1) & \cdots & \chi_N(1) \\ \chi_1(2) & \chi_2(2) & \cdots & \chi_N(2) \\ \vdots & \vdots & & \vdots \\ \chi_1(N) & \chi_2(N) & \cdots & \chi_N(N) \end{vmatrix} \equiv \left| \begin{array}{cccc} \chi_1 & \chi_2 & \cdots & \chi_N \end{array} \right\rangle \qquad [2.8]$$

2.1.4 The Hartree-Fock Method

Given $\Psi = |\chi_1\chi_2\cdots\chi_N\rangle$ the energy $E = \langle\Psi^*| \quad |\Psi\rangle$ is a functional of the spin orbitals $\{\chi_i\}$. In most electronic structure calculations we are trying to calculate the spin orbitals. The *variation theorem* provides us to the best approximate wave function by minimizing the energy $E\left[\{\chi_i\}\right]$ with respect to the spin orbitals, subject to the constraint that the spin orbitals remain orthonormal:

$$\int d\mathrm{x}_1\chi_i^*(1)\chi_j(1) = \delta_{ij} \qquad [2.9]$$

That is, the constraints are of the form:

$$\int d\mathrm{x}_1\chi_i^*(1)\chi_j(1) - \delta_{ij} = 0 \qquad [2.10]$$

where $\delta_{ij} = 0$ for $i \neq j$; otherwise $\delta_{ij} = 1$. Here, the label '1' is used wherever there is an integral involving the coordinates of a single electron, even though the actual electron may

not be 'electron 1'. Similarly, when two electrons are considered, then the labels 1 and 2 are employed.

Using Lagrange's method (   ) of undetermined multipliers, we can set up the following equation:

$$[\{\chi_i\}] = E[\{\chi_i\}] - \sum_{i=1}^{N}\sum_{j=1}^{N}\epsilon_{ij}(\int d\mathrm{x}_1\chi_i^*(1)\chi_j(1) - \delta_{ij}) \qquad [2.11]$$

where ϵ_{ij} is the Lagrange multiplier. Minimization of E, subject to the constraints, is thus obtained by minimizing   in which the first variation in   equals zero:

$$\delta \quad [\{\chi_i\}] = \delta E[\{\chi_i\}] - \sum_{i=1}^{N}\sum_{j=1}^{N}\epsilon_{ij}\delta(\int d\mathrm{x}_1\chi_i^*(1)\chi_j(1)) = 0 \qquad [2.12]$$

It should be noted that δ here is not a variable like δ_{ij}, but, it means the variation by infinitesimal amount of any variable it operates on. The energy E contains three terms: (i) the kinetic and potential energy of electron moving in the field of M nuclei ($^{core}(1)$), (ii) the electrostatic repulsion between pairs of electrons ($_j(1)$) and (iii) the exchange interaction which arises from the motions of electrons with parallel spins ($_j(1)$). Equation 2.12 expanded in these three terms can be written as:

$$\delta \quad [\{\chi_i\}] = \sum_{i=1}^{N}\int d\mathrm{x}_1\delta\chi_i^*(1)\left[\quad^{core}(1)\chi_i(1) + \sum_{j=1}^{N}(\quad_j(1) - \quad_j(1))\chi_i(1) - \sum_{j=1}^{N}\epsilon_{ij}\chi_j(1)\right]$$
$$+\text{complex conjugate} = 0 \qquad [2.13]$$

where

$$^{core}(1) = -\frac{1}{2}\nabla_i^2 - \sum_{A=1}^{M}\frac{Z_A}{r_{iA}} \qquad [2.14]$$

$$_j(1) = \int d\mathrm{x}_2 \chi_j(2)\chi_j(2)\frac{1}{r_{12}} \tag{2.15}$$

$$_j(1) = \int d\mathrm{x}_2 \chi_j(2)\frac{1}{r_{12}} \; _{12}\chi_j(2) \tag{2.16}$$

Since $\delta\chi_i^*(1)$ is arbitrary, it must be the quantity in square brackets which is zero for all i. Therefore,

$$\left[\; ^{\text{core}}(1) + \sum_{j=1}^{N}(\; _j(1) - \; _j(1)) \right]\chi_i(1) = \sum_{j=1}^{N}\epsilon_{ij}\chi_j(1) \tag{2.17}$$

$$f_i(1)\chi_i(1) = \sum_{j=1}^{N}\epsilon_{ij}\chi_j(1) \tag{2.18}$$

$f_i(1)$ is called the Fock operator whose theory assumes that each electron move in a 'fixed' field comprising the nuclei and the other electrons. Equation 2.18 is not eigenvalue form because any single determinant wave function Ψ formed from a set of spin orbitals $\{\chi_i\}$ retains a certain degree of flexibility in the spin orbitals. The spin orbitals can be mixed among themselves without changing the expectation value E. Fortunately, it is possible to manipulate Equation 2.18 with unitary transformation to obtain a standard eigenvalue equation.

$$f_i(1)\chi_i(1) = \epsilon_i\chi_i(1) \tag{2.19}$$

Let's consider Equations 2.15-2.16. We can see that Hartree-Fock equation is non-linear. Solving equation for one electron will affect the solutions for the other electrons in the system. The general strategy called *self-consistent field* (SCF) approach is a way to solve this equation. First, a set of trial solutions χ_i to the Hartree-Fock equations are obtained. These

are used to calculate the Coulomb and exchange operators. The Hartree-Fock equations are solved, giving a second set of solutions χ_i, which are used in the next iteration.

2.1.5   Roothan-Hall Equations

Numerical solutions are common in solving the Hartree-Fock equations [50] for atoms; however, for molecules, introduction of a known set of basis functions, which was contributed by Roothaan and Halls, converts the differential equations to a set of algebraic equations and solved by standard matrix techniques.

The unknown molecular orbitals ψ_i can be expanded as a linear combination of a set of K known basis functions $\{\phi_\nu | \nu = 1, 2, \cdots, K\}$:

$$\psi_i = \sum_{\nu=1}^{K} c_{\nu i} \phi_\nu \qquad [2.20]$$

Basis functions are one-electron orbitals and correspond to the atomic orbitals. For a given basis set and a given functional form of the wave function, the best set of coefficients is that for which the energy is a minimum at which point

$$\frac{\partial E}{\partial c_{\nu i}} = 0 \qquad [2.21]$$

for all coefficients $c_{\nu i}$. The objective is thus to determine the set of coefficients that gives the lowest energy for the system. The corresponding Fock operator for a closed-shell system with N electrons in $N/2$ orbitals is

$$f_i(1) = {}^{\text{core}}(1) + \sum_{j=1}^{N/2} \{2\;_j(1) -\;_j(1)\} \qquad [2.22]$$

By multiplying by $\phi_\mu(1)$ on the left and integrating, the integro-differential equation, then, transforms into a matrix equation:

$$\sum_{\nu=1}^{K} c_{\nu 1} \int d\mathrm{r}_1 \phi_\mu(1) f_i(1) \phi_\nu(1) \; = \; \epsilon_i \sum_{\nu=1}^{K} c_{\nu 1} \int d\mathrm{r}_1 \phi_\mu(1) \phi_\nu(1) \qquad [2.23]$$

$$\sum_{\nu=1}^{K} F_{\mu\nu} c_{\nu i} \; = \; \epsilon_i \sum_{\nu=1}^{K} S_{\mu\nu} c_{\nu i} \qquad [2.24]$$

where

$$S_{\mu\nu} \; = \; \int d\mathrm{r}_1 \phi_\mu(1) \phi_\nu(1) \qquad [2.25]$$

$$F_{\mu\nu} \; = \; \int d\mathrm{r}_1 \phi_\mu(1) f_i(1) \phi_\nu(1) \qquad [2.26]$$

$S_{\mu\nu}$ is the overlap integral between the basis functions ϕ_μ and ϕ_ν. Although the basis functions are normalized and linearly independent, they are not necessarily orthogonal to each other and, hence, $0 \le |S_{\mu\nu}| \le 1$.

The elements $F_{\mu\nu}$ of the Fock matrix can be expanded by substituting Equation 2.22 for the Fock oprerator:

$$F_{\mu\nu} \; = \; \int d\mathrm{r}_1 \phi_\mu(1) \; {}^{\mathrm{core}}(1) \phi_\nu(1) + \sum_{i=1}^{N/2} \int d\mathrm{r}_1 \phi_\mu(1)[2 \;{}_j(1) - \;{}_j(1)]\phi_\nu(1) \qquad [2.27]$$

$$= \; H_{\mu\nu}^{\mathrm{core}} + \sum_{j=1}^{N/2} \sum_{\lambda=1}^{K} \sum_{\sigma=1}^{K} c_{\lambda j} c_{\sigma j}[2(\mu\nu|\lambda\sigma) - (\mu\lambda|\nu\sigma)] \qquad [2.28]$$

The shorthand notation is used for the integrals in Equation 2.28 in which

$$(\mu\nu|\lambda\sigma) \equiv \int d\mathrm{r}_1 d\mathrm{r}_2 \phi_\mu(1)\phi_\nu(1)\frac{1}{r_{12}}\phi_\lambda(1)\phi_\sigma(1) \qquad [2.29]$$

$$(\mu\lambda|\nu\sigma) \equiv \int d\mathrm{r}_1 d\mathrm{r}_2 \phi_\mu(1)\phi_\lambda(1)\frac{1}{r_{12}}\phi_\nu(1)\phi_\sigma(1) \qquad [2.30]$$

Note that the two-electron integrals may involve up to four different centers. Thus, four different indices $\mu, \nu, \lambda, \sigma$ are used for the basis functions.

Equation 2.28 can be simplified by introducing the *charge density* matrix, P, whose elements are defined as:

$$P_{\lambda\sigma} = 2\sum_{i=1}^{N/2} c_{\lambda i}c_{\sigma i} \qquad [2.31]$$

The expression for each element $F_{\mu\nu}$ of the Fock matrix element for a closed-shell system of N electrons, thus, becomes:

$$F_{\mu\nu} = H_{\mu\nu}^{\mathrm{core}} + \sum_{\lambda=1}^{K}\sum_{\sigma=1}^{K} P_{\lambda\sigma}[(\mu\nu|\lambda\sigma) - \frac{1}{2}(\mu\lambda|\nu\sigma)] \qquad [2.32]$$

Equation 2.32 is the standard form for the expression for the Fock matrix in the Roothaan-Haal equations.

Equation 2.24 can be written more compactly as the single matrix equation:

$$\mathrm{FC} = \mathrm{SCE} \qquad [2.33]$$

Because the Fock matrix depends on the expansion coefficients $F = F(C)$, Equation 2.33 is nonlinear. It, thus, must be solved iteratively. Besides, to solve the problem using standard eigenvalue methods, an equation of the form FC = CE is required. This can be manipulated by pre-multiplying Equation 2.33 with matrix $S^{-1/2}$ and then inserting the unit matrix, in the form $S^{-1/2}S^{1/2}$ into the left-hand side of the equation:

$$S^{-1/2}F(S^{-1/2}S^{1/2})C \;=\; S^{-1/2}SCE \qquad\qquad [2.34]$$

$$(S^{-1/2}FS^{-1/2})(S^{1/2}C) \;=\; (S^{1/2}C)E \qquad\qquad [2.35]$$

$$F'C' \;=\; C'E \qquad\qquad [2.36]$$

The basis function coefficients C can be obtained from C' using $C = S^{-1/2}C'$.

2.1.6 Basis Sets

A basis set in chemistry is a set of functions used to create the molecular orbitals, which are expanded as a linear combination of such functions with the weights or coefficients to be determined. There are many basis sets defined for polyatomic calculation. The basis sets defined in a series of papers by Pople and collaborators, which have been used extensively, are briefly mentioned here as "minimal basis sets" and "advanced basis sets". However, a general treatment of contraction will be presented first.

Contracted Gaussian Functions Though, Slater functions are desired as the most efficient and accurate functions in which the fewest possible terms will be required. Gaussian functions have an advantage of speed of two-electron integral evaluation, comparing to Slater functions. Contracted Gaussian functions might be chosen to approximate Slater functions. By using a basis set of "contracted Gaussian functions", each basis function is a fixed linear

combination (contraction) of Gaussian functions (primitives). Integrals involving such basis functions reduce to sums of integrals involving the primitive Gaussian functions. Even though many primitive integrals may need to be calculated for each basis function integral, the basis function integrals will be rapidlz calculated provided the method of computing primitive integrals is very fast. A contraction has the form.

$$\phi_\mu^{\text{CGF}}(r - R_A) = \sum_{p=1}^{L} d_{p\mu} g_p(\alpha_{p\mu}, r - R_p) \qquad [2.37]$$

where $\alpha_{p\mu}$ and $d_{p\mu}$ are the contraction exponents and coefficients and L is the length of the contraction. g_p stands for normalized Gaussian primitive functions are of the $1s$, $2p$, $3d$, $\ldots$ type. The origins R_p of the primitives are almost always equal to R_A. Different origins for the primitives in a contraction are used only with Gaussian lobe basis sets. In these basis sets $s, p, d, \ldots$ functions as combinations of spherical $1s$ Gaussians (lobes= placed appropiately in space.

Minimal Basis Sets

A common naming convention for minimal basis sets is STO-XG, where X is an integer. This X value represents the number of Gaussian primitive functions comprising a single basis function. In these basis sets, the same number of Gaussian primitives comprise core and valence orbitals. The minimal basis sets are known for several deficiencies: (i) The atoms at the end of a period are described using the same number of basis functions as the atoms at the beginning of the period. (ii) The radial exponents are not allowed to vary and the function can not expand or contract in size in accordance with the molecular environment. (iii) They can not describe non-spherical aspects of the electronic distribution because the same radial component are used for all functions that incorporate anisotropy.

Advanced Basis Sets

Using more than one function for each orbital can address the problems with minimal basis sets. For any molecular system, the valence electrons principally take part in the bonding. In recognition of this fact, basis functions are added to valence orbitals. The notation for these split-valence basis sets is typically X-YZg. In this case, X represents the number primitive Gaussian functions comprising each core atomic orbital basis function. The Y and Z indicate that the valence orbitals are composed of two basis functions each, the first one composed of a linear combination of Y primitive Gaussian functions, the other composed of a linear combination of Z primitive Gaussian functions. In this case, the presence of two numbers after the hyphens implies that this basis set is a split-valence double-zeta basis set. Split-valence triple- and quadruple-zeta basis sets are also used, denoted as X-YZWg, X-YZWVg, etc.

Simply increasing the number of basis functions can not overcome the problems with non-isotropic charge distribution completely. The charge distribution about an atom in a molecule is usually perturbed in comparison with the isolated atom, for example, the electron cloud in an isolated hydrogen atom is symmetrical, but when the hydrogen atom is present in a molecule the electrons are attracted toward the other nuclei. The most common solution to this problem is to introduce polarization functions into the basis set. The polarization functions have a higher angular quantum number and correspond to p orbitals for hydrogen and d orbitals for the first- and second-row elements. An asterisk (*) indicates the use of polarization functions. That is 6-31G* refers to a 6-31 basis set with polarization functions on non-hydrogen atoms. Use of polarization function on hydrogen can be denoted by adding one more asterisk (e.g. 6-31G**).

So far the basis sets fail to deal with species such anions and molecules containing lone pairs. The failure arises because the amplitudes of the Gaussian basis functions are rather low far from the nuclei while such species have a significant amount of electron density away from the nuclear centers. This deficiency can be cured by adding highly diffuse functions to the basis set. To use these functions, a '+' or '++'is added, for example, 6-31+G** contains an additional single set of diffuse s- and p-type and 6-31++G** includes the diffuse functions for hydrogen as well as for heavy atoms.

2.1.7 Basis Set Superposition Error

Suppose one wishes to calculate the energy of formation of a bimolecular complex AB. This energy could be obtained by subtracting the energy of the two isolated molecules A and B from that of complex A-B. However, the energy difference obtained by such an approach will overestimate of the true value. This discrepancy arises from a phenomenon known as *basis set superposition error* (BSSE). As the molecules A and B approach each other, the energy of the system falls not only because of the favorable intermolecular interactions but also because the basis functions on each molecule that provide a better description of the electronic structure around the other molecule. It is clear that the BSSE would be expected to be particularly significant when small, inadequate basis sets are used. They do not provide for an adequate representation of the electron distribution far from the nuclei, particularly in the region where non-covalent interactions are strongest. Counterpoise correction offered by Boys and Bernadi can be performed by including the entire basis set in all calculations:

$$A + B \rightarrow AB \qquad\qquad [2.38]$$

$$\Delta E = E_{AB}(AB) - [E_A(AB) + E_B(AB)] \qquad\qquad [2.39]$$

The calculation of the energy of the speicies A is performed in the presence of ghost orbitals of B; that is without the nuclei or electrons of B. Similar calculation is performed for B using the ghost orbitals on A.

2.1.8 Møller-Plesset Perturbation

Since the Hartree-Fock calculation takes into account the average affect of electron repulsion, but, not the explicit electron-electron interaction, this method lacks electron correlation. Consequently, the probability of finding an electron at some location around an

atom is determined by the distance from the nucleus but not the distance to the other electrons. This is not physically true. Correlation is important for several reasons. These include improvement of the accuracy of computed energies and molecular geometries.

A number of types of calculations begin with a Hartree-Fock calculation and then correct for correlation. Møller and Plesset proposed the way to tackle the problem of electron correlation based upon Rayleigh-Schrödinger perturbation theory, in which the 'true' Hamiltonian   is expressed as the sum of the Hartree-Fock Hamiltonian as a 'zeroth order' Hamiltonian $_0$ and a perturbation   .

$$ =   _0 + \qquad [2.40]$$

Suppose we wish to solve the eigenvalue problem

$$ \Psi_i = (_0 +   )\Psi_i = E_i \Psi_i \qquad [2.41]$$

where we know the eigenfunctions and eigenvalues of $_0$,

$$ _0 \Psi_i^{(0)} = E_i^{(0)} \Psi_i^{(0)}. \qquad [2.42]$$

If the perturbation,   is small enough, it was expected Ψ_i and E_i to be close to $\Psi_i^{(0)}$ and $E_i^{(0)}$, respectively. A procedure which gradually improve the known eigenfunctions, $\Psi_i^{(0)}$ and eigenvalues, $E_i^{(0)}$ to the eigenfunctions and eigenvalues of the true Hamiltonian,   is devised by introducing an ordering parameter λ, which will later, be set equal to unity

$$ =   _0 + \lambda . \qquad [2.43]$$

The exact eigenfunctions and eigenvalues are now expanded in a Taylor series of λ,

$$\Psi_i = \Psi_i^{(0)} + \lambda\Psi_i^{(1)} + \lambda^{(2)}\Psi_i^2 + ... \qquad [2.44]$$

$$E_i = E_i^{(0)} + \lambda E_i^{(1)} + \lambda E_i^{(2)} + ... \qquad [2.45]$$

The $E_i^{(n)}$ is called the nth-order correction.

$$E_i^{(0)} = \int \Psi_i^{(0)} \quad {}_0\Psi_i^{(0)}\mathrm{d}\tau \qquad [2.46]$$

$$E_i^{(1)} = \int \Psi_i^{(0)} \quad \Psi_i^{(0)}\mathrm{d}\tau \qquad [2.47]$$

$$E_i^{(2)} = \int \Psi_i^{(0)} \quad \Psi_i^{(1)}\mathrm{d}\tau \qquad [2.48]$$

$$E_i^{(3)} = \int \Psi_i^{(0)} \quad \Psi_i^{(2)}\mathrm{d}\tau \qquad [2.49]$$

In Møller-Plesset perturbation theory the unperturbed Hamiltonian $\quad{}_0$ is the sum of Fock operators for N electrons:

$$_0 = \sum_{i=1}^{N} f_i = \sum_{i=1}^{N} \left({}^{\text{core}} + \sum_{j=1}^{N}(\quad_i + \quad_i) \right) \qquad [2.50]$$

The Hartree-Fock wave function, $\Psi_0^{(0)}$ is an eigenfunction of $\quad{}_0$ and the corresponding zeroth-order energy $E_0^{(0)}$ is equal to the sum or orbital energies for the occupied molecular orbitals:

$$E_0^{(0)} = \sum_{i=1}^{\text{occupied}} \epsilon_i \qquad [2.51]$$

The true Hamiltonian is equal to the sum of the nuclear attraction terms and electron repulsion terms:

$$= \sum_{i=1}^{N} (\quad^{\text{core}}) + \sum_{i=1}^{N} \sum_{j=i+1}^{N} \frac{1}{r_{ij}} \qquad [2.52]$$

Thus, the perturbation   which is the difference between the true Hamiltonian   and the zeroth order Hamiltonian $_0$ is given by:

$$= \sum_{i=1}^{N} \sum_{j=i+1}^{N} \frac{1}{r_{ij}} - \sum_{j=1}^{N} (\quad_j + \quad_j) \qquad [2.53]$$

Substituting Equation 2.53 in Equation 2.47, then, the first-order energy $E_0^{(1)}$ can be given as:

$$E_0^{(1)} = -\frac{1}{2} \sum_{i=1}^{N} \sum_{j=1}^{N} [(ii|jj) - (ij|ij)] \qquad [2.54]$$

The sum of the zeroth-order and first-order energies corresponds to the Hartree-Fock energy for a closed-shell system:

$$E_0^{(0)} + E_0^{(1)} = \sum_{i=1}^{N} \epsilon_i - \frac{1}{2} \sum_{i=1}^{N} \sum_{j=1}^{N} [(ii|jj) - (ij|ij)] \qquad [2.55]$$

Therefore, it is necessary to use at least second order Møller-Plesset perturbation theory, which is referred to as MP2, to obtain an improvement on the Hartree-Fock energy. The higher-order wave function $\Psi_0^{(1)}$ in Equation 2.48 can be expressed as linear combinations of solutions to the zeroth-order Hamiltonian:

$$\Psi_0^{(1)} = \sum_j c_j^{(1)} \Psi_j^{(0)} \qquad [2.56]$$

The $\Psi_j^{(0)}$ in Equation 2.56 will include single, double, etc. excitations obtained by promoting electrons into the virtual orbitals obtained from a Hartree-Fock calculation. The second-order energy is given by:

$$E_0^{(2)} = \sum_i \sum_{j>i} \sum_a \sum_{b>a} \frac{\int \int d\mathrm{x}_1 d\mathrm{x}_2 \chi_i(1) \chi_j(2) \frac{1}{r_{12}} \left[\chi_a(1) \chi_b(2) - \chi_b(1) \chi_a(2) \right]}{\epsilon_a + \epsilon_b - \epsilon_i - \epsilon_j} \qquad [2.57]$$

where i and j are indices for summations over occupied orbitals while a and b are indices for summations over virtual orbitals.

The advantage of perturbation theory is that it is size-consistent; however, Møller-Plesset is not variational and can give energies that are lower than the 'exact' energy.

2.2 Curve Fitting: Least Square Estimation

One method of building mathematic model to describe scientific phenomena is to correlate between variables in the experiment as a function or an equation to explain the phenomena. Estimation by a least square method would yield the best function because of the least of a summation over all the errors in the data. Thus, when a curve of a function is written, it will pass in the area that data are distributed around and it will intersect over

some points of the data. The principle of the least square method is as follows:

If there are n sets of coordinates (x, y), a given function estimating these data is $G(x)$ in whose form is as follows:

$$G(x) = a_1 g_1(x) + a_2 g_2(x) + \ldots a_m g_m(x) \ldots \qquad [2.58]$$

where $m \leq n$ and $g_1(x), \ldots g_m(x)$ are functions of x which can be in forms of polynomial, logarithm or exponential. Equation 2.58 will be complete only if values of coefficients, $a_1, a_2, \ldots a_m$ enable the function $G(x)$ yields the estimate values with least deviation from the data. If a variance over all data   is defined as follows:

$$= \sum_{i=1}^{n} [y_i - G(x_i)]^2 \qquad [2.59]$$

Required coefficients, $a_1, a_2, \ldots a_m$ which minimize   can be determined from the following relations:

$$
\begin{aligned}
\frac{\partial}{\partial a_1} &= 0 \\
\frac{\partial}{\partial a_2} &= 0 \\
&\vdots \\
\frac{\partial}{\partial a_m} &= 0
\end{aligned}
\qquad [2.60]
$$

From the relations 2.60, m Equations are derived and coefficients $a_1, \ldots a_m$ can be solved using linear equation system.

Fitting functions to estimate the data by the least square method is also called "Regression" and if a relation of n given points is linear, the method determining the linear equation is called "Linear Regression":

$$G(y) = A + Bx \qquad [2.61]$$

Comparing Equation 2.61 to Equation 2.58, it can be found that $g_1(x) = 1, g_2(x) = x$ and other terms is zero. Variance over all these data is

$$= \sum_{i=1}^{n} (y_i - A - Bx_i)^2 \qquad [2.62]$$

A, B are parameters we wish to find which minimize   . That is

$$\frac{\partial}{\partial A} = -2 \sum_{i=1}^{n} (y_i - A - Bx_i) = 0 \qquad [2.63]$$

$$\frac{\partial}{\partial B} = -2 \sum_{i=1}^{n} (y_i - A - Bx_i)(x_i) = 0 \qquad [2.64]$$

Rearrange Equations and :

$$nA + B \sum x_i = \sum y_i \qquad [2.65]$$

$$A \sum x_i + B \sum x_i^2 = \sum x_i y_i \qquad [2.66]$$

A and B, thus, can be solved

$$A = \frac{\sum y_i \sum x_i^2 - \sum x_i \sum x_i y_i}{n \sum x_i^2 - \left(\sum x_i\right)^2} \qquad [2.67]$$

$$B \;=\; \frac{n\sum x_i y_i - \sum x_i \sum y_i}{n\sum x_i^2 - \left(\sum x_i\right)^2} \qquad\qquad [2.68]$$

The method of linear regression can applied to those data which their relations are not linear. For example, a given $G(x) = A + B\ln x$. If we give $X = \ln x$ and $Y = G(x)$, then the equation becomes $Y = A + BX$.

2.3 Statistical Mechanics

2.3.1 Introduction

Statistical mechanics [51] is the mathematical tool that provides a framework for relating the microscopic properties of individual atoms and molecules to the macroscopic or bulk properties of materials, explaining thermodynamics as a natural result of statistics and mechanics (classical and quantum) at the microscopic level.

Suppose certain macroscopic properties of a complex system are known, they do not characterize the system completely because there are a huge number of possible microstates that all have the same macroscopic properties. Knowing those macroscopic properties, the microstate of the system is still unknown.

An ensemble is defined as an idealization consisting of a huge number of mental copies of a system, considered all at once, each of which represents a possible microstate that the real system might be in. It is introduced into the statistical mechanics as a basic tool to obtain explicit formulas for many of the thermodynamic quantities of interest, often in terms of the appropriate partition function.

2.3.2 Ensembles and Thermodynamic Connection

Among many possible ensembles the most common ones are the microcanonical, the canonical and the grand canonical ensemble that are consistent with isolated, closed and opened systems. Only the basic knowledge of first two types, which were used in the present study, are given here

Microcanonical Ensemble

A microcanonical ensemble is an ensemble consisting of copies of an isolated system and its analysis is correspondingly simple. By the assumption that the system is isolated, each copy in the ensemble has a common fixed energy E. The system may have many different microstates corresponding to the energy E. If $\Omega(E)$ is the number of microstates corresponding to the same energy E, the probability that a system chosen at random from the ensemble would be in a given microstate is simply $\frac{1}{\Omega}$. This leads to a formula for entropy:

$$S = k_{\mathrm{B}}\ln\Omega(\mathrm{E})$$ [2.69]

where k_{B} is the Boltzmann constant. Or, equivalently,

$$\Omega(E) = \mathrm{e}^{k_{\mathrm{B}}S}$$ [2.70]

The entropy S, which describes the physical situation is the characteristic function of this ensemble.

Canonical Ensemble

A canonical ensemble is an ensemble of dynamically similar systems, each of which can share its energy with a large heat reservoir, or heat bath. The distribution of the total energy amongst the possible dynamical states (*i.e.* the members of the ensemble) is given by the partition function. A generalization of this is the grand canonical ensemble, in which the systems may share particles as well as energy.

In some derivations, the heat bath is considered to comprise a large number of copies of the original system, loosely coupled to the original and to each other, so as to share the same total energy - this then makes the combined (system+heat bath) describable by the statistics

of a microcanonical ensemble

Given a system A and the reservoir B are in thermal equilibrium, which the total energy E^* is a sum of the energy of the $m-th$ state E_m for the system and the energy associated with the heat bath E':

$$E^* = E' + E_m \qquad [2.71]$$

Notice E is constant, since the system C which is a combination of A and B is thought to be isolated. Therefore the probability of A being in the $m-th$ state is proportional to corresponding number of microstates available to the reservoir:

$$p_m = c'\Omega'(E') \qquad [2.72]$$

Taking the logarithm gives

$$\ln p_m = \ln c' + \ln\Omega'(E') = \ln c' + \ln\Omega'(E^* - E_m) \qquad [2.73]$$

Since E_m is small compared to E^*, a Taylor series expansion can be performed on the logarithm around the energy E'. An appropriate approximation can be obtained by keeping the first two terms of the Taylor series expansion:

$$\ln p_m = \ln c' + ln\Omega'(E^*) - \frac{1}{k_\mathrm{B}T}E_m = \ln c' + ln\Omega'(E^*) - \beta E_m \qquad [2.74]$$

where T is the temperature in Kelvin.

Exponentiating Equation 2.74 gives

$$p_m = c\mathrm{e}^{-\beta \mathrm{E_m}} \qquad [2.75]$$

where

$$c = c'\Omega'(E^*) \qquad [2.76]$$

The probabilities must sum to 1, thus

$$\sum_m p_m = 1 \;=\; \sum_m c\mathrm{e}^{-\beta \mathrm{E_m}}$$
$$c \;=\; \frac{1}{\sum_m \mathrm{e}^{-\beta \mathrm{E_m}}} = \frac{1}{Z(\beta)} \qquad [2.77]$$

$Z(\beta)$ is known as the partition function for the canonical ensemble. The partition function can be used to find the expected value of any microscopic property of the system, which can then be related to macroscopic variables. For instance, the expected value of the microscopic energy E is interpreted as the microscopic definition of the thermodynamic variable internal energy U which can be obtained by taking the derivative of the partition function with respect to the temperature:

$$U =< E >= \frac{\sum_i E_i e^{-\beta E_i}}{Z} = -\frac{\mathrm{d}\ln Z}{\mathrm{d}\beta} \qquad [2.78]$$

The entropy can be calculated by

$$\frac{S}{k_{\mathrm{B}}} = -\sum_i p_i \ln p_i = \sum_i \frac{\mathrm{e}^{-\beta \mathrm{E_i}}}{Z}(\beta E_i + \ln Z) = \ln Z + \beta U \qquad [2.79]$$

which implies that

$$-\frac{\ln Z}{\beta} = U - TS = F \qquad [2.80]$$

is the Free energy of the system or in other words,

$$Z = \mathrm{e}^{-\beta \mathrm{F}} \qquad [2.81]$$

The free energy F is the characteristic function for this kind of ensemble. Having microscopic expressions for the basic thermodynamics potentials U, S and F is sufficient to derive expressions for other thermodynamics quantities. For example, pressure which is a combination of known thermodynamics relation ships between U and V can be expressed in terms of temperature, volume and the partition function:

$$P = \frac{1}{\beta}\left(\frac{\partial \ln Z}{\partial V}\right)_{N,T} \qquad [2.82]$$

2.4 Molecular Dynamics Simulations

2.4.1 Introduction

A brief concept of statistical mechanics was presented. Statistical mechanics provides a means for determining physical properties that are associated with a macroscopic sample of the bulk liquid, solid and so on as the net result of the properties of many molecules in many conformations, energy states and the like. In practice, the difficulty is not the statistical mechanics, but obtaining all the information about possible energy levels, conformations and so on. Molecular dynamics (MD) simulations is one of two methods for obtaining this information. (Another method is called 'Monte Carlo' simulations whose details will be not mentioned, except for technical details which are applied to both two simulation methods.)

MD simulation is a simulation of the time-dependent behavior of a molecular system. It uses (in most cases classical) mechanics to calculate the trajectories of the particles that form the system. The energy expression is used to compute the forces on the atoms for any given geometry. To carry out the MD simulation, the program is constructed in the rule, as following:

1. The parameters specifying the conditions of the system, *e.g.*, initial temperature, particle number, time step, total time, are read in.

2. The system is initialized.

3. The forces for each pair of paricles in the system have been computed.

4. The Newton's equation has been integratd. This step and the previous steps of force calculations, the core of MD simulation, will be repeated until the total or evaluation time is reached.

5. After the core loop is completed, either dynamic or structural quantities could be carried out now.

2.4.2 Newton's Laws of Motion

In MD, successive configurations of the system are generated by integrating Newton's laws of motion. The result is a trajectory that specifies the positions and velocities of the particles in the system with respect to time. Newton's law can be stated as follows:

1. A body continues to move in a straight line at constant velocity unless a force acts upon it.

2. Force equals the rate of change of momentum.

3. To every action there is an equal and opposite reaction.

The trajectory is obtained by solving the differential equations incorporated Newton's second law ($F = ma$):

$$\frac{\mathrm{d}^2 x_i}{\mathrm{d}t^2} = \frac{F_{x_i}}{m_i} \qquad [2.83]$$

This equation describes the motion of a particle of mass m_i along coordinate x_i with the force on the particle F_{x_i}.

2.4.3 Finite Difference Methods

In realistic models of intermolecular interactions, the force on each particle will change whenever the particle changes its position, or whenever any of the other particles with which it interacts changes position. This leads to the coupled motions of all the particles in the system or many-body problem that can not be solved analytically. A *finite different method* is introduced to integrate the equations of motion under such circumstances.

The essential idea of the finite difference method is that the integration is broken down into many small stages, each separated in time by a fixed time δt. The net force on each particle

at a time t is calculated as the vector sum of its interactions with other particles. From the force the accelerations of the particles are determined. Then, they are combined with the positions and velocities at a time t to calculate the positions and velocities at a time $t + \delta t$. The force is assumed to be constant during the time step.

There are many algorithm for integrating the equations of motion using finite difference methods. All algorithms assume that the positions and dynamics properties (velocities, accelerations, etc.) can be approximated as Taylor series expansions:

$$r(t + \delta t) \quad = \quad r(t) + \delta t v(t) + \frac{1}{2}\delta t^2 a(t) + \frac{1}{6}\delta t^3 b(t) + ... \qquad [2.84]$$

$$v(t + \delta t) \quad = \quad v(t) + \delta t a(t) + \frac{1}{2}\delta t^2 b(t) + ... \qquad [2.85]$$

$$a(t + \delta t) \quad = \quad a(t) + \delta t b(t) + ... \qquad [2.86]$$

where v is the velocity (the first derivative of the position r with respect to time), a is the acceleration (the second derivative), b is the third derivative, and so on. The *Verlet integrator* [52] is probably the most widely used algorithm for integrating the equations of motion in MD simulations. Several variation on the Verlet integrator have been developed. The velocity Verlet integrator developed by Swope gives positions, velocities and accelerations at the same time and does not compromise precision:

$$r(t + \delta t) \quad = \quad r(t) + \delta t v(t) + \frac{1}{2}\delta t^2 a(t) \qquad [2.87]$$

$$v(t + \delta t) \quad = \quad v(t) + \frac{1}{2}\delta t[a(t) + a(t + \delta t)] \qquad [2.88]$$

Three stages have been performed. First, the positions at $t + \delta t$ are calculated according to Equation 2.87 using the velocities and the accelerations at time t. Then, the velocities at time $t + \frac{1}{2}\delta t$ are then determined using:

$$v(t + \frac{1}{2}\delta t) = v(t) + \frac{1}{2}\delta t a(t) \qquad \text{[2.89]}$$

New forces are next computed from the current positions, giving $a(t + \delta t)$. In the final step, the velocities at time $t + \delta t$ are determined using:

$$v(t + \frac{1}{2}\delta t) = v(t + \frac{1}{2}\delta t) + \frac{1}{2}\delta t a(t + \delta t) \qquad \text{[2.90]}$$

2.4.4 Energy Expression

All of the information needed to calculate the dynamics of a system can be found from the potential energy function U of the system. From Newton's laws, the force on atom i in the system can then be determined from the equation.

$$f_i = -\nabla_i u \qquad \text{[2.91]}$$

An integrator is then used to calculate the trajectories of the atoms from the forces. Potential functions and parameter sets are derived from both experimental work and high-level quantum mechanical calculations. Potential functions may provide parameters for every atom in a system or may treat the hydrogen atoms and their connected atom as a single interaction center or psudo atom.

The basic functional form of a potential function encapsulates both bonded terms relating to atoms that are linked by covalent bonds, and non-bonded terms describing the long-range electrostatic and van der Waals forces. The various contributions are schematically represented in Figure 2.1
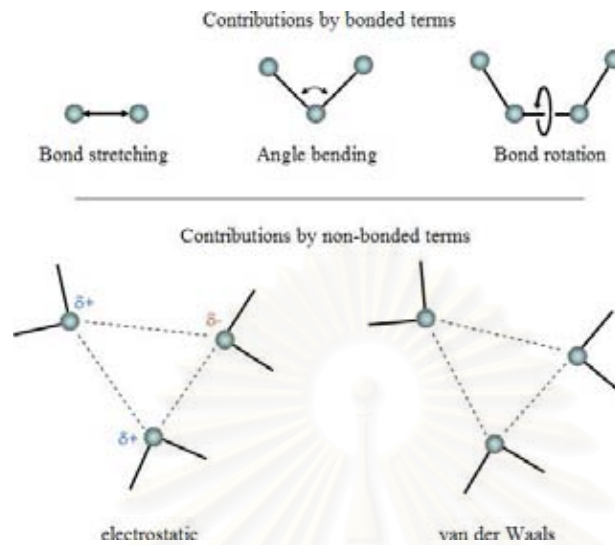
Figure 2.1 Schematic representation of the four key contributions to potential for a molecular system: bond strecthing, angle bending and torsional terms and non-bonded interactions

Bond Stretching

Potential energy curve for a typical bond stretching can be modeled by the Morse potential:

$$u(l) = D_{\mathrm{e}}\{1 - \exp[-a(l - l_0)]\}^2 \qquad [2.92]$$

D_e is the depth of the potential energy minimum and $a = \omega\sqrt{\mu/2D_{\mathrm{e}}}$, where μ is the reduced mass and ω is the frequency of the bond vibration. ω is related to the bond stretching constant k by $\omega = \sqrt{k/\mu}$. l_0 is the reference bond length. Though, the Morse potential is not amenable to efficient computation and requires three parameters to be specified for each bond. It's useful in calculations for bonds to deviate significantly from their reference values; the Morse curve describes a wide range of behavior from the strong equilibrium behavior to dissociation.

A simpler functional form is to use a Hooke's law formula in which the energy varies with the square of the displacement from the reference bond length l_0:

$$u(l) = \frac{k}{2}(l - l_0)^2 \qquad [2.93]$$

The model is reasonable approximation to the shape of the potential energy curve at the bottom of the bottom of the potential well, at distances that correspond to bonding in ground-state molecules. Therefore, it is usually used in molecular mechanics calculations where bond dissociation is rare.

Angle Bending

The deviation of angles from their reference values is also often described using a Hooke's law or harmonic potential:

$$u(\theta) = \frac{k}{2}(\theta - \theta_0)^2 \qquad [2.94]$$

The contribution of each angle is characterized by a force constant k and a reference value θ_0. For linear molecules $\theta = 180$ can cause problems. In this case, the harmonic cosine potentials are more suitable for MD simulations by avoiding a factor $1/\sin 180^0$ which will be derived from calculating force from Equation 2.94. The general form of the harmonic cosine potentials can be express as:

$$u(\theta) = \frac{k}{2}(\cos\theta - \cos\theta_0)^2 \qquad [2.95]$$

Bond Rotation (Torsional)

Deformation from the reference value by bond-stretching and angle-bending requires quite substantial energy. The variation in structure and relative energies is mostly due to the complex interplay between the torsional and non-bonded contributions.

Torsional potentials are almost always expressed as a cosine series expansion:

$$u(\omega) = \sum_{n=0}^{N} \frac{V_n}{2}[1 + \cos(n\omega - \gamma)] \qquad [2.96]$$

ω is the torsion angle. V_n in Equation 2.96 give a qualitative indication of the relative barriers to rotation. n is the multiplicity; its value gives the number of minimum points in the function as the bond is rotated through 360^0. γ is the phase factor that determines where the torsion angle passes through its minimum value.

An alternative equivalent expression is:

$$u(\omega) = \sum_{n=0}^{N} C_n \cos(\omega)^n \qquad [2.97]$$

Electrostatic

Each element can attract electrons differently, giving rise to an unequal distribution of charge in a molecule. This charge distribution can be represented in a number of ways. One common approach is to arrange fractional point charges to the nuclear centers. These charges, then, are often referred to as partial atomic charges or net atomic charges. The electrostatic interaction between two molecules or between different parts of the same molecule can be calculated as a sum of interactions between pairs of point pcharges, using Coulomb's law:

$$u = \sum_{i=1}^{N_A} \sum_{j=1}^{N_B} \frac{q_i q_j}{4\pi\epsilon_0 r_{ij}} \qquad [2.98]$$

N_A and N_B are the numbers of point charges in molecules A and B, respectively. However, an accurate representation of a molecule's electrostatic properties may require charges to be placed at locations other than at the atomic nuclei. For example, molecular nitrogen has a dipole moment of zero. Its total charge is also zero. But, nitrogen molecule has a quadrupole moment. The simplest way to model this is to place three partial charges along the bond. A charge of $-q$ at each nucleus and $+2q$ at the center of mass.

Van der Waals

Electrostatic interactions can not account for all of the non-bonded interactions in a system. Noble gases are an obvious example. They are very stable and tend not to interact. This is why it is difficult to condense them into liquids. However, the larger the atom of the noble gas (the more electrons it has) the easier it is to condense the gas into a liquid. This happens because, when the electron cloud surrounding the gas atom gets large, it becomes a temporary dipole. This induces the same shift in neighboring atoms and spreads from one atom to the next. Deviations from ideal gas behavior were famously quantitated by van der Waals. Thus, the forces that give rise to such deviations are often referred to as van der Waals forces.

The van der Waals interactions arise from a balance between dispersive and exchange-repulsive interactions between atoms and molecules. An instantaneous dipole arises during the fluctuations in the electron clouds induce a dipole in neighboring atoms, giving rise to a long-range attractive inductive effect while, at short distance, decrease in the separation cause a large increase in the energy. The interaction is due to electrons with the same spin, therefore, it is often referred to as exchange force. The effect of exchange is to reduce the electrostatic repulsion between pairs of electrons. This reduces electron density in the inter-nuclear region and leads to repulsion between between incompletely shielded nuclei.
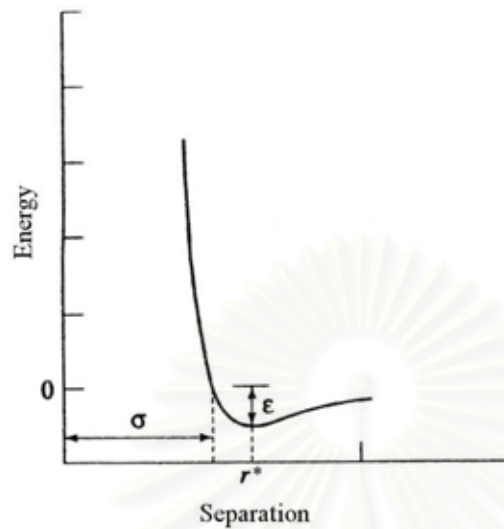
Figure 2.2 The Lennard-Jones potential

The best known of the van der Waals potential functions is the *Lennard-Jones 12-6 function*, which takes th following form for the interaction between two atoms:

$$u(r) = 4\epsilon \left[\left(\frac{\sigma}{r} \right)^{12} - \left(\frac{\sigma}{r} \right)^{6} \right]$$

[2.99]

There exist just two adjustable parameters in Equation 2.99: the collision diameter σ for which the separation at the energy is zero and the well depth ϵ The Lennard-Jones potential is characterized by an attractive part that varies as r^{-6} and a repulsive part that varies as r^{-12}. Different powers have also been used for the repulsive part of the potential. Lennard-Jones potential can be written in the following general form:

$$u(r) = k\epsilon \left[\left(\frac{\sigma}{r} \right)^{n} - \left(\frac{\sigma}{r} \right)^{m} \right]$$

[2.100]

where $k = \frac{n}{n-m}\left(\frac{n}{m}\right)^{m/(n-m)}$.

Several formulations have been proposed. Buckingham potential replaces the r^{-12} term with exponential term:

$$u(r) = \epsilon\left[\frac{6}{\alpha-6}\exp[-\alpha(r/r^* - 1)] - \frac{\alpha}{\alpha-6}\left(\frac{r^*}{r}\right)^6\right] \qquad [2.101]$$

There are three adjustable parameters in the Buckingham potential (σ, r^* and α). It must be noted here that this function give strongly attractive at very short distances. So the program must check that atoms are not becoming to close.

Two main reasons for developing the functional form is to obtain a more accurate reproduction for the dispersion interaction and keep the potential finite as the interatomic potential approach zero (unlike the Lennard-Jones function, which becomes infinite).

2.4.5 Technical Details

In this section, the important computational tricks which compromise between computational time and accuracy of the results will be discussed. Actually, these useful tricks have no deeply physical significance.

Periodic Boundary Conditions

Normally, only a small number of particles are performed in a simulation. Thus, one must give an appropriate surroundings to the simulated particles in order to forbid surface effect. Otherwise, the particles will behave like a tiny drop. Therefore, a trick called periodic boundary condition [53] is employed: a cubic box containing the system particles is replicated in all directions to give a periodic array. Replication of two-dimensional box is shown in Figure 2.3.
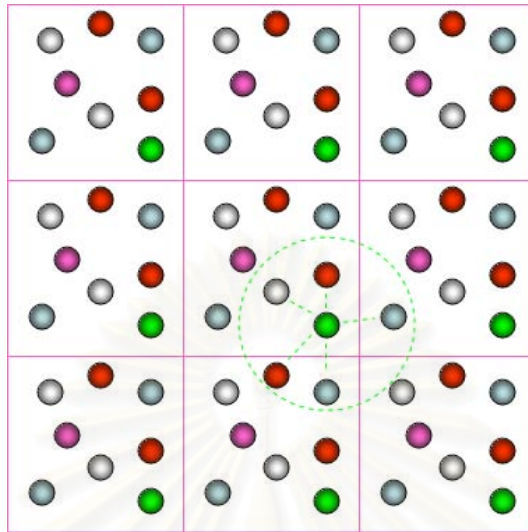
Figure 2.3 Two-dimensional periodic boundary conditions: minimum image convention is applied when cutoff radius is as small as a half of boxlength.

An interested box is called a *central box* while neighbors surrounding it are called *image boxes*. In the two-dimensional a central box is surrounded by eight images; in three dimensions central box would have 26 nearest images. The coordinates of the particles in the image boxes can be computed simply by adding or subtracting integral multiples of the box sides. If a particle leave the central box during the simulation, then, an image particle will enter the central box from the opposite side, as displayed in Figure 2.3. The number of particles within the central box thus remains constant.

Cutoff Radius

Employing the periodic boundary condition, uncountable particles interact an interested particle. Calculating all these pairs is impractical and meaningless because the non-bonded potential falls off very rapidly with distance. For example, at a distance of 2.5σ, the Lennard-Jones potential has just 1% of its value at σ. Pair interactions will be calculated within a certain distance, called *cutoff radius* (r_C). Potential energy and force is set to be zero for a distance larger than cutoff radius.

Minimum Image Convention

When the range r_C of the potential is as small as the half of the box length, the so called *minimum image convention* is applied. Pairs of interested atom with the other closest atoms or images that fall in the cutoff radius will be calculated for potential energies and forces as illustrated in Figure 2.3. If the cutoff radius must be large enough to cover an interatomic distance where potential energy becomes insignificant, it should be noted here that box length L should not be larger than the cutoff diameter. Otherwise, an atom sees other atoms twice.

Shifted Potential

A cutoff introduces a discontinuity in both the potential energy and the force near the cutoff value. This creates problems in MD simulations where energy conservation is required. There are several ways to counteract the effect of this continuity. One approach is to use a shifted potential by adding a linear term that make the derivative zero at the cutoff. Given the original Lennard-Jones potential $u_{LJ}(r)$, shifted potential $u(r)$ can be written as follows:

$$u(r) = u_{\mathrm{LJ}}(r) - (r_\mathrm{C} - r)\Delta f - u_{\mathrm{LJ}}(r_\mathrm{C}) \qquad [2.102]$$

In Equation 2.102, $u(r) = 0$ for $r > r_\mathrm{C}$.
Though, the shift improves the validity of energy conservation and numerical stability, in some cases, it makes significant deviation from the true potential and calculated thermodynamic properties.

2.5 Evaluation

2.5.1 Heat of Adsorption

The isosteric heat of adsorption (Q_{st}) is a property often used to validate fitted potential functions. At infinite dilution it is easy to evaluate [47] by the relation

$$Q_{st} = -\left(\langle U \rangle_{gz} - \langle U \rangle_{z} - \langle U \rangle_{g}\right) + k_{B}T \qquad [2.103]$$

where $\langle U \rangle_{gz}$, $\langle U \rangle_{g}$ and $\langle U \rangle_{z}$ are the ensemble average of the potential energy of the zeolite-guest system, the energy of an isolated hydrocarbon and the average zeolite energy, respectively. For the rigid zeolite lattice at high dilution, *e.g.*, 1 molecule per unit cell, the terms $\langle U \rangle_{z}$ can be neglected. Then, Q_{st} in Equation 2.103 becomes

$$Q_{st} = -\left(\langle U \rangle_{gz} - \langle U \rangle_{g}\right) + k_{B}T. \qquad [2.104]$$

2.5.2 Self Diffusion

Diffusion is one type of transport phenomena. The expression "diffusion" is used for the movement of particles from one place to another [54] by Brownian motion. In the case of the so called transport diffusion which is often simply but unprecisely called diffusion it causes a particle flux reducing concentration gradients. This flux must be distinguished from other fluxes caused by pressure gradients. If there is no concentration gradient, then, the spread of some marked particles which initially were close to each other over the total system is called self diffusion. It is a physical process rather than a chemical reaction, which requires no net energy expenditure. In cell biology, diffusion is often described as a form of passive transport, by which substances cross membranes.

The different forms of diffusion can be modeled quantitatively using the diffusion equation, which goes by different names depending on the physical situation.

In the late 1820s Robert Brown gave the expression of a phenomenon, which is closely related to diffusion. It is about the behavior resulting from the continuously changing inter-action between particles of the surrounding fluid. Analogy, the individual particles undergo a sequence and apparently random movements. This phenomenon is referred to as Brownian motion [55].

An experimentally accessible quantity that describes Brownian motion is the time dependence of the concentration distribution, starting from the assumptions that the particles do not interfere with each other and may step with equal probability in any direction. Self diffusion were elaborated from Brownian motion by Einstein [56]. The self diffusion coefficients are calculated from the particle displacements. The process of self-diffusion was generally related to the moments of the propagator [57, 58, 59]. The propagator $P(r,t)$ represents the probability density to find a particle at position r at time t.

The nth moment of the propagator is defined by the relation,[59]

$$\left\langle |r - r_0|^n \right\rangle = \int |r - r_0|^n P(r,t)\mathrm{dr}. \qquad [2.105]$$

In the case of isotropic diffusion and of a homogeneous system the propagator is

$$P(r,t) = (4\pi Dt)^{-3/2}\exp\left\{\frac{-(r)^2}{4Dt}\right\} \qquad [2.106]$$

The moments of displacement yield in this case:

$$\langle |r - r_0| \rangle = 4\sqrt{\frac{Dt}{\pi}} \qquad [2.107]$$

$$\left\langle (r - r_0)^2 \right\rangle = 6Dt \qquad [2.108]$$

$$\left\langle \left| (r - r_0)^3 \right| \right\rangle = \frac{32(Dt)^{3/2}}{\sqrt{\pi}} \qquad [2.109]$$

$$\left\langle (r - r_0)^4 \right\rangle \;=\; 60(Dt)^2 \qquad\qquad [2.110]$$

$$\vdots$$

and D can be obtained from each one of these moments.

In the case of anisotropy, the three components of the probability distribution (propagator) are assumed to be uncorrelated and hence

$$
\begin{aligned}
P(r,t) &= P_x(x,t)P_y(y,t)P_z(z,t) \\
&= \frac{(4\pi t)^{-3/2}}{\sqrt{D_x D_y D_z}} \exp\left\{ -\frac{x^2}{4D_x t} - \frac{y^2}{4D_y t} - \frac{z^2}{4D_z t} \right\}
\end{aligned}
\qquad [2.111]
$$

The moments for each direction $e.g.$ $x-$ direction [60] are

$$\left\langle |x - x_0| \right\rangle \;=\; 2\sqrt{\frac{D_x t}{\pi}} \qquad\qquad [2.112]$$

$$\left\langle (x - x_0)^2 \right\rangle \;=\; 2D_x t \qquad\qquad [2.113]$$

$$\left\langle \left| (x - x_0)^3 \right| \right\rangle \;=\; \frac{8(D_x t)^{3/2}}{\sqrt{\pi}} \qquad\qquad [2.114]$$

$$\left\langle (x - x_0)^4 \right\rangle \;=\; 12(D_x t)^2 \qquad\qquad [2.115]$$

$$\vdots$$

The D values estimated from these moments must synchronize each other in the case of normal diffusion for t values larger than the decay time of the velocity auto-correlation function. The elements of the diffusion tensor, corresponding to the $x-$, $y-$ and z-axes.

2.5.3 Anisotropic Effect on Self Diffusion

It has been observed experimentally and theoretically that the diffusion of alkanes and light gases in silicalite–1 is anisotropic [61, 62, 63, 64, 65]. To visualize this effect, a formula for the relation between the components of the diffusivity tensor (D) proposed by Kärger et al [65]. Equation 2.116 has been applied,

$$\frac{a^2}{D_x} + \frac{b^2}{D_y} = \frac{c^2}{D_z} \qquad [2.116]$$

where a, b and c are the unit cell parameters (see Figure 1.1b). The deviation from Equation 2.116 can be accounted by introducing a parameter [61, 66],

$$\beta = \frac{c^2/D_z}{a^2/D_x + b^2/D_y} \qquad [2.117]$$

where $\beta = 1$ denotes random processing, e.g., a guest molecule passing an intersection continues the diffusion path independent of how it gets to the intersection. A hint on preferentially continuative diffusion path either along in one or the same channel type is when $\beta > 1$. Vice versa, a higher diffusivity in z-direction, that is only possible by changes between straight and sinusoidal channels, occurs if $\beta < 1$. The interchange between the two channel types is more probable in this case.

2.5.4 Radial Distribution Function

The radial distribution function (RDF) allows a straightforward theoretical measurement in a simulation to the real laboratory experiment measurements, e.g., neutron on X-ray scattering. It is basically defined as the ratio between the average number density at a distance from any determined atom r and the overall number density [67, 68]:

$$g_{ij}(r) = \frac{N_j(r)}{\rho_{ij}\Delta V(r)} \qquad [2.118]$$

where $\Delta V(r)$ is a volume of spherical shell of thickness δr at a distance r. ρ_{ij} is a number density of unrepeated pair between atom i and atom j. A number of particles of type b around a particle i in the volume ΔV are collected as $N_j(r)$. The evaluation of $g(r)$ as shown in Equation 2.118 is displayed in Figure 2.4.
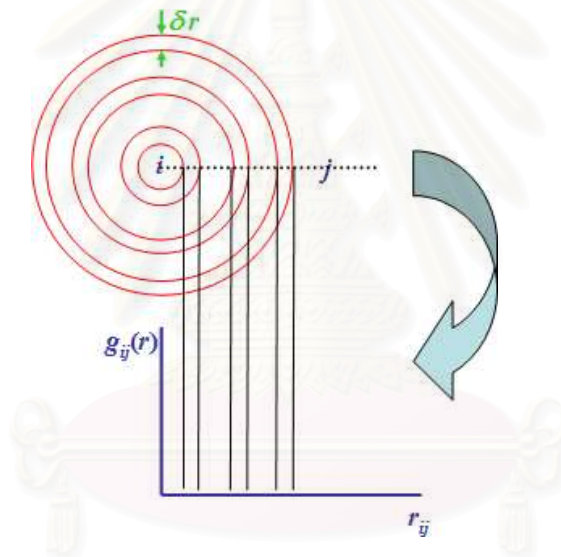
Figure 2.4 Evaluation of number of particles of the type j around a particle of type i in the volume ΔV.

CHAPTER III

METHODOLOGY

As it was written in Chapter that aim of this work is to study the structural details of the system using MD simulation method applying intermolecular potentials which developed from the *ab initio* data. Content of this chapter starts with detailed development of the *ab initio* fitted potentials. Then, followed by declaration of detailed modeling in MD simulations.

3.1 Development of *Ab Initio* Fitted Potentials

3.1.1 Fragment Representing Silicalite-1

To develop the n-pentane/silicalite-1 potentials, it is not possible to perform quantum chemical calculation using complete unit cell of the crystal. Therefore, a fragment consisting of 10 oxygen and 10 silicon atoms, or 10 O-membered ring, has been used to represent the silicalite–1. The fragment was, then, saturated with hydrogen atoms as shown in Figure 3.1b.
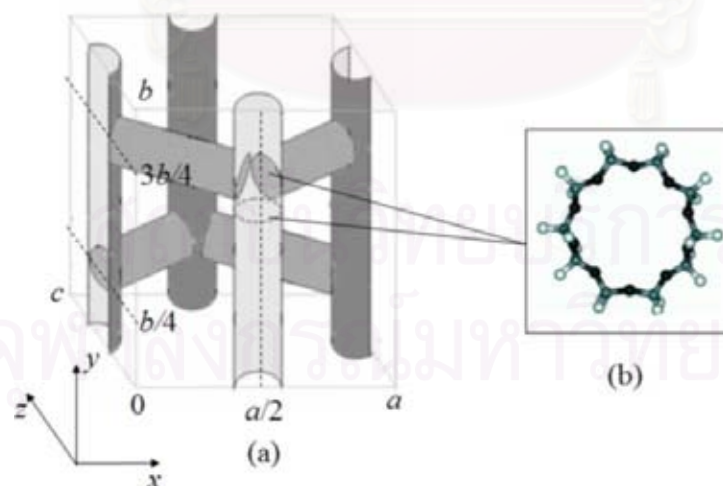
Figure 3.1 Schematic representation of: (a) the channel system within one unit cell of silicalite-1; (b) a 10-oxygen membered ring-fragment of silicalite-1.

Positions and orientations of the hydrogen atoms were optimized at the Hartree Fock (HF) level with 6-31G(d).

3.1.2   *Ab Initio* Calculations

Energies representing both n-pentane/silicalite–1 fragment and n-pentane/n-pentane interactions were calculated for the configurations which were generated as follows:

n-pentane/silicalite-1

The n-pentane molecule was first positioned at the center of the fragment in the configuration shown in Figure 3.2.
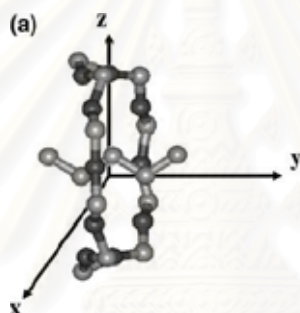
Figure 3.2 Schematic representation of n-pentane/silicalite–1 complex where n-pentane was positioned at the origin of the cartesian coordinates (hydrogen atoms connected to heavy atoms are not displayed).

Then, 189 configurations were generated by varying coordinates of n-pentane in terms of molecular translation and rotation along x, y and z-axes.

n-pentane/n-pentane

Similar procedures as performed for the guest/host intermolecular potential, it was also applied to the guest/guest system. The center of mass of the first n-pentane was located at the origin and that of the second one at 3 Å on the x-axis (Figure 3.3).

Positions and orientations of the second n-pentane were varied in terms of its translation and rotation along the x-, y- and z-axes. The distance between the two molecules was extended until the interaction approaches zero. In addition, flexibility of the n-pentane was also taken into account by varying all CCCC torsional angles of both molecules. With
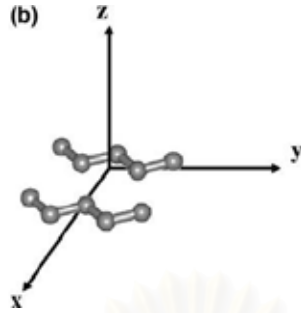
Figure 3.3 Starting configuration of n-pentane/n-pentane dimer which was used to develop the intermolecular pair potential.

this procedure, 1300 configurations of the n-pentane dimer have been generated. Quantum chemical calculations were performed at MP2 level [17, 69]. The basis set superposition error (BSSE) was also taken into account for all data points.

3.1.3 Analytical Form of the Fitted Functions

The calculated interaction energies, $E(r)$, were fitted to analytical functions of the type:

$$\Delta E(r) = \sum_{i}^{n} \sum_{j \neq i}^{n} \left\{ \frac{A_{ij}}{r_{ij}^6} + \frac{B_{ij}}{r_{ij}^{12}} + \frac{C_{ij}}{r_{ij}^4} \right\} \qquad [3.1]$$

where A_{ij}, B_{ij} and C_{ij} are fitting parameters. r_{ij} is the distance between atoms i and j, belonging to different molecules. Note that, the highly repulsive configurations were excluded from the fitting procedure due to the negligible likeliness of occurrence. The n-pentane molecule is represented by a united atom model [70], in which interaction sites of CH_2 or CH_3 groups are positioned at the carbon atoms. Therefore, n in Equation 3.1 is equal to 5, numbers of interaction site in n-pentane molecule

Only oxygen atoms of the fragment were included in the n-pentane/silicalite–1 fitted potential as it is done in most of the MD simulations for guest/zeolite systems while the quantum calculations include, of course, also the silicon atoms.

3.2   MD simulations

3.2.1   The Model

All details on the silicalite-1 and n-pentane models used in MD simulations with varying loadings and temperatures were given below.

The Silicalte-1 Model

Zeolite Silicalite-1 used in this study is assumed to be purely silicious. The zeolite structure was extracted from the database of the Structure Commission of the International Zeolite Association (IZA). The zeolite structure was furthermore assumed to be rigid to reduce computational requirements. However, the lack of exchange in energy due to the rigid lattice was compensated by applying thermalization by a virtual heat bath [71]. Flexibility of the framework is not an issue for adsorption of linear and branched alkanes [72]. The zeolite structure, thus, was assumed to be rigid to reduce computational requirements.

The n-Pentane Model

The n-pentane molecule were modelled using united atom models, whereby the methyl and methylene groups were treated as single interaction centers. The reference bond length between two interaction sites, r_0 is 1.54 Å and was allowed to fluctuate under the influence of the Morse potential [73] as shown in Equation 3.2:

$$u(r) = D \left[1 - e^{\beta(r-r_0)} \right]^2 \qquad [3.2]$$

where $D = 83.9$ kJ/mol, $\beta = 1.84$ Å^{-1}.

A Harmonic potential [74] was assumed for three adjacent interaction sites:

$$u(\theta) = \frac{k}{2} \left(\theta - \theta_0 \right)^2 \qquad [3.3]$$

where reference bond angle $\theta_0 = 1.99$ rad and the force constant $k = 519.398$ kJ·mol^{-1}·rad^{-2}. Torsion is modelled using a four-term cosine expansion in the dihedral angle [75]:

$$u(\omega) = \sum_{n=0}^{3} C_n \cos^n(\omega) \qquad [3.4]$$

where $C_0 = 8.4029$ kJ/mol, $C_1 = 16.7974$ kJ/mol, $C_2 = 1.1346$ kJ/mol and $C_3 = -26.3349$ kJ/mol.

3.2.2 Simulation Details

The general details for setting MD simulations are as follows. The simulation program is a home made package. The temperature of the system has been controlled by a virtual heat bath [71]. The Newton equation of motion has been solved through Verlet algorithm [76]. Each simulation run was for 200 ns long with time step of 0.5 fs. The potential functions was first calibrated by applying to the MD program and predicting the heat of adsorption (Q_{st}) at zero coverage and the diffusion coefficients (D_s). Therefore, several MD simulations were carried out in order to valiate the newly developed functions.

the validated n-pentane/silicalite–1 and n-pentane/n-pentane potential functions, were, then, applied to the MD program. The simulations were performed by varying number of n-pentane and temperature range. Variation of the n-pentane for 3 concentrations from 0.5 to 8 molecules per unit cell and 4 temperatures from 200 K upto 350 K.

CHAPTER IV

RESULTS AND DISCUSSIONS: POTENTIAL DEVELOPMENT

4.1   General Remarks on the *Ab Initio* Fitted Potential

Some comments could be made concerning the *ab initio* fitted potential. The main
concept of this kind of potential function is to seek for direct relation one to one corresponding
between the *ab initio* data and the fitted energy. This is in contrast to the empirical force
field in which the parameters were adjusted to represent the experimental observation such
as diffusion coefficient and adsorption isotherm *etc.* Therefore, the following remarks could
be made. (*i*) in order to get the best function representing the *ab initio* potential surface,
the physical meaning of the analytical function as well as the fitted parameters may be
disregarded. (*ii*) Although, the representation of energy on each atomic pair might not
reasonable. This would be eliminated by summation over all pairs as the parametrization
of the potential function are performed on molecular base, *i.e.*, the overall energy represents
molecular interaction that is calculated directly from the *ab inito* method. (*iii*) The potential
function developed under this method is always presented in the form of $A/r^m + B/r^n +
C/r^l + \cdots$ instead of collision diameter (σ) and well depth (ϵ) as done in 12-6 Lennard-Jones
force-field potential (see Equation 2.99). Here A, B and C are fitting constants, r denotes
interatomic distance and $m \neq n \neq l$ are the integers. These concepts have been a topic
on debate. Some examples are the guest-zeolite systems studied by simulations applying *ab
initio* fitted potential functions, *e.g.* water/silicalite–1 and methane/silcalite–1. The two
systems were conducted by Bussai *et. al.*[11, 12, 13, 14, 17]. The fitted parameters on the
term of r^{-12} are negative. However, such function can describe the structural properties of
the systems satisfactorily.

The remainder of this chapter is organized as follows. Section 4.2, accuracy of the
ab initio data with and without basis set supposition error (BSSE) was explained. Next,
the fitting results such as optimized potential parameters and quality of the fit, were given

in Sections 4.3 and 4.4 for guest/host and guest/guest potentials. Then, several attempts in refitting functions based on reproducibility of experimental heat of adsorption (Q_{st}) at zero coverage quantitatively and self diffusion coefficient (D_s) qualitatively were reported in Sections 4.6-4.8.

4.2 Accuracy of the *Ab Initio* Data

As the analytical function was directly fitted to the *ab initio* data, therefore, accuracy of the *ab initio* method used was concerned. Taking into account of the importance of dispersive interaction in the alkane/silicalite–1 system, Møller-Plesset perturbation (MP2) method was chosen [69]. The basis set superposition error (BSSE) was, then, examined.
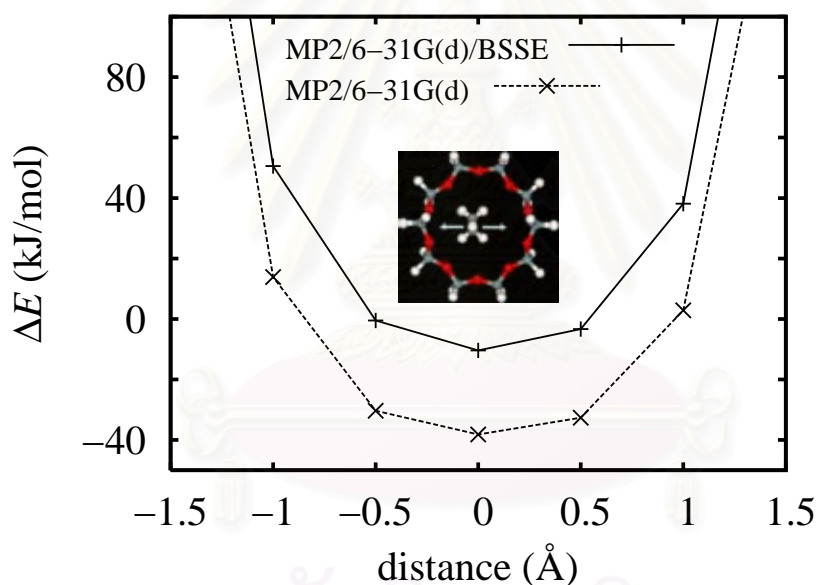
Figure 4.1 Interaction potential energies (ΔE) obtained from the *ab initio* calculations at the MP2/6-31G(d) level with and without BSSE correction. Inset shows starting configuration which the distance was defined to be 0.00 Å.

Comparison between the MP2 energies calculated with and without BSSE was given in Figure 4.1. At the optimal configuration, the BSSE energy of -10.40 kJ/mol is about 3.7 times higher than that of -38.18 kJ/mol without BSSE. An artifact due to an unbalance of the basis set is very large. Thus, *ab initio* calculation with BSSE correction can not be neglected and was applied for all data points for both guest/host and guest/guest interactions.

4.3 n-Pentane/Silicalite–1 Intermolecular Potential

To compromise between the accuracy and computational time required, a 10-oxygen membered ring shown in Figure 3.1 was chosen as a fragment representing silicalite–1 channel.

For the first attempt, the functional form shown in Equation 4.1 was given:

$$\Delta E(r) = \sum_i \sum_j \left\{ \frac{A_{ij}}{r_{ij}^6} + \frac{B_{ij}}{r_{ij}^{12}} + \frac{C_{ij}}{r_{ij}^4} \right\} \qquad [4.1]$$

The fitting parameters were optimized and and their final values were summarized in Table 4.1.

Table 4.1 *Ab initio* fitted potential parameters for the n-pentane/silicalite–1 intermolecular potential as the functional form shown in Equation 4.1.

Sort	Parameters		
	$A(\text{kJ·Å}^6/\text{mol})$	$B(\text{kJ·Å}^{12}/\text{mol})$	$C(\text{kJ·Å}^4/\text{mol})$
O-CH$_3$	-2.111·10^4	3.774·10^7	4.212·10^2
O-CH$_2$	-1.149·10^4	1.510·10^7	5.212·10^2

Due to the use of the united atom model, the total charge of each united atom of type CH_2 or CH_3 is almost zero. Therefore, no Coulombic term was included in Equation 4.1. Another argument to leave out this term is that the proposed model with the effective parameters employed in this study already yields very good agreement between the predicted (by the potential function) and the observed (by the *ab initio* calculation) interaction energies. In addition, the CH_n-Si pairs were not presented in the prepared function. The description is that these type of pair interactions were already included into the CH_n-O pairs. Furthermore, the silicalite–1 surface was prevented by the surrounding oxygens.

To visualize the quality of the guest/host fitted potentials, energies yielded from the *ab initio* calculations (ΔE_{MP2}) were compared with those obtained from the analytical pair potential. ΔE_{FIT}. The result was shown in Figure 4.2 for numerous configurations where each point on the symmetry line would mean 1:1 agreement of model and *ab initio* calculations.
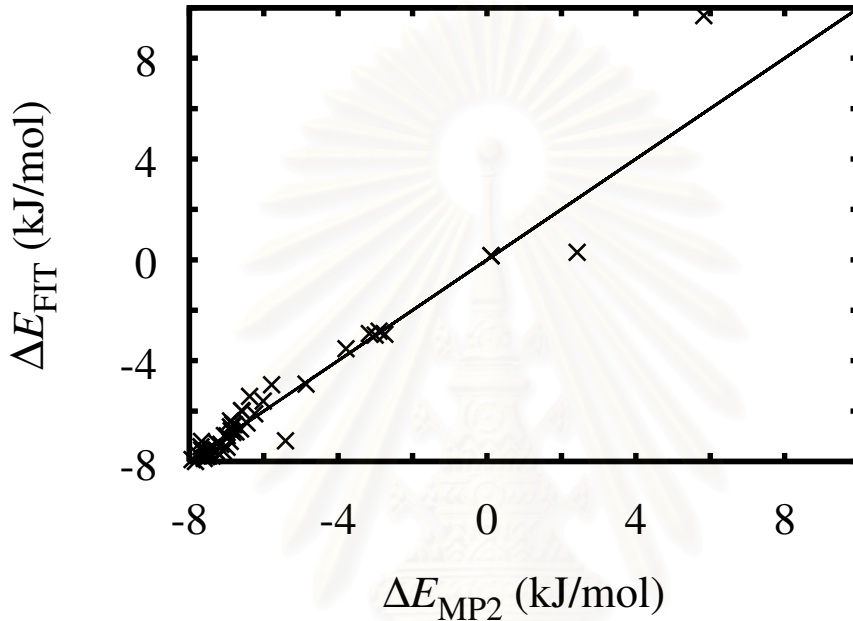
Figure 4.2   The correlation between potential energy values arising from the *n*-pentane/silicalite–1 interaction calculated from *ab initio* method (ΔE_{MP2}) compared to those yielded from Equation 4.1 with the optimal parameters shown in Table 4.1 (ΔE_{FIT}).

The plot shows that the *n*-pentane/silcalite–1 potential reproduced the *ab initio* data very well, especially for the low energy configurations that would frequently appear during MD simulations.

A comparison between the *ab initio* calculated energies and those from the model for the *n*-pentane/silicalite–1 potential energy in the configurations where the *n*-pentane molecule lied at the center of the fragment (Figure 3.2) and moved along the $\pm x$ direction approaching the inner surface of the wall was shown in Figure 4.3, where the $\pm$ distances correspond to those along $\pm x$ axes. The same plots for methane molecule were also given for comparison.
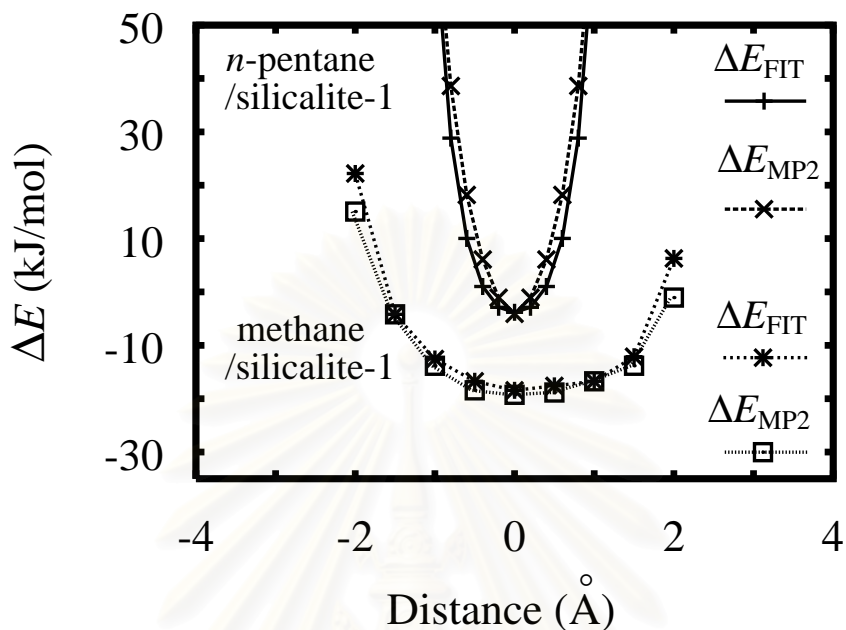
Figure 4.3 Interaction potential energies (ΔE) for the n-pentane/silicalite–1 obtained from the *ab initio* calculations at the MP2 level with the extended 6-31G(d) basis sets (ΔE_{MP2}) and from the potential function (ΔE_{FIT}) according to Equation 4.1 where the n-pentane molecule lies in the configuration shown in Figure 3.2 and moves along the $\pm x$ axes to the inner surface of the silicalite–1. For methane/silicalite–1, the ΔE_{MP2} and ΔE_{FIT} were defined in a similar manner.

Good agreement between the two curves confirmed the reliability and quality of the fitted potential. Rapid increase of the interaction energy indicated strong repulsion between n-pentane and the inner wall of the silicalite–1. This is in contrast to what takes place for methane molecules as well as water (data not shown) in the pore of silicalite–1 [17, 77].

4.4 n-Pentane/n-Pentane Intermolecular Potential

As mentioned above, the most simple species of hydrocarbon series, *e.g.*, methane, was investigated as a guest in zeolite silicalite–1 by Bussai *et. al.* Considering from a success of Bussai's work [14, 17, 78], the same method and basis sets 6-31G(d) used for methane was chosen and applied for the n-pentane/n-pentane. The functional form used is the same as that of n-pentane/silicalite–1 potential (Equation 4.1).

The final values for the n-pentane/n-pentane were summarized in Table 4.2.

Table 4.2 *Ab initio* fitted potential parameters for the n-pentane/n-pentane intermolecular potential as the functional form shown in Equation 4.1.

Sort	Parameters		
	A(kJ·Å^6/mol)	B(kJ·Å^{12}/mol)	C(kJ·Å^4/mol)
CH$_3$-CH$_3$	-5.719·10^3	3.956·10^7	0.0
CH$_3$-CH$_2$	-9.904·10^3	3.568·10^7	0.0
CH$_2$-CH$_2$	-3.856·10^3	2.828·10^6	0.0

Interestingly, the r^{-4} terms become zero for all pairs. The function, then, becomes a simple 12-6 Lennard-Jones form.

Quality of the fitted function in reproducing the *ab initio* data was first examined by the three trajectories as given in Figure 4.4.
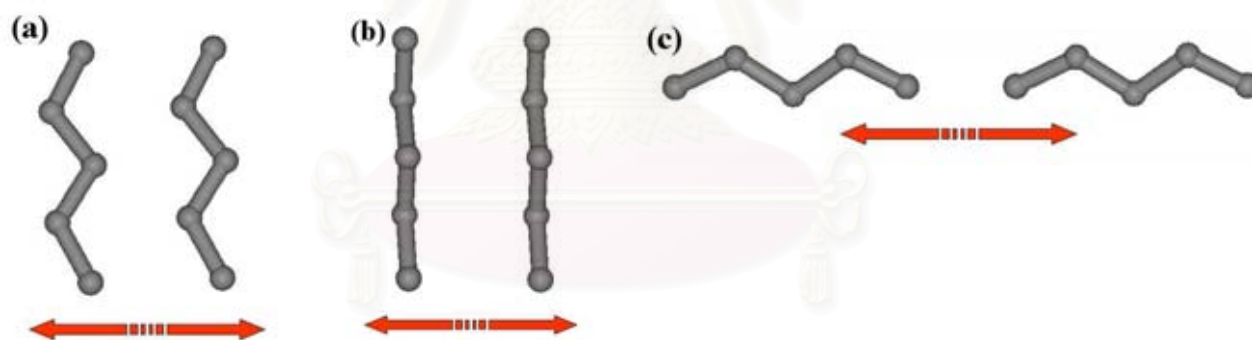
Figure 4.4 Orientations of the n-pentane dimer used in testing the quality of the fitted functions.

The corresponding values calculated from the 3 empirical force fields [79, 80, 81] were also given for comparison. The plot were displayed in Figure 4.5

According to the three sampling potential curves, our fitted potential function yields no better reproducing *ab initio* data than the other 3 force fields taken from the literatures. The all data comparison was also shown in Figure 4.6.
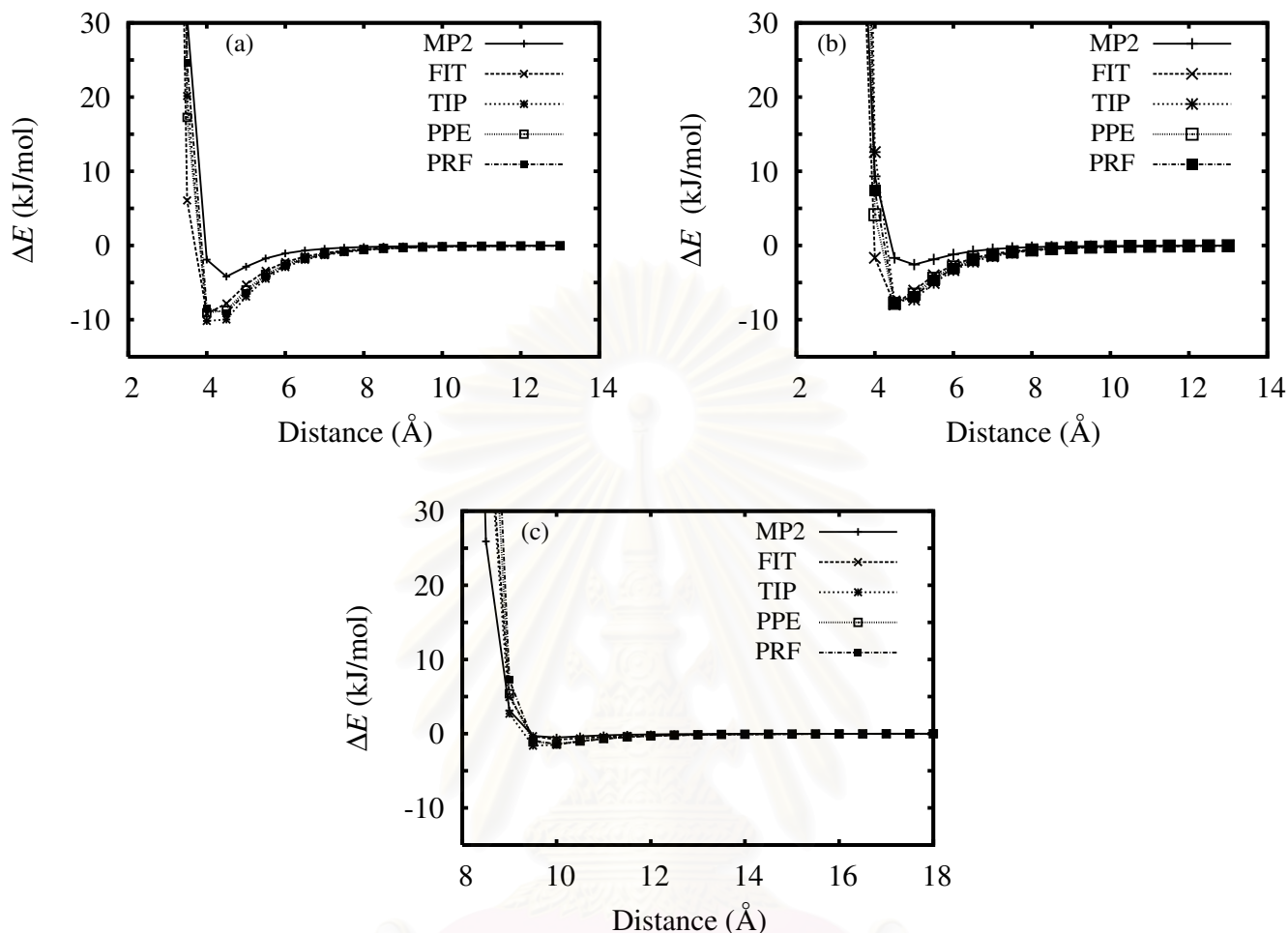
Figure 4.5 Potential curves arising from moving n-pentane molecules in the configurations shown in Figure 4.4. The distance between pentane dimer was measured from center of mass of each pentane. MP2: 2nd-order Møller-Plesset Perturbation; FIT: fitted potentials(This study); TIP: Transferable Intermolecular Potentials [79]; PPE or TraPPE-UA: Transferable Potentials for Phase Equilibria United-Atom [81]; PRF: Poncela-Rubio-Freire (Authors'names) [80].

Some remarks should be noted here on the three force fields taken from the literatures. Three sampling forces fields, TIP, PPE and PRF were parametrized to reproduce specific properties. The first one, TIP potential, was developed to determine densities and heat of vaporization with 2% deviation for 15 liquid hydrocarbons including alkane, branced alkane, alkene, and benzene. The second one, PPE, aims to develop as transferable potentials for phase equilibrium. The PPE potential reproduced experimental saturated vapor pressures
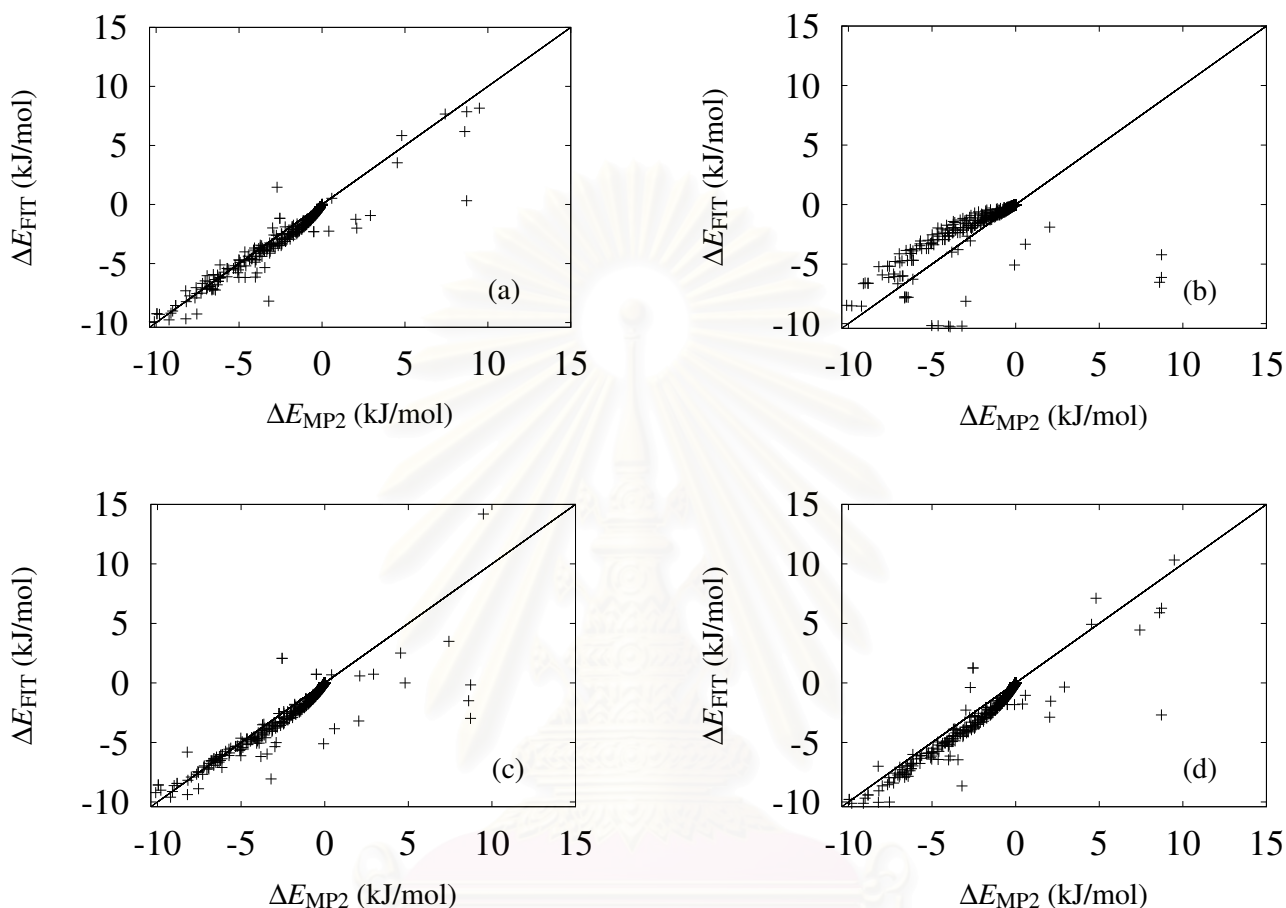
Figure 4.6 Correlation between potential energy values from the n-pentane/n-pentane interaction calculated using *ab initio* method (ΔE_{MP2}) compared to those yielded form Equation 4.1 (ΔE_{FIT}) with (a) the optimal parameters shown in Table 4.2; (b) TIP potentials; (c) PPE potentials and (d) PRF potentials.

and densities, but overpredicted the critical temperature of the large branched alkanes. For the PRF potential, it was developed to reproduce adequately the virial coefficient data of linear and branched molecules. Though, these force fields were expressed in microscopic term. They were fitted from macroscopic properties. All of them were parametrized by varying collision parameters and well depth until results from Monte Carlo (MC) simulations reproduce the experimental ones. In Figure 4.6, it was obvious that good agreement between

two sources of the energy was yielded, especially in the attractive region ($\Delta E < 0$). Among the three force fields taken, all, except for TIP, fits to the correlation line.

4.5   Validation of *Ab Initio* Fitted Potential

On one hand, discrepancy of the unbalance of the ratio of the atomic pairs in the molecular pair interaction is usually exhibited through the dynamic and thermodynamic properties and is still in debated. On the other hand, calibrating the potential function with the experimental diffusion is complicated by large discrepancies between microscopic and macroscopic measurement methods. The same measurement technique, there are many disagreements between the results reported by different recent groups [36]. While adsorption results seem to be well established and provide a more solid basis for a detailed comparison between experiment and simulation. Moreover, a large amount of data exists on adsorption of hydrocarbons in siliceous zeolites [10, 36]. Therefore, the fitted potential function was chosen to calibrate with the experimental zero-coverage heat of adsorption (Q_{st}).

The functions were applied to the MD program. Simulations was carried out and the trajectories were collected after equilibration. The Q_{st} was calculated and the value of -45.78 kJ/mol was yielded. It is clear that the negative value of the Q_{st} is not possible. The error can, surely, arise from only the n-pentane/silicalite–1 potential function since the Q_{st} was calculated at zero coverage of guest molecules, *i.e.*, there is no guest/guest interaction. To examine the ratio of the CH_3-O and CH_2-O atomic pairs in the total n-pentane/silicalite–1 potential pair, calculations were performed and the results were plotted in Figure 4.7. Figure 4.7 gives the information opposing the remark *ii* in Section 4.1 and indicates an unbalance of the atomic pairs.

The fitted potential function can reproduce the *ab initio* data very well (Figures 4.2 and 4.3). But, in Figure 4.7, no attractive part takes place on the CH_2-O curve. When the CH_2-O distance gets larger, the potential energy decays to zero rapidly. This also means that CH_2 groups would move through the silicalite–1 channel under the constraint due to repulsive force from the channel.
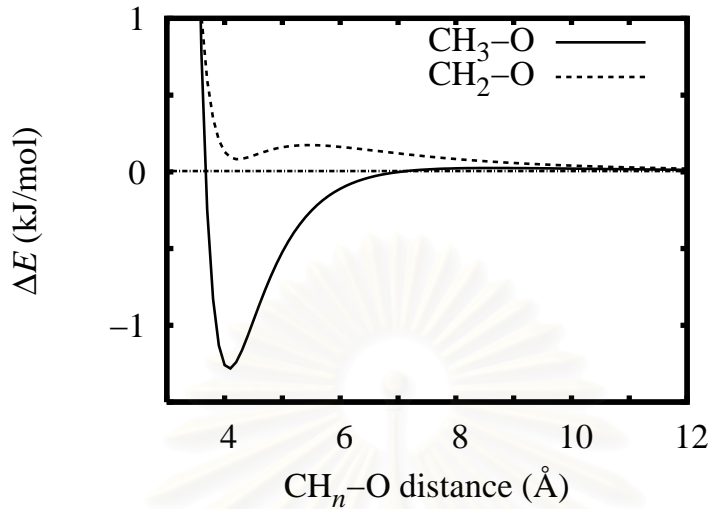
Figure 4.7 Potential energies with respect to CH_3-O (solid line) and CH_2-O distances (dash line).

Therefore, it was necessary to refit the n-pentane/silicalite–1 potential function. Note that, the parameters A and B of CH_2-O pair are about half of those of the CH_3-O while C_{CH_2-O} is a bit larger than C_{CH_3-O} (Table 4.1). This could be source of the repulsive contribution. Then, this term was removed from the functional form.

4.6 The 1st Revision of the n-Pentane/Silicalite–1 Potential: Removing C/r^4

Omitting terms C_{CH_n-O} (see Equation 3.1), the optimized parameters of the 1st refitted potential function representing the n-pentane/silicalite–1 interaction were given in Table 4.3. The atomic pairs were plotted separately in Figure 4.8 where the force-field function taken from Reference [9] was also given for comparison.

Comparison between correspondence pairs, the 1st refitted potential function gives the minimum energies at larger distances than the force-field does. A minimum energy for the CH_3-O pair of the *ab initio* potential of -0.64 kJ/mol is 0.13 kJ/mol higher than that of the force-field potential. The corresponding value for the *ab initio* CH_2-O is 0.35 kJ/mol higher than that of the CH_3-O. Though, all the atomic pair potentials decays to zero at about the

Table 4.3 *Ab initio* fitted potential parameters for the *n*-pentane/silicalite–1 intermolecular potential in the form of $A/r^6 + B/r^{12}$.

Sort	Parameters	
	$A(\text{kJ}\cdot\text{Å}^6/\text{mol})$	$B(\text{kJ}\cdot\text{Å}^{12}/\text{mol})$
CH_3-O	$-7.584\cdot10^3$	$2.231\cdot10^7$
CH_2-O	$-2.575\cdot10^3$	$1.084\cdot10^7$
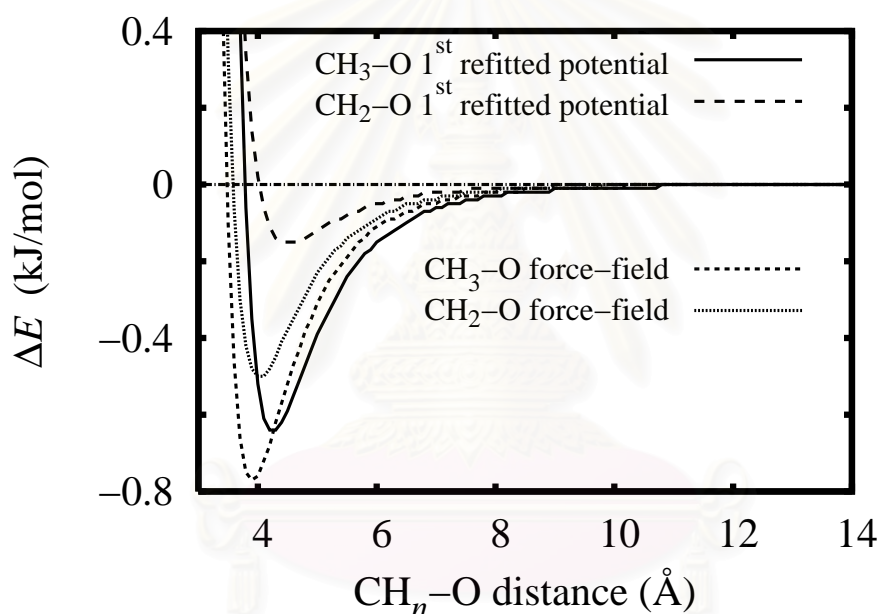
Figure 4.8 Pair potential energy with respect to CH_n-O distance belonging to the 1st refitted potential function and empirical force field [9].

same distance (about 10 Å). The atomic pair potentials of the fitted potential, especially CH_2-O pair, become repulsive faster than those of the force field. Collision distances of the fitted potential are 3.79 and 4.02 Å for CH_3-O and CH_2-O pairs whereas those of the force field is 3.48 and 3.58 Å for, respectively.

The calculated Q_{st} obtained from this refitted function is 31.6 kJ/mol. This value deviates from the experimental result of 57.7 kJ/mol [82] by 45.23%. It is known that

quality of the *ab initio* data points depends directly on the level of theory and the basis sets used. As the minimum of the *ab initio* energy (Figure 4.8) is almost 70% higher than that obtained from the force field. Therefore, quality of data points were, then, examined. The *ab initio* data with the same method (MP2) but larger basis set, changing from 6-31G(d) to 6-31+G(d,p), leads to significantly lower energies. Here, it was decided to recalculate all data points. Note that at the beginning of the project, computer facility could not effort the use of MP2(FC)/6-31+G(d,p) for the investigated system size.

4.7 The 2nd Revision of the *n*-Pentane/Silicalite–1 Potential: Recalculation using MP2(FC)/6-31+G(d,p)

With the MP2 method that was approved to well represent of the dispersion force for the hydrocarbon/zeolite system [15, 83], calculations were performed by varying the basis sets used. The results were summarized in Table 4.4.

Table 4.4   The obtained interaction energy and CPU time needed to perform *ab initio* calculations at MP2 level with different basis sets (Computing Center, University of Leipzig).

Method	Interaction energy (kJ/mol)	CPU time (Hrs)
MP2/6-31G(d)	-38.80	
MP2/6-31G(d)(BSSE)	-7.55	4.56
MP2(FC)/6-31G(d)(BSSE)	-7.55	3.26
MP2(FC)/6-31G(d,p)(BSSE)	-9.94	7.55
MP2(FC)/6-31+G(d)(BSSE)	-14.11	14.49
MP2(FC)/6-31+G(d,p)(BSSE)	-16.53	24.02
MP2(FC)/6-31++G(d,p)(BSSE)	-17.02	30.10

FC stands for frozen core in which only valence orbitals are involved in correlation calculations.

As the results, some conclusions could be made: (*i*) there is no significant difference between the energies obtained from the MP2 and MP2(FC). (*ii*) As expected, the energy

becomes lower as the basis sets is larger. (*iii*) The MP2(FC)/6-31+G(d,p)(BSSE) and MP2(FC)/6-31++G(d,p)(BSSE) give almost the same values of interaction data but the second one consumed much CPU time. In addition the energy difference among two methods of 0.49 kJ/mol is within the thermal fluctuation as the simulations were carried out at the temperature range between 200 and 350 K. Therefore, the MP2(FC)/6-31+G(d,p)(BSSE) was chosen to be used to generate the energies. The same fitting procedure and number of data points were used. The parameters of the 2nd refitted potential function were listed in Table 4.5.

Table 4.5 The potential parameters for the *n*-pentane/silicalite–1 intermolecular potential in the form of $A/r^6 + B/r^{12}$ where the ab initio energies were calculated using the MP2(FC)/6-31+G(d,p)(BSSE).

Sort	Parameters	
	A(kJ·Å^6/mol)	B(kJ·Å^{12}/mol)
CH$_3$-O	-4.292·10^3	1.129·10^7
CH$_2$-O	-5.976·10^3	1.555·10^7

To control physical meaning of the function, positive for r^{-12} and negative for r^{-6} terms, the energy points of higher than 10 kJ/mol were excluded from the fit. The correlation plot which indicates the quality of the potential function to reproduce the *ab initio* data was shown in Figure 4.9. For the low energy region, the fitted energies reproduce to the *ab initio* data nicely.

This function was, then, applied for the MD simulation with 1 *n*-pentane molecule in the system. The Q_{st} was evaluated and the value of 49.79 kJ/mol was obtained. This is 13.71% deviated from the experimental value. However, regarding the details of the simulation technique, it was found that the shifted force-potential technique (Equation 2.104) which is used to smooth the function at cut-off radius (r_C) cause higher energy than that of the original function. The difference of the potential energy between shifted and original
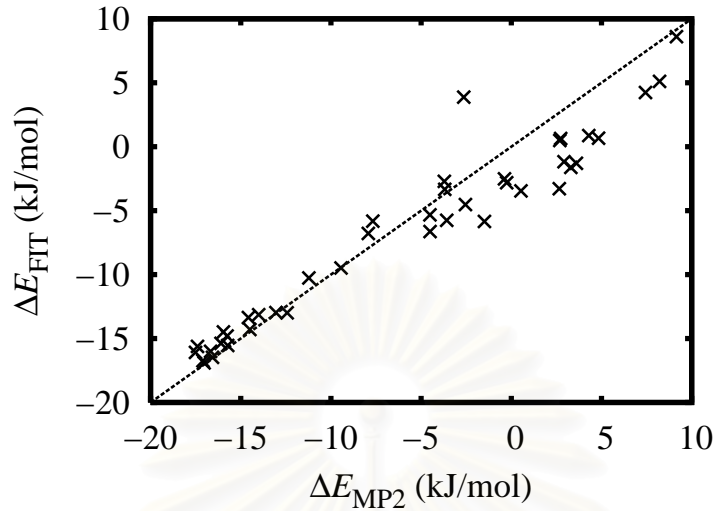
Figure 4.9   The correlation between potential energy values arising from the *n*-pentane/silicalite–1 interaction calculated from *ab initio* method (ΔE_{MP2}) and those yielded from the 2$^{\text{nd}}$ refitted potential function (ΔE_{FIT}).

potentials at a certain distance, thus, would depend on the r_{C}. Practically, calculations of the Q_{st} at infinite r_{C} could not be performed. The real (if known) Q_{st}, thus, would be possible to be estimated by extrapolating the heat of adsorption at different cutoff radius ($Q_{\text{st}}(r_{\text{C}})$). Here, MD simulations were carried out for the loading of 0.5 molecules per unit cell at r_{C} of 12, 14, 16, 18 and 20 Å. The MD box is larger than two times of the maximum r_{C} ($2 \times 2 \times 2$ unit cells). The obtained Q_{st} at $r_{\text{C}} = 12, 14, 16, 18$ and 20 Å are 50.54, 53.76, 55.68, 56.51 and 56.59 kJ/mol, respectively. It can clearly be seen that the calculated Q_{st} is very sensitive against the choice of the r_{C}. This sensitivity is, of course, a general feature of Lennard-Jones type potentials used to describe the Q_{st} of *n*-pentane in silicalite–1 and is not related to the parameter set proposed in this study. Nevertheless, this effect is not taken into account by many other articles, *e.g.* [9, 10, 45, 84, 85, 86, 87, 88]. As the system size is restricted by computational possibilities it was decided to estimate the limiting value by fitting the results for 5 different r_{C} to a decay law.

The decay law used to fit the Q_{st} at different r_{C} can be written as:

$$Q_{st}(r_C) = Q_{st}^{\infty} \left[1 - \frac{\alpha}{r_C^{\beta}} \right]. \qquad\qquad [4.2]$$

where Q_{st}^{∞} is the estimated heat of adsorption at infinite r_C. α and β are fitting constants. Figure 4.10 displays fitted values according to Equation 4.2 compared to those reported Q_{st} obtained from simulations at different r_C. The obtained Q_{st}^{∞} of 58.93 kJ/mol is excellently agreed with the experiment value of 57.7 kJ/mol [82] by 2.13% error.
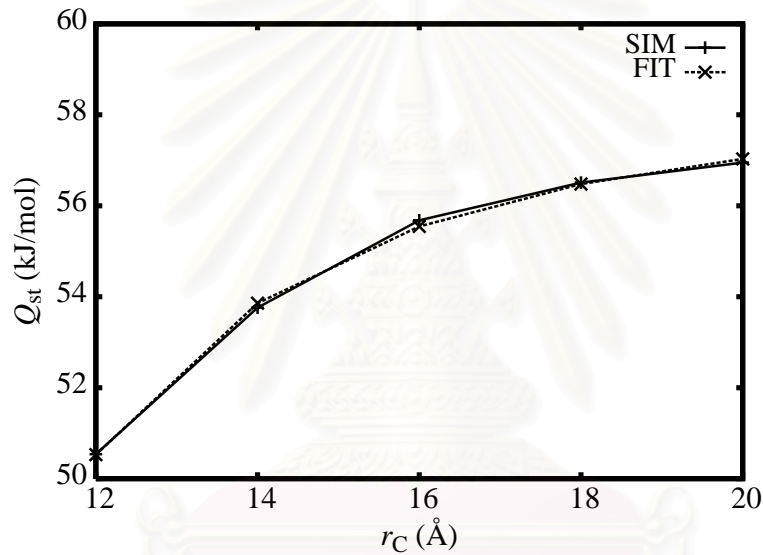
Figure 4.10 Dependency of heat of adsorption on cut-off radius from MD simulations (SIM) and fitting simulation results to Equation 4.2 (FIT) where $\alpha = 1295.29$ and $\beta = 3.7$.

The agreement between the Q_{st} yielded from MD simulations and those fitted by Equation 4.2 (Figure 4.10) confirms the fit for the interval which is accessible.

Diffusion coefficients at the two loadings (4 and 8 molecules per unit cell) were given in Table 4.6 in comparison with the experimental observations. It can be seen that comparable D_s of 7.52×10^{-10} and 6.99×10^{-10} m^2/s for MPC=4 and 8 are not reasonable, i.e., at high loading, the D_s is expected to decrease. This is in contrast to those found from an empirical force field as well as from the PFG-NMR measurements.

Table 4.6 Self diffusion coefficients (D_s) from MD simulations applying 2nd refitted potential and the force filed in Reference [9].

potential	D_s (10^{-10} m^2/s)	
	4 MPC at 330 K	8 MPC at 298 K
2nd refitted	7.52	6.99
force field [9]	8.98	2.20
PFG-NMR	3.90[89]	0.41[90]

MPC=molecules per unit cell.

Source of discrepancy can be, of course, due to the potential function used. The main difference between the *ab initio* and the force-field functions still remain, especially at the repulsive region where the function approaches zero for the first time (see Figure 4.11), the collision diameter. The collision diameters of this function are 3.71 Å for both CH$_3$-O and CH$_2$-O pairs which is smaller than those of the 2nd refitted potential function, but still larger than those of the force field.

To examine this, the function was, then, refitted by keeping the collision diameter fixes.

4.8 The 3rd Revision of the *n*-Pentane/Silicalite–1 Potential: Fixing σ

The final values of the parameters were given in Table 4.7. The collision parameters (σ) used to fix for CH$_3$-O and CH$_2$-O pairs were taken from values proposed by Dubbeldam [9].

To examine effect of the σ for the guest/guest interaction, the *n*-pentane/*n*-pentane function was also refitted. The σ parameters for the CH$_2$ and CH$_3$ groups for guest/guest interaction are in the range 3.76-4.00 Å [79, 80, 81]. Variation was done manually and the values of 4.00, 3.85 and 4.00 Å for CH$_3$-CH$_3$, CH$_3$-CH$_2$ and CH$_2$-CH$_2$ pairs were found to yield the

Figure 4.11 Pair potential energy with respect to CH_n-O distance belonging to the 2nd refitted potential function and empirical force field [9]

Table 4.7 The 3rd refitted potential parameters for the (a) n-pentane/silicalite–1 and (b) n-pentane/n-pentane intermolecular potential in the form of 12-6 Lennard-Jones potentials (Equation 2.99) where collision parameter, σ, were kept fix.

	Sort	Parameters	
		σ_{Fix} (Å)	ϵ(K)
(a) Guest/Host	CH_3-O	3.48*	61.53
	CH_2-O	3.58*	58.18
(b) Guest/Guest	CH_3-CH_3	4.00**	42.51
	CH_3-CH_2	3.85**	14.59
	CH_2-CH_2	4.00**	32.99

* from Reference [9]; ** from Reference [79, 80, 81] and manually adjusted.

best numerical fitting. The ΔE_{FIT} and ΔE_{MP2} for both systems were compared in Figure 4.12.
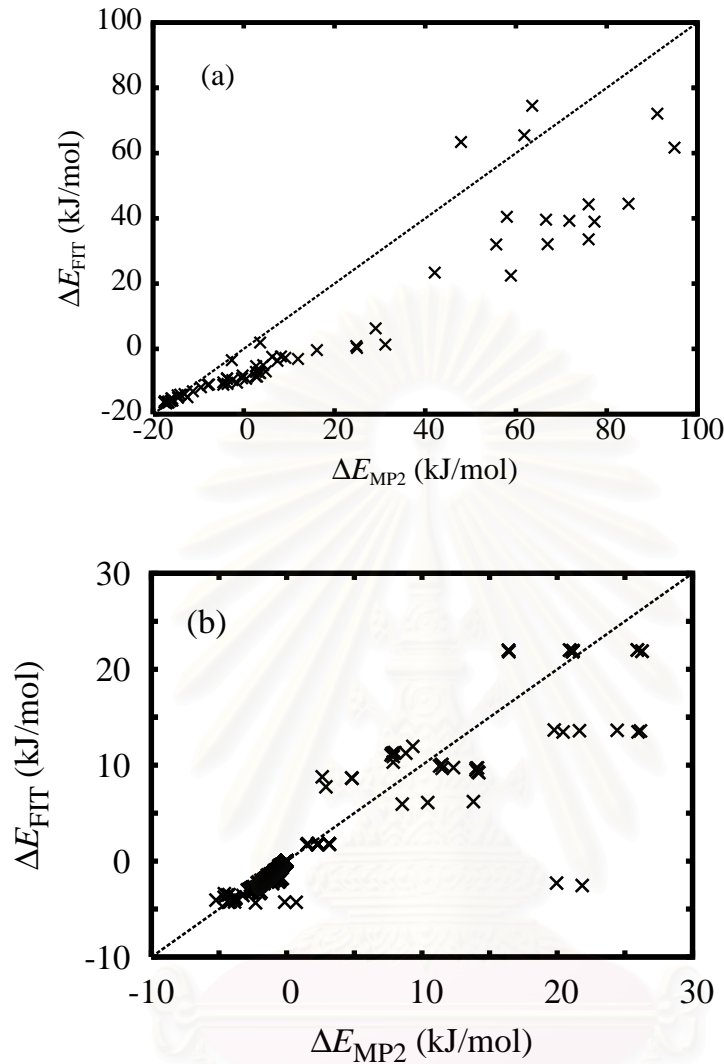
Figure 4.12 The correlation between potential energy values arising from the interaction calculated from *ab initio* method (ΔE_{MP2}) compared to those yielded from the 3$^{\mathrm{rd}}$ refitted potential function (ΔE_{FIT}): (a) *n*-pentane/silicalite–1 (b) *n*-pentane/*n*-pentane.

Though, less variables in the fitting procedure cause the fitted energies deviate from the *ab initio* energies. The fitted energies reproduce to the *ab initio* data satisfactorily for the low energy region.

With the fix σ parameters, simulations were performed. The Q_{st} and D_{s} were calculated and given in Table 4.8. Simulations were also performed using Dubbeldam's parameters. The Q_{st} and D_{s} were also given in Table 4.8.

Table 4.8 Diffusion coefficients (D_s) at the 2 loadings (4 and 8 MPC) and zero coverage heat of adsorption (Q_{st}) from MD simulations applying 3rd refitted potentials where "Free" and "Fix" represent the guest/guest.

GH	GG	$D_s(10^{-10}$ m^2/s)		Q_{st} (kJ/mol)
		4 MPC	8 MPC	
3rd fitted potential	Free	8.03	7.68	52.28
3rd fitted potential	Fix	11.03	4.26	52.28
Dubbeldam's potential [9]		8.98	2.20	50.21
PFG-NMR		3.90 [89]	0.41 [90]	-
Pulse-Chromatography		-	-	57.7 [82]

GH denotes n-pentane/silcalite-1 fitted potential. GG represents n-pentane/n-pentane.

With the same extrapolation process used in Section 4.7, five MD simulations with the cut-off radius of 12, 14, 16, 18 and 20 Å were performed. The extrapolated Q_{st} is 52.28 kJ/mol, 9.39% lower than the experimental value. The Q_{st} data in Dubbeldam's paper is 1% less than the experimental one. However, we have performed the MD simulations using both intra- and intermolecular potentials reported in their paper. The obtained Q_{st} of 50.21 kJ/mol is 12.98% error. The difference might be from technical details that the authors did not reveal.

In terms of the concentration dependence of the self diffusion coefficient, guest/host and guest/guest intermolecular potentials with fix collision diameters yield qualitatively results as the D_s get smaller with the higher concentrations. Though, the error in Q_{st} produced in this σ-fix potential function is larger than that of the 2nd refitted function. The Q_{st} is yet in the acceptable range and the qualitative D_s can be obtained. Therefore, the 3rd would be best one and were used to determine the structural data with variation of loading of guest molecule and temperature.

By taking σ from Dubbeldam's force field, this potential function and the force field have one more common characteristic. That is the position of minimum energies of correspondence pairs are equal (See Figure 4.13). Unlike the CH_2-O pairs, the minimum CH_3-O pair energy of this potential is as -0.3 kJ/mol as higher than that of the force field.
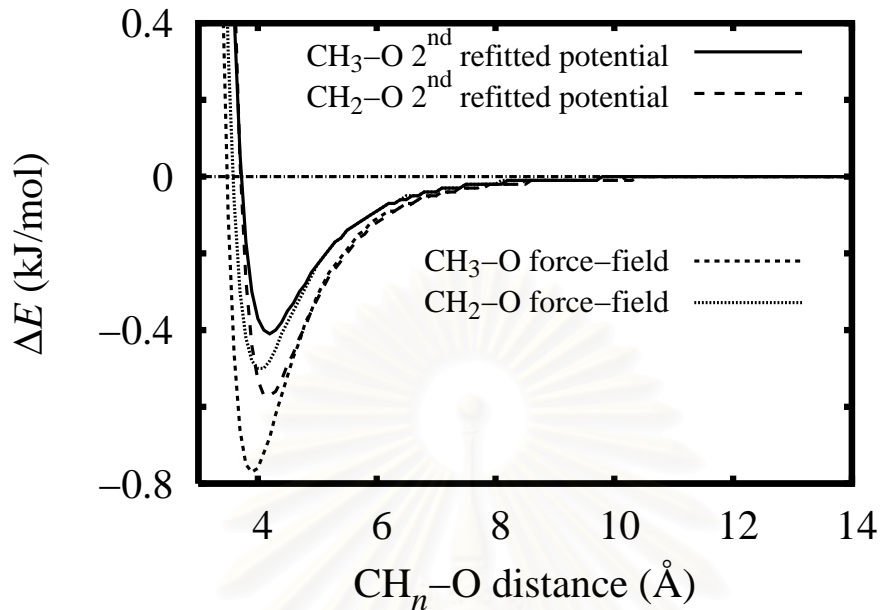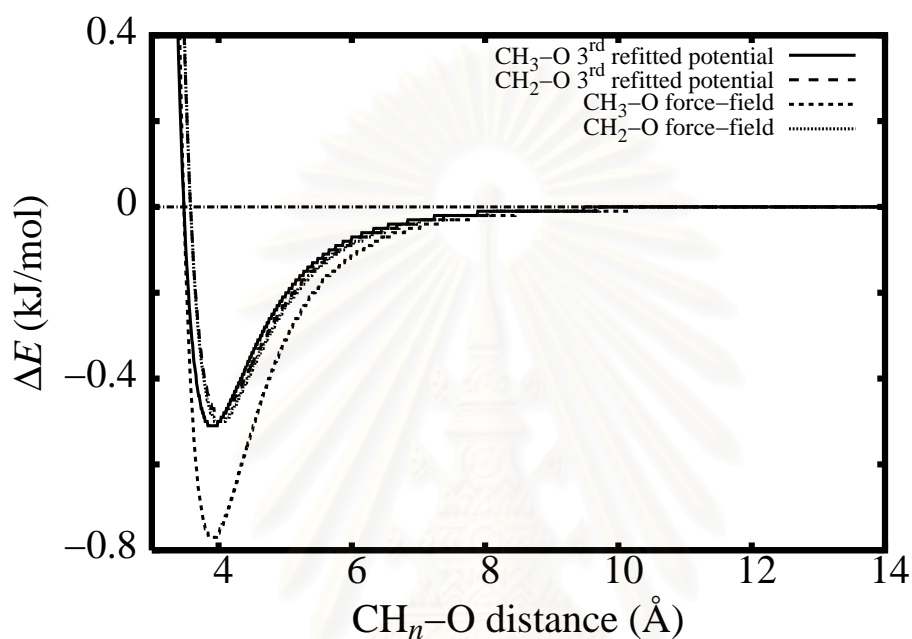

Figure 4.13 Pair potential energy with respect to CH_n-O distance belonging to the 3rd refitted potential function and empirical force field [9]

There could be some differences in molecular properties. Thus, comparison of structural properties belonging to the 3rd refitted function and Dubbeldam's force field is also available.

CHAPTER V

RESULTS AND DISCUSSIONS: MOLECULAR PROPERTIES AS A FUNCTION OF LOADING AND TEMPERATURE

The 3rd refitted functions for n-pentane/silicalite–1 and n-pentane/n-pentane with constant σ from Chapter IV were applied to study structure and dynamic properties of the system. Changes of these properties as a function of temperatures and loading were respectively investigated.

5.1 Temperature Dependence of the Molecular Properties

In order to monitor how diffusing molecules distribute in the channels of silicalite–1, the positions of center of mass of guest molecules in the sinusoidal and straight channels were registered during the simulations. However, arranging the registered positions with general radial distribution function (RDF) is not sufficient to describe the distribution of the guest molecule along the channels (See Subsection 2.5.4 for details of the RDF calculation). Because of anisotropic effect introduced by the silicalite–1, RDF would give neither qualitative nor quantitative picture. The number density at each distance r would be the summation overall the atoms found at this distance, even, they might align along different channels. However, a general concept of RDF to arrange data into small intervals is useful. To facilitate the numerical evaluation in this study, channel intersection was considered as part of straight channel. Thus, the probability around the intersection would not appear along the sinusoidal channel. The reference positions which have been defined to be 0.0 Å is the center of intersection (see Figure 3.1a where positions of the centers of intersection are $b/4$ and $3b/4$ along y-axis). For straight channel, instead of starting at a certain atom and find out neighbor atoms radially, residence probability along silicalite–1 channels can be performed by separating channels into several very short cylinders and registering the position of guest molecule in each cylinder. The temperature effect on the dilute pentane in silicalite–1 in the term of the residence distribution are presented in Figure 5.1.
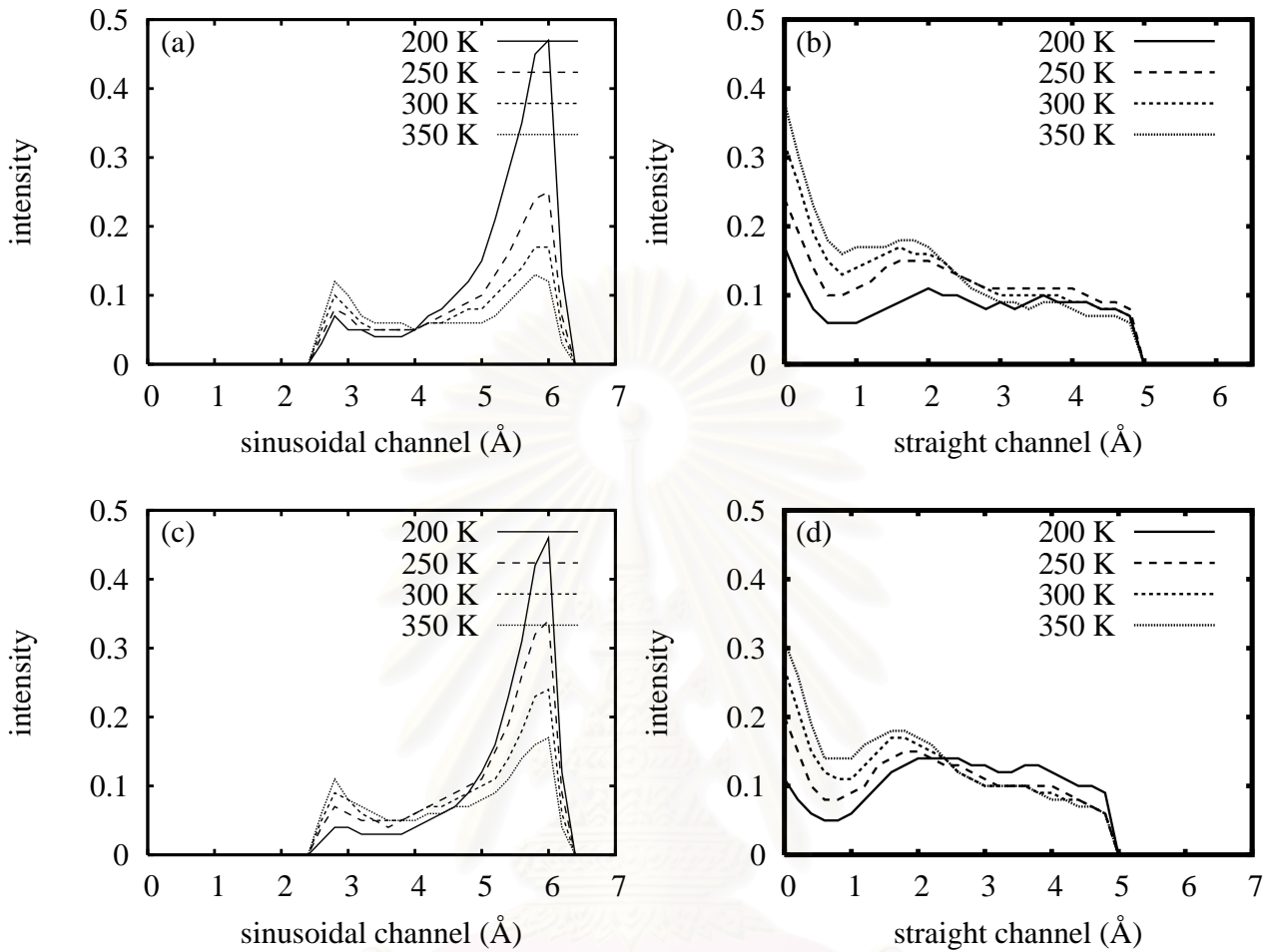
Figure 5.1 Residence probability for very low loading of the n-pentane molecule in silicalite–1 at 200-350 K: (a)-(b) 3$^{\text{rd}}$ refitted potential function, (c)-(d) Dubbeldam's force field.

Some characteristics of the residence probabilities can be concluded as follows: (i) At low temperature, $e.g.$, 200 K, a high peak at 6 Å in either Figures 5.1a or 5.1c indicates the most preferential site is around the middle of sinusoidal channel. (ii) The probability at this position decreases when temperature increases. Increment of temperature from 200 K to 250 K, decreases the peak height dramatically while it looks decrease monotonically from 200-350 K for Dubbeldam's potential. (iii) Though, obvious change in residence probability along the sinusoidal channel can be detected as change in area under the curve from around the distance 4-6.5 Å (see Figure Figures 5.1a and 5.1c). The change in residence probability along the straight channel can be noticed from 0-3.0 Å for our function (Figure 5.1b) and

from 0-2.5 Å for Dubbeldam's force field (Figure 5.1d). There appears no significant change at larger distance. (iv) Therefore, higher the temperature is, more frequency the molecule moves toward the channel intersection. The reason for more migration of the molecule toward the intersection when the temperature increases was firstly determined by average potential along the channel as given in Figure 5.2.
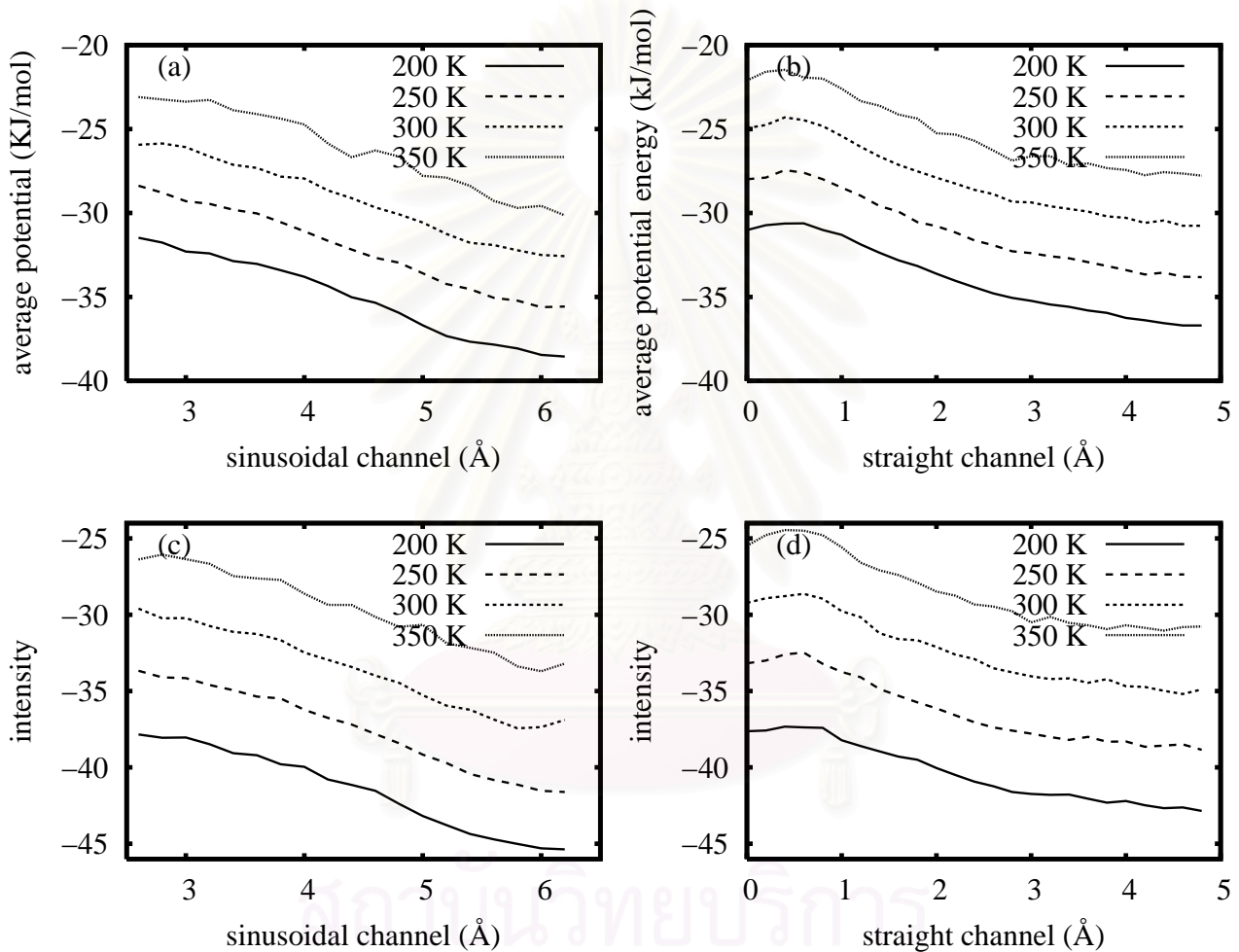
Figure 5.2   Average potential energy of the n-pentane molecule for zero loading of the n-pentane molecule in silicalite–1 at 200-350 K: (a)-(b) our refitted potential function, (c)-(d) Dubbeldam's force field.

Patterns of average potential surfaces along either sinusoidal or straight channel are very similar for both our and Dubbeldam's potentials. That is the potential energy increases

gradually from around the middle of the channel to the intersection. The effect of temperature just is to shift the potential surface to higher potential energy. Since the change in residence probability depends on to temperature directly. It was assumed that the kinetic energy cause the migration of the guest molecule by increasing internal or tumble movement. Upon this assumption, temperature-independent probabilities along the sinusoidal at the distance less than 4 Å and the straight channel at distance larger than 3.0 Å for our potential and 2.5 Å for Dubbeldam's potential can be explained as follows: (i) When the temperature decreases, the molecule would have lower internal and/or tumble movement, then, the potential plays a stronger role. The molecule, then, moves to the lower potential region. Sinusoidal channel whose shape is more curvious than straight channel obstructs the molecule to move out from the channel when it reaches to around the center of the channel. Then, the molecule spends more time in the region. In contrast, the straight channel's topology lets the molecule move toward/backward the intersection easier. There's more competition between molecular movement and potential field exerted by host for the distribution in this region. Even, the lowest temperature in the study (200 K), it does not show up higher residence probability at around the middle of the channel (at distance of about 5 Å). (ii) When the temperature increases, the molecule would have higher internal and/or tumble movement. The molecule would prefer to move in the channel intersection because it has more space or less confinement than in the channel. When the molecule in the sinusoidal channel arrives the region of about 2.7-4.0 Å, they would hop to the intersection easily.

As it has been assumed that the temperature effects the residence probability by increasing or decreasing internal and/or tumble movement. Then, the next destination on structural determination is to figure out how much each kind of movement has influenced on the residence probability. There are 3 terms to represent the internal movement. These are bond stretching, bond bending and bond rotation. A net movement by these terms has been investigated in the term of the end-to-end length distribution. The end-to-end length stands for the length measured between two CH_3-groups of n-pentane molecule. While the tumble movement has been represented by distribution of angles that are formed from y-axis

and end-to-end vectors. Here, let's call this angle "end-to-end angle". Since the potential energy gradually increase from the middle of the channel to the intersection. It can not be partitioned the region energetically. Because of aiming to movement that is caused by the temperature, only configurations in the peak area with obvious change in Figure 5.1 were contributed into the end-to-end length and angle distributions. This covers the distance range 4-6.5 Å for sinusoidal channel and the range 0-3 Å for straight channel. Since there exists a node at about 1 Å along the straight channel. It was proposed to sub-partition this region. Therefore, 3 regions have been investigated for the movement of the molecule. Each region was, for simplicity named as follows: (i) Sinusoidal refers to distance along the sinusoidal channel between 4 and 6.5 Å. (ii) Inner-intersection and (iii) outer-intersection occupy distances along the straight channel between 0 and 1 Å and between 1 and 3 Å, respectively. Only the trajectories belonging to the lowest (200 K) and highest (350 K) temperatures were compared for the end-to-end length and angle distributions.

Some common characteristics found in the end-to-end length distribution in all regions (Figure 5.3) are: (i) Each area under the curve corresponds to that of residence probability. Comparison, thus, can be done qualitatively and quantitatively. (ii) There are 2 peaks in each region at both temperatures. The first one has a maximum at 4.5 Å and the second peak has the maximum at 5.1 Å. (iii) The end-to-end length of 5.1 Å corresponds to the n-pentane in elongated conformation. The other form which is shorter by up to 0.6 Å would correspond to the conformation which deviates from the elongated form by a bond rotation as a main contribution of internal movement. (iv) There is no significant difference between the distributions under both potential fields.

Starting at the sinusoidal region (Figures 5.3c and 5.3f), molecules, which arrive here, usually contribute the conformation with end-to-end length of 5.1 Å at low temperature. Instead of changing conformation, the molecule would spend more time in other regions when the temperature increases. Otherwise, the peak centered at 4.5 Å should increase to compensate the decrease of the end-to-end peak centered at 5.1 Å. While no significant reduction in the peak centered at 5.1 Å has been found in either the inner (Figures 5.3a and 5.3d) or outer intersections (Figures 5.3b and 5.3e) when the temperature increases. Instead,

the peaks in these two regions get boarder and their peak at 4.5 Å are, at least, 2-time higher than those at low temperature. This would mean that the inner and outer intersection let the molecule be more flexible or have less confinement than the sinusoidal does.

Tumble movement can be understood by the end-to-end angle distribution as given in Figure 5.4.

Characteristics of molecular orientation through the end-to-end angle distribution due to our and Dubbeldam's potentials are very similar. Therefore, the following discussions are true for both cases. (i) Maxima of the distribution take place at 10^0 and 90^0 which would correspond to the molecular alignment parallel to the straight and sinusoidal channel, respectively. (ii) Broadening the distribution by the temperature can be seen in both the inner (see Figures 5.4a and 5.4d) and outer intersections (see Figures 5.4b and 5.4e), but not in the sinusoidal region.

Like the end-to-end length distribution, tumble movement of the molecule is limited in the sinusoidal channels. As the results, the peak at 90^0 decreases when the temperature increases as the molecule would spend shorter time in this region (see Figures 5.4c and 5.4f). Unlike the sinusoidal region, the inner and outer intersections have more space which are large enough for tumble movement as evidenced by broadening the curve in Figures 5.4a, 5.4b, 5.4d, 5.4e when the temperature increases. It is assumed that, at high temperature, after the molecule escapes from the sinusoidal channel, it still retains memory where it was from or it still aligns parallel the sinusoidal channel. The assumption was confirmed by Figures 5.4a and 5.4c. The height of the peak at 10^0 is comparable to that at 90^0 at low temperature. The latter one becomes larger than the former at high temperature. This would be interpreted that part of the molecule might insert in the straight channel and the other part might stick out the channel intersection.

All the distributions presented have provided static pictures of the structural data. Dynamic details in this study were mentioned through the diffusion coefficient (D_s) and memory factor (β) as shown in Table 5.1 (See Subsection 2.5.3 for derivation of β).

According to Table 5.1, the following conclusions can be made: (i) All the diffusion components increase as a function of temperature. (ii) D_y is the fastest component for all

Table 5.1 Diffusion coefficients and memory factor at 200 and 350 K obtained from the MD simulation using our and Dubbeldam's potentials.

.

Potentials	T	Diffusion coefficient ($\times 10^{-9}$ m^2/s)				β
	(K)	D_x	D_y	D_z	D_s	
3$^{\mathrm{rd}}$ Refit	200	0.27 (0.73)	0.76 (2.06)	0.08 (0.22)	0.37	1.11
	350	1.27 (0.94)	2.48 (1.84)	0.29 (0.22)	1.35	1.26
Dubbeldam's	200	0.24 (0.49)	1.18 (2.41)	0.06 (0.12)	0.49	1.38
	350	1.10 (0.75)	3.03 (2.08)	0.23 (0.16)	1.46	1.55

Each number in parenthesis is a diffusion tensor along principle axis divided average value (D_s)

temperatures. This supports the residence probability data (Figure 5.1) that the molecule can move along the straight channel easier than the sinusoidal channels. (*iii*) Interestingly, along the sinusoidal channel, higher relative D_x has been detected when the residence probability decreases or temperature increases (Figures 5.1a and 5.1c). In contrast, higher residence probability along the straight channel at high temperature (Figures 5.1b and 5.1d), the lower relative D_y has been detected. Since the self diffusion relates directly to the molecular displacement per time unit. This would mean that the molecule would spend less time to stay in the region where the relative diffusion coefficient is higher. (*iv*) β are greater than 1 for both low and high temperatures. This indicates the molecule prefers to continue diffusing along the same channel type where it came from when it arrives the intersection. β and end-to-end angle distribution, thus, confirm each other. Although, the molecule shows tumble movement, this movement would hardly switch the molecule which aligns along one type of the channel to the other type of the channel. Otherwise, other peaks between two broad peaks could be detected in Figures 5.4a and 5.4d can be detected.

Till to now, the results are on very low loading of *n*-pentane. Next section, the structural investigation would include the contribution of higher loading of guest molecule.

5.2   *n*-Pentane Loading Dependence on the Molecular Properties

In this section, 3 different loadings of 0.5, 2 and 4 MPC were investigated. The loading of 4 MPC corresponds to the concentration that half of total channel space is occupied by *n*-pentane molecules. Since the distribution at low and high temperatures are different as discussed in previous section. 2 series categorized by temperature were performed in which each series containing 3 loadings. The residence distributions with various loadings of *n*-pentane at both low and high temperatures were given in Figure 5.5. Some conclusions are (*i*) Loading more guest molecule causes the residence intensity increase for all regions. (*ii*) Patterns of the distribution plots at higher loadings are very similar to that at low loading of 0.5 MPC as shown in Section 5.1. (*iii*) As we know from the previous section that, at low temperature (see Figures 5.5a and 5.5b), the field of the potential exerted by the zeolites plays more important role than the molecular movement and the potential in the channel is much lower than that in the intersection. Loading more guest molecules, then, lets the role of the potential to be more obvious because higher intensity can be observed around the middle of the channel (around 6 Å in Figure 5.5a). (*iv*) At high temperature (see Figures 5.5c and 5.5d), molecular movements play a stronger role. Increase in intensity of the residence distribution, thus, can be seen in the straight channel around 0-3 Å where molecular movement can occur easier than the other place.

Though, at high temperature, the intensity at 0 Å along the straight channel (see Figures 5.5a) increases, the maximum along the sinusoidal channel at about 6 Å (see Figure 5.5c) is still comparable.

The explanation of retaining high intensity of residence probability along sinusoidal channel was given through the change of relative self-diffusion coefficients.

The self-diffusion coefficients, their element along principle axes and memory factors at different loadings have been summarized in Table 5.2.

It can be seen in Table 5.2 that all components and D_s decrease when the loading increases. At 200 K, the relative D_y increases from 2.05 to 2.46 when the loading increases from 0.5 to 4.0 MPC. This is not a case for D_x. As the results, the *n*-pentane molecules relatively

Table 5.2 Diffusion coefficients and memory factor at different loadings at 200 and 350 K.

T(K)	Loading (MPC)	Diffusion coefficient ($\times 10^{-9}$ m^2/s)					β
		D_x	D_y	D_z	D_s		
200	0.5	0.27 (0.73)	0.76 (2.05)	0.08 (0.22)	0.37	1.11	
	2.0	0.20 (0.53)	0.93 (2.35)	0.06 (0.15)	0.40	1.24	
	4.0	0.12 (0.42)	0.71 (2.46)	0.36 (0.12)	0.29	1.29	
350	0.5	1.27 (0.94)	2.48 (1.84)	0.29 (0.22)	1.35	1.26	
	2.0	1.07 (0.92)	2.24 (1.93)	0.19 (0.16)	1.16	1.70	
	4.0	0.56 (0.71)	1.68 (2.14)	0.11 (0.14)	0.78	1.73	

Each number in parenthesis is a diffusion tensor along principle axis divided average value (D_s)

spend longer time in sinusoidal region than the other region. That is the reason why high intensity along the sinusoidal region was obtained.

At 350 K, of course, the same explanation can be used. As the relative D_y increases from 1.84 to 2.14, the relative D_x decreases from 0.94 to 0.71.

Table 5.2, all the loadings at both low and high temperatures yields the memories factors (β) that are greater than 1. Besides, the β is larger when the loading is higher. The molecules would retain the same behavior by keeping diffusing along the same channel type where they were before arriving the channel intersection.
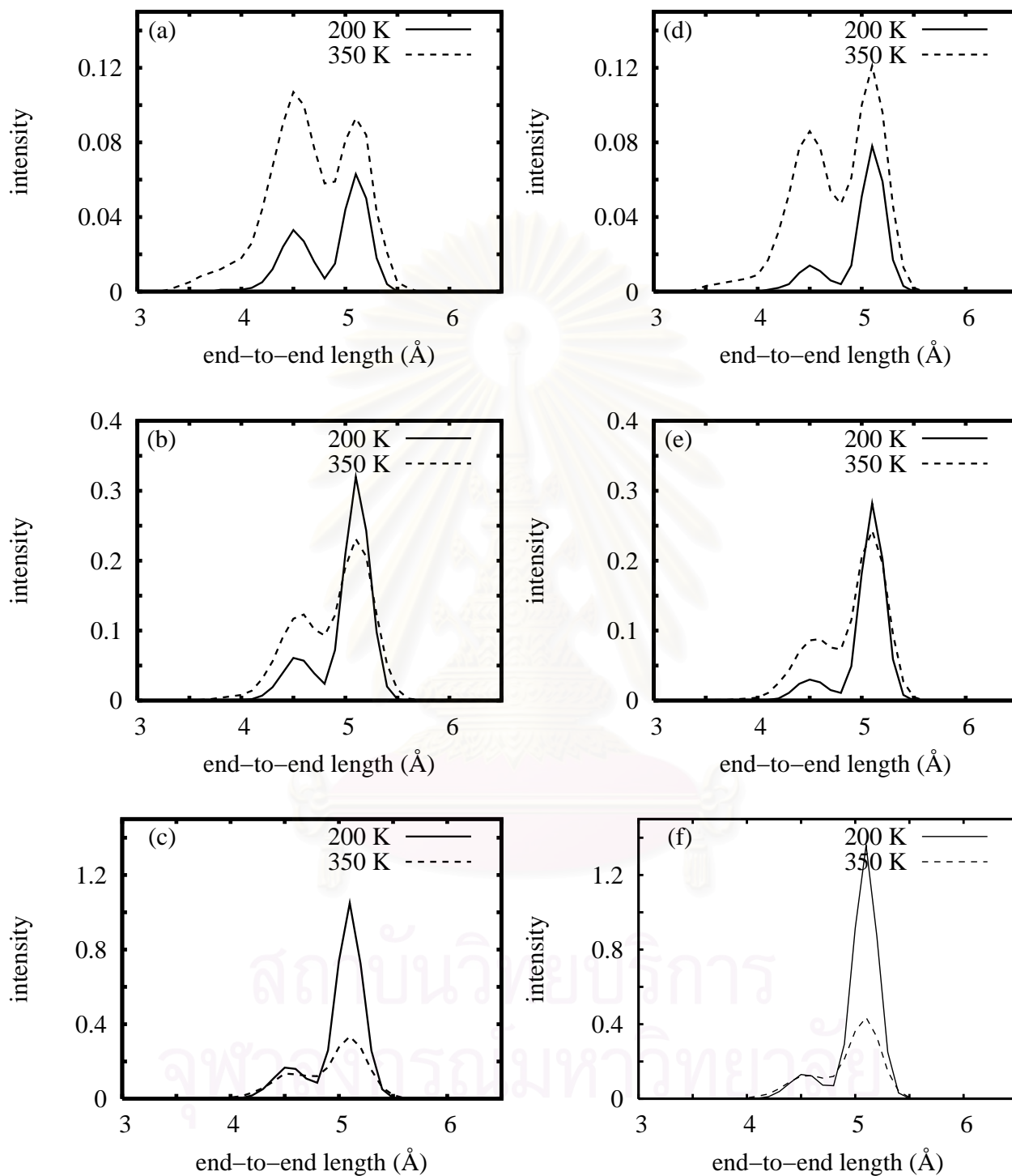
Figure 5.3 End-to-end length for very low loading of the n-pentane molecule in silicalite–1 at 200 and 350 K where (a)-(c) belong to 3rd refitted potential function, (d)-(f) belong to Dubbeldam's force field: (a) and (d) are inner intersections; (b) and (e) are outer intersections; (c) and (f) are sinusoidal regions.

Figure 5.4 End-to-end angle for very low loading of the n-pentane molecule in silicalite–1 at 200 and 350 K where (a)-(c) belong to 3rd refitted potential function, (d)-(f) belong to Dubbeldam's force field: (a) and (d) are inner intersections; (b) and (e) are outer intersections; (c) and (f) are sinusoidal regions.
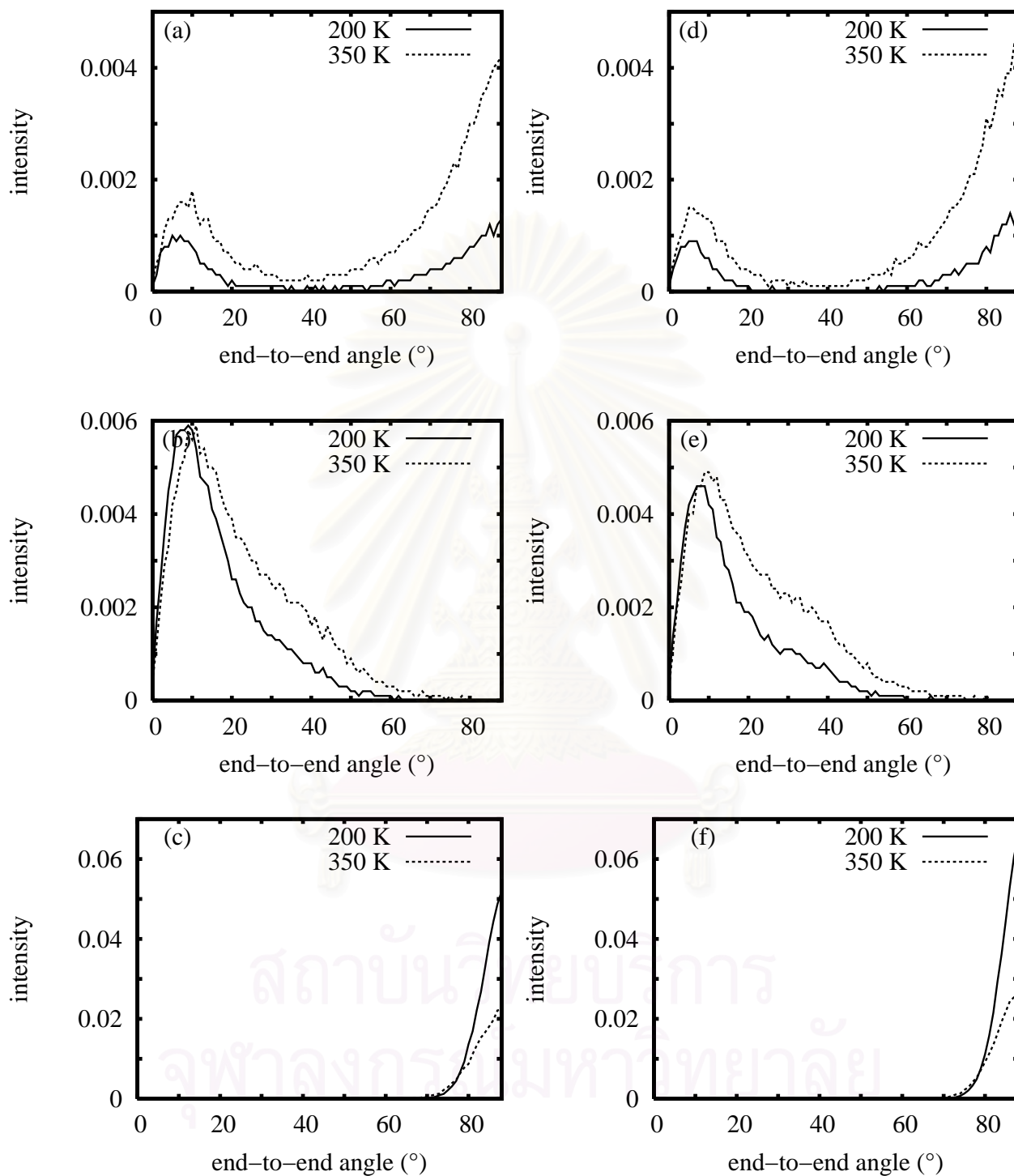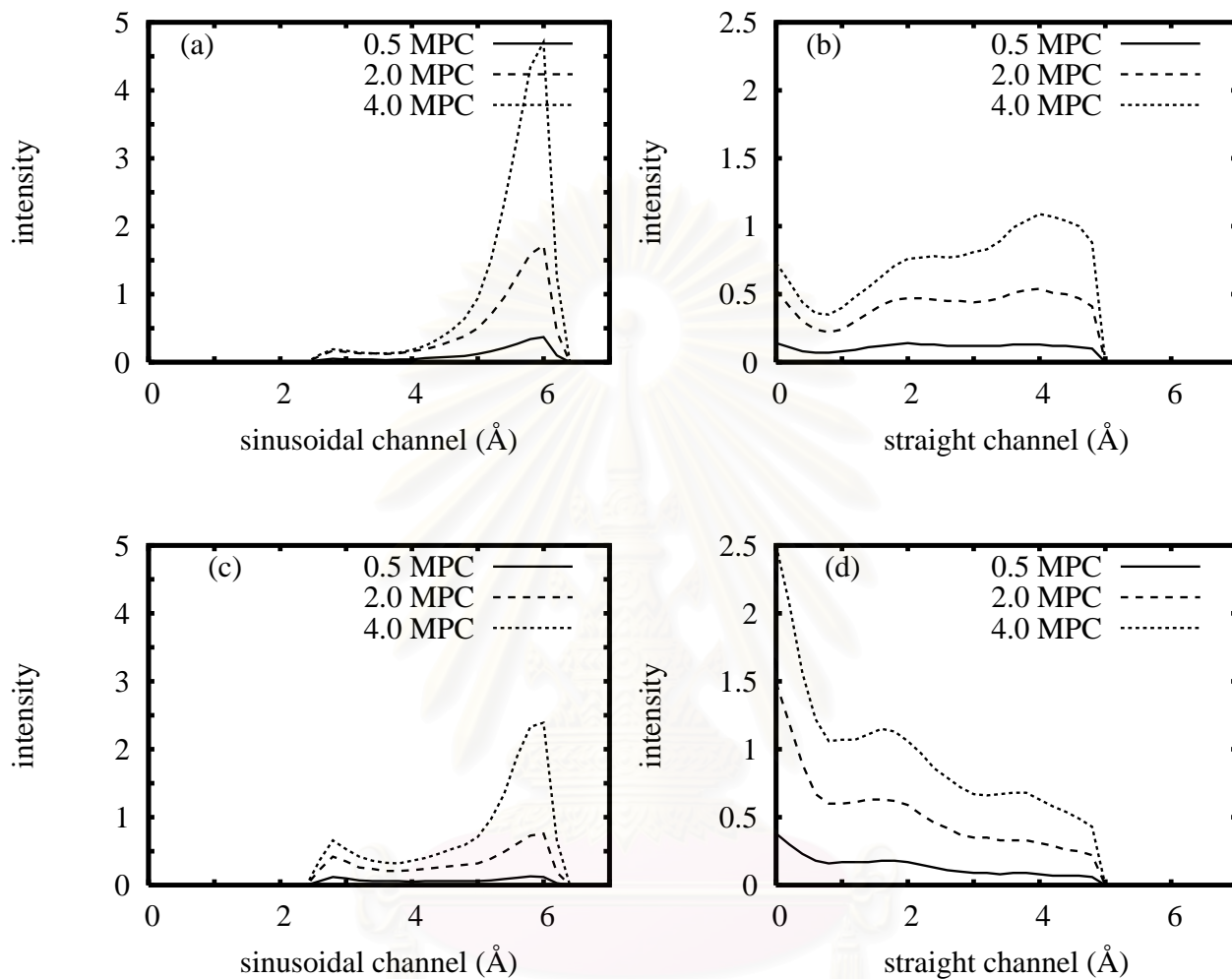
Figure 5.5 Residence distribution of n-pentane molecule in silicalite–1 at 200 K (a,b) and 350 K (c,d)

CHAPTER VI

CONCLUSION

The intermolecular potential function for the system of n-petane/silicalite–1 were developed. The small fragment of silicalite–1 consisting of 20 heavy atoms in which the chemical composition is $O_{10}Si_{10}H_{20}$ was used to represent the silicalite–1 channel. 189 configurations of n-pentane/silicalite–1 fragment and 1300 configurations of n-pentane/n-pentane dimer interactions were calculated on the basis of *ab initio* at Møller Plesset levels with the 6-31G(d) basis sets. In order to get reproducibility on experimental heat of adsorption and diffusion coefficients, several attempts were spent to fit the obtained *ab initio* data to the analytical function representing n-pentane/silicalite–1. Problems were arisen and solved step by step that can be summarized as follows. On the first attempt, the analytical fitted function are in the form of $A/r^6 + B/r^{12} + C/r^4$. Though, this functional form gives the best fit to the *ab initio* data, the non-reasonably partitioning energy to each pair leads to positive interaction energies obtained from the MD simulations. With this function, no attractive contribution was found on the CH_2-O pair. This lead to the second attempt, where the C/r^4 terms were excluded. Then, the problem of the repulsive contribution on the CH_2-O pair was solved. However, the obtained potential function did not yet reproduce the experimental heat of adsorption at zero coverage (Q_{st}), the calculated and the experimental Q_{st} are 31.6 kJ/mol and 57.7 kJ/mol, respectively. It was found, then, that energy obtained from the MP2/6-31G(d) is significantly higher than that of the MP2/6-31+G(d,p) method. Note that when the project started, computer facility could not report the later calculation type. Therefore, recalculations of the n-pentane/silicalite–1 configurations with the larger basis sets were performed.

The refitted function on the third attempt using MP2(FC)/6-31+G(d,p) method was found to reproduce the experimental Q_{st} very well, *i.e.*, the calculated Q_{st} of 58.93 kJ/mol is 2.13% higher than that obtained experimentally. Problem still remain, the function does not represent the experimental self diffusion ceofficient, D_s. This is in contrast to that proposed

by Dubbeldam. Among two functional types, difference was found at the repulsive region where the function approach zero for the first time. Here, the fitted collision parameters are significantly larger than that of the force field. Therefore, the forth attempt was made by replacing the fitting parameter using the atomic collision constants. By applying this function for the MD simulations, the calculated Q_{st} of 52.28 kJ/mol is 9.39% lower than the experimental value and change of the D_s as a function of temperature is in good agreement with that of the experiment. Note that the collision constants were also applied to the n-pentane/n-pentane potential function.

After the potential functions were validated. The structural and dynamical data were investigated. Distribution of the resident probability at the low temperature shows that molecule prefers to locate at the sinusoidal channel. This is different for high temperature where high resident probability takes place at the intersection. The reason for the difference were explained by the average potential energy along the channels and the distributions of the end-to-end length and end-to-end angle. At low temperature, potential will play more important role, comparing to molecular movement. At higher temperature, the internal and tumble movements dominate the potential well. In addition, increasing temperature leads to an increase of relative diffusion rate along the x-axis, $i.e.$, molecule spends less time in the sinusoidal channel.

The effect of concentration was investigated at two temperatures. The patterns of the residence distribution for all concentrations are rather similar. Either temperature or loading does not effect behavior of the diffusing molecule in the term of memory factor. That is, the molecules prefer to the diffuse path along the same channel type.

In summary, collision constants were introduced into the ab $initio$ fitted potential. Here ratio of the atomic pairs in the molecular potential was reasonably partitioned. An advantage of the approach is that the newly develop guest/host and guest/guest potential functions were found to represent structural, dynamic and thermodynamic properties of the simulated systems very well. This overcome an issue of currently debate where the force field parameters can not well represent structural data while the ab $initio$ fitted potential is often fail to represent dynamic and thermodynamic properties of the system.

REFERENCES

[1] Blauwhoff, P. M. M., Gosselink, J. W., Kieffer, E. P., Sie, S. T., and Stork, W. H. J., Fundamentals and Applications, in *Catalysis and Zeolites*, edited by Weitkamp, J. and Puppe, L., Berlin, Springer, 1999, pages 437–538.

[2] Thomas, J. M., Solid Acid Catalysis, *Sci. Am.* 266 (1992): 112–118.

[3] Kärger, J. and Ruthven, D. M., *Diffusion in Zeolites and Other Microporous Solids*, Wiley: New York, 1992.

[4] Theodorou, D. N., Snurr, R., and Bell, A. T., Molecular Dynamics and Diffusion in Microporous Materials, in *Comprehensive Supramolecular Chemistry, Edt. G. Alberti and T. Bein*, volume 7, Oxford, Pergamon, 1996, pages 507–548.

[5] Keil, F., Krishna, R., and Coppens, M.-O., Modelling of Diffusion in Zeolites, *Rev. Chem. Eng.* 16 (2000): 71–197.

[6] Reyes, S. C., Sinfelt, J. H., and DeMartin, G. J., Diffusion in Porous Solids: The Parallel Contribution of Gas and Surface Diffusion Processes in Pores Extending from the Mesoporous Region into the Microporous region, *J. Phys. Chem. B* 104 (2000): 5750–5761.

[7] Bezus, A., Kiselev, A., Lopatkin, A., and Du, P. Q., Molecular Statistical Calculation of the Thermodynamic Adsorption Characteristics of Zeolites Using the Atom - Atom Approximation. Part 1.–Adsorption of Methane by Zeolite NaX, *J. Chem. Soc. Faraday Trans.II* 74 (1978): 367–379.

[8] Lachet, V., Boutin, A., Pellenq, R., Nicholson, D., and Fuchs, A., Molecular Simulations of the Structural Rearrangement of Methane Adsorbed in Aluminophosphate $AlPO_4$–5, *J. Phys. Chem.* 100 (1996): 9006–9013.

[9] Dubbeldam, D. et al., United Atom Force Field for Alkanes in Nanoporous Materials, *J. Phys. Chem. B* 108 (2004): 12301–12313.

[10] Dubbeldam, D. et al., Force Field Parametrization through Fitting on Inflection Points in Isotherms, *Phys. Rev. Lett.* 93 (2004): 1–4.

[11] Bussai, C., Hannongbua, S., Fritzsche, S., and Haberlandt, R., Diffusion of water in silicalite by molecular dynamics simulations: *Ab Initio* based interactions, *Studies in Surface Science and Catalysis* 142 (2002): 1979–1986.

[12] Bussai, C., Hannongbua, S., Fritzsche, S., and Haberlandt, R., Ab initio potential energy surface and molecular dynamics simulations for the determination of the diffusion coefficient of water in silicalite-1, *Chem. Phys. Lett.* 354 (2002): 310–315.

[13] Bussai, C. et al., On the diffusion of water in silicalite-1: Md simulations using ab initio fitted potential and pfg nmr measurements, *Applied Catalysis A* 232 (2002): 59–66.

[14] Bussai, C., Fritzsche, S., Haberlandt, R., and Hannongbua, S., Concentration Dependence of the Methane Structure in Silicalite-1: A Molecular Dynamics Study Using the Möller-Plesset-Based Potential, *Langmuir* 21 (2005): 5847–5851.

[15] Bussai, C., Fritzsche, S., Haberlandt, R., and Hannongbua, S., A Molecular Dynamics (MD) Study of Methane in Silicalite-1: A Novel Möller-Plesset Potential Energy Surface, in *Abstracts of the 14th International Zeolite Conference in Cape Town*, edited by van Steen, E. W. J., Callanan, L. H., Claeys, M., and O'Connor, C. T., Cape Town, The Catalyst Society of South Africa, 2004, pages 2104–2109.

[16] Bussai, C., Fritzsche, S., Hannongbua, S., and Haberlandt, R., Formation of Low-Density Water Clusters in the Silicalite-1 Cage: A Molecular Dynamics Study, *J. Phys. Cem. B* 107 (2003): 12444–12450.

[17] Bussai, C., Fritzsche, S., Haberlandt, R., and Hannongbua, S., A Novel Møller-Plesset Perturbation Based Potential for Determining the Structural and Dynamical Properties of Methane in Silicalite–1: A Molecular Dynamics Study, *J. Phys. Chem. B* 108 (2004): 13347–13352.

[18] Breck, D. W., *Zeolite Molecular Sieves*, John Wiley & Sons: New York, 1974.

[19] Galarneau, A., Renzo, F. D., and Fajula, F., *Zeolites and Mesoporous Materials at the Dawn of the 21st Century, 13th International Zeolite Conference Montepellier, France*, Elsevier Science: Amsterdam, 2001.

[20] Ruthven, D. M., *Principles of Adsorption and Adsorption Processes*, John Wiley & Sons: New York, Chichester, Brisbane, Toronto, Singapore, 1984.

[21] Baerlocher, C., Meier, W. M., and Olson, D. H., *Atlas of Zeolite Framework Types*, Elsevier: Amsterdam, fifth revised edition edition, 2001.

[22] Kokotailo, G. T. and Meier, W. M., Properties and Applications of Zeolites, *Chem. Soc. (Special Publ.)* 33 (1979): 133.

[23] Naber, J. E., de Jong, K. P., Stork, W. H. J., Kuipers, H. P. C. E., and Post, M. F. M., Industrial applications of zeolite catalysis, *Stud. Surf. Sci. Catal.* 84 (1994): 2197–2219.

[24] Chen, N., Personal perspective of the development of para selective zsm-5 catalysts, *Ind. Eng. Chem. Res.* 40 (2001): 4157–4161.

[25] Liu, X. and Yan, Z., Optimization of nanopores and acidity of usy zeolite by citric modification, *Ind. Eng. Chem. Res.* 68 (2001): 145–154.

[26] Funke, H. H., Argo, A. M., Falconer, J. L., and Noble, R. D., Separations of cyclic, branched, and linear hydrocarbon mixtures through silicalite membranes, *Ind. Eng. Chem. Res.* 36 (1997): 137–143.

[27] Krishna, R., Smit, B., and Vlugt, T. J. H., Sorption–Induced Diffusion–Selective Separation of Hydrocarbon Isomeres Using Silicalite, *J. Phys. Chem. A* 102 (1998): 7727–7730.

[28] Schenk, M., Vidal, S. L., Vlugt, T. J. H., and Krishna, B. S. R., Separation of alkane isomers by exploiting entropy effects during adsorption on silicalite-1: A configurational-bias monte carlo simulation study, *Langmuir* 17 (2001): 1558–1570.

[29] Calero, S., Smit, B., and Krishna, R., Configurational entropy effects during sorption of hexane isomers in silicalite, *J. of Catal.* 202 (2001): 395–401.

[30] Allen, M. P. and Tildesley, D., *Computer Simulation of Liquids*, Clarendon Press: Oxford, 1989.

[31] Haberlandt, R., Fritzsche, S., Peinel, G., and Heinzinger, K., *Molekulardynamik - Grundlagen und Anwendungen, mit einem Kapitel über Monte-Carlo-Simulationen von H. - L. Vörtler*, Vieweg–Verlag: Wiesbaden, 1995.

[32] Demontis, P. and Suffritti, G. B., Structure and Dynamics of Zeolites Investigated by Molecular Dynamics, *Chemical Reviews* 97 (1997): 2845–2878.

[33] Kärger, J., Molecular Transport in ZeolitesMiracles, Insights and Practical Issues, in *Proceedings of the 12th International Zeolite Conference, Baltimore 1998*, edited by Treacy, M. M. J., Marcus, B. K., Bisher, M. E., and Higgins, J. B., Warrendale, Materials Research Society, 1999, pages 35–42.

[34] Auerbach, S. M., Jousse, F., and Vercauteren, D. P., Dynamics of Sorbed Molecules in Zeolites, in *Computer Modelling of Microporous and Mesoporous Materials*, edited by Catlow, C. R. A., van Santen, R. A., and Smit, B., Amsterdam, Elsevier, 2004, pages 49–108.

[35] Haberlandt, R., Fritzsche, S., and Vörtler, H. L., Simulation of Microporous Systems: Confined Fluids in Equilibrium and Diffusion in Zeolites, in *Handbook of Surfaces and Interfaces of Materials*, edited by Nalwa, H. S., volume 5, San Diego, London, Boston, New York, Sidney, Tokyo, Toronto, Academic Press, 2001, pages 358–444.

[36] Kärger, J., Vasenkov, S., and Auerbach, S. M., Diffusion in Zeolites, in *Handbook of Zeolite Science and Technology*, edited by S. M. Auerbach, K. A. C. and Dutta, P. K., New York, Marcel Dekker, 2003, pages 341–422.

[37] Vlugt, T. J. H., Krishna, R., and Smit, B., Molecular Simulations of Adsorption Isotherms for Linear and Branched Alkanes and Their Mixtures in Silicalite, *J. Phys. Chem. B* 103 (1999): 1102–1118.

[38] Ramanan, H. and Auerbach, S. M., Modeling Jump Diffusion in Zeolites: I. Principles and Methods, in *NATO-ASI Series C: Fluid Transport in Nanopores*, edited by Fraissard, J. and Conner, W. C., Dordrecht, Kluwer Academic Publishers,, 2004.

[39] Keil, F. and Coppens, M., Dynamic Monte Carlo Simulations of Diffusion and Reaction in Zeolites, in *Computer Modelling of Microporous and Mesoporous Materials*, edited by Catlow, C. R. A., van Santen, R. A., and Smit, B., San Diego, London, Boston, New York, Sidney, Tokyo, Toronto, Academic Press, 2004, pages 109–127.

[40] Kamat, M. R., Dang, W., and Keffer, D., Agreement between Analytical Theory and Molecular Dynamics Simulation for Adsorption and Diffusion in Crystalline Nanoporous Materials, *J. Phys. Chem. B* 108 (2004): 376–386.

[41] Ramanan, H., Auerbach, S. M., and Tsapatsis, M., Beyond Lattice Models of Activated Transport in Zeolites: High-Temperature Molecular Dynamics of Self-Diffusion and Cooperative Diffusion of Benzene in NaX, *J. Phys. Chem. B* 108 (2004): 17171–17178.

[42] Schüring, A., Vasenkov, S., and Fritzsche, S., Influence of boundaries of nanoporous crystals on the molecular exchange under conditions of single-file diffusion, *J. Phys. Chem. B* 109 (2005): 16711–16717.

[43] van de Graaf, J., Kapteijn, F., and Moulijn, J., Diffusivities of Light Alkanes in a Silicalite–1 Membrane Layer, *Microporous and Mesoporius Materials* 35 (2000): 267–281.

[44] Millot, B. and Methivier, A., Adsorption of *n*-alkanes on silicalite crystals. a temperature-programmed desorption study, *J. Phys. Chem. B* 102 (1998): 3210–3215.

[45] Sun, M., Shah, D., Xu, H., and Talu, O., Adsorption equilibria of c_1 to c_4 alkanes, co_2, and sf_6 on silicalite, *J. Phys. Chem. B* 102 (1998): 1466–1473.

[46] Yun, J. H., Düren, T., Keil, F. J., and Seaton, N. A., Adsorption of Methane, Ethane, and Their Binary Mixtures on MCM–41: Experimental Evaluation of Methods for the Prediction of Adsorption Equilibrium, *Langmuir* 18 (2002): 2693–2701.

[47] June, R., Bell, A. T., and Theodorou, D. N., Prediction of Low Occupancy Sorption of Alkanes in Silicalite, *J. Phys. Chem.* 94 (1990): 1508–1516.

[48] June, R. L., Bell, A. T., and Theodorou, D. N., Molecular Dynamics Studies of Butane and Hexan in Silicalite, *J. Phys. Chem.* 96 (1992): 1051–1060.

[49] Maginn, E. J., Bell, A. T., and Theodorou, D. N., Sorption Thermodynamics, Siting, and Conformation of Long *n*-Alkanes in Silicalite Predicted by Configurational–Bias Monte Carlo Integration, *J. Phys. Chem* 99 (1995): 2057–2079.

[50] Roothaan, C., New developments in molecular orbital theory, *Rev. Mod. Phys.* 23 (1951): 69–89.

[51] Huang, K., *Statistical Mechanics*, Wiley: New York, 1987.

[52] Verlet, L., Computer Experiments on Classical Fluids. II. Equilibrium Correlation Functions, *Phys. Rev.* 165 (1968): 201–214.

[53] Born, M. and von Karman, T., über schwingungen in raumgittern, *Physik. Z* 13 (1912): 297–309.

[54] Wilkinson, D., *Mass Transport in Solids and Fluids*, Cambridge University Press: London, 2000.

[55] Brown, R., A Brief Account of Microscopical Observations Made in the Months on June, July and August 1827, on the Particles Contained in the Pollen of Plants; and on the General Existence of Active molecules in Organic and Inorganic Bodies, *Phil. Mag.* 4 (1828): 161–173.

[56] Einstein, A., On a Heuristic Point of View concerning the Production and Transformation of Light, *Ann. Phys.* 17 (1905): 349.

[57] Kärger, J., Pfeifer, H., and Heink, W., *Principles and Application of Self-Diffusion Measurements by Nuclear Magnetic Resonance*, Advances in Magnetic Resonance Vol. 12, Academic Press: New York, 1988.

[58] Haberlandt, R. and Kärger, J., Molecular dynamics under the confinement by the host lattice in zeolitic adsorbat-adsorbent systems, *Chem. Eng. J.* 74 (1999): 15–24.

[59] Fritzsche, S., Haberlandt, R., Kärger, J., Pfeifer, H., and Heinzinger, K., An MD Simulation on the Applicability of the Diffusion Equation for Molecules Adsorbed in a Zeolite, *Chem. Phys. Lett.* 198 (1992): 283–287.

[60] Fritzsche, S., Wolfsberg, M., and Haberlandt, R., The Importance of Various Degrees of Freedom in the Theoretical Study of the Diffusion of Methane in silicalite–1, *Chem. Phys.* 289 (2003): 321–333.

[61] June, R., Bell, A. T., and Theodorou, D. N., Molecular Dynamics Study of Methane and Xenon in Silicalite, *J. Phys. Chem* 94 (1990): 8232–8240.

[62] Heink, W., Kärger, J., Pfeifer, H., Datema, K., and Nowak, A., High–temperature Pulsed Field Gradient Nuclear Magnetic Resonance Self-diffusion Measurements of n-Alkanes in MFI–type Zeolites, *J. Chem. Soc. Faraday Trans.* 88 (1992): 3505–3509.

[63] Runnebaum, R. C. and Maginn, E. J., Molecular Dynamics Simulations of Alkanes in the Zeolite Silicalite: Evidence for Resonant Diffusion Effects, *J. Phys. Chem. B* 101 (1997): 6394–6408.

[64] Maginn, E. J., Bell, A. T., and Theodorou, D. N., Dynamics of Long n-Alkanes in Silicalite: A Hierarchical Simulation Approach, *J. Phys. Chem* 100 (1996): 7155–7173.

[65] Kärger, J., Random Walk Through Two-Channel Networks: A Simple Means to Correlate the Coefficients of Anisotropic Diffusion in ZSM-5 Type Zeolites, *J. Phys. Chem* 95 (1991): 5558–5560.

[66] Kärger, J., Demontis, P., Suffritti, G. B., and Tilocca, A., Two Steps Model of Molecular Diffusion in Silicalite, *J. Chem. Phys.* 110 (1999): 1163–1172.

[67] McQuarrie, D., *Statistical Mechanics*, Harper & Row: New York, Evanston, San Francisco, London, 1976.

[68] Gray, C. G. and Gubbins, K. E., *Theory of Molecular Fluids. Part 1. Fundamentals.*, Clarendon Press: Oxford, 1984, Intermolecular Forces, Statistical Mechanics, Perturbation Theory, BBGKY, Ornstein–Zernicke, Percuss–Yevick, Buch in Abteilung MDC vorhanden.

[69] Cremer, D., Mϕller-plesset perturbation theory, in *Encyclopedia of Computational Chemistry*, volume 3, Chichester, Wiley, 1998, pages 2110–2117.

[70] Ryckaert, J. and Bellemans, A., Molecular dynamics of liquid alkanes, *Faraday Discuss. Chem. Soc.* 66 (1978): 95–106.

[71] Kast, S. and Brickmann, J., Constant Temperature Molecular Dynamics Simulations by Means of a Stochastic Collision Model. II. The Harmonic Oscillator, *J. Chem. Phys.* 104 (1996): 3732–3741.

[72] Vlugt, T. J. H. and Schenk, M., Influence of Framework Flexibility on the Adsorption Properties of Hydrocarbons in the Zeolite Silicalite, *J. Phys. Chem. B* 106 (2002): 12757–12763.

[73] Demontis, P., Suffritti, G. B., and Tilocca, A., Diffusion and Vibrational Relaxation of a Diatomic Molecule in the Pore Network of a Pure Silica Zeolite: A Molecular Dynamics Study, *J. Chem. Phys.* 105 (1996): 5586–5594.

[74] Schuring, D., Jansen, A., and van Santen, R. A., Concentration and Chainlength Dependence of the Diffusivity of Alkanes in Zeolites Studied with MD Simulations, *J. Phys. Chem. B* 104 (2000): 941–948.

[75] Smit, B., Loyens, L., and Verbist, G., Simulation of Adsorption and Diffusion of Hydrocarbons in Zeolites, *Faraday Discuss.* 106 (1997): 93–104.

[76] Verlet, L., Computer Experiments on Classical Fluids. (I). Thermodynamical Properties of Lennard Jones Molecules, *Phys. Rev.* 159 (1967): 98–103.

[77] Bussai, C., Hannongbua, S., and Haberlandt, R., Understanding the Movement, Encapsulation, and Energy Barrier of Water Molecule Diffusion into and in Silicalites Using Ab Initio Calculations, *J. Phys. Chem. B* 105 (2001): 3409–3414.

[78] Bussai, C., Fritzsche, S., Haberlandt, R., and Hannongbua, S., A Molecular Dynamics (MD) Study of Methane in Silicalite-1: A Novel Mller-Plesset Potential Energy Surface, in *Studies in Surface Sciences and Catalysis*, volume 154, Amsterdam, Elsevier, 2004, pages 2104–2109.

[79] Jorgensen, W. L., Madura, J. D., and Swenson, C. J., Optimized Intermolecular Potential Functions for Liquid Hydrocarbons, *J. Am. Chem. Soc.* 106 (1984): 6638–6646.

[80] Poncela, A., Rubio, A., and Freire, J., Determination of the potential parameters of a site model from calculations of second virial coefficients of linear and branched alkanes, *Mol. Phys.* 91 (1997): 189–201.

[81] Martin, M. G. and Siepmann, J. I., Novel Configurational-Bias Monte Carlo Method for Branched Molecules. Transferable Potentials for Phase Equilibria. 2. United-Atom Description of Branched Alkanes, *J. Phys. Chem. B* 103 (1999): 4508–4517.

[82] Denayer, J., Souverijns, W., Jacobs, P., Martens, J., and Baron, G., High-temperature low-pressure adsorption of branched c_5–c_8 alkanes on zeolite beta, zsm-5, zsm-22, zeolite y, and mordenite, *J. Phys. Chem. B* 102 (1998): 4588–4597.

[83] Tuma, C. and Sauer, J., Treating dispersion effects in extended systems by hybrid mp2:dft calculations-protonation of isobutene in zeolite ferrierite, *Phys. Chem. Chem. Phys.* 8 (2006): 3955–3965.

[84] Eder, F. and Lercher, J. A., Alkane sorption in molecular sieves: The contribution of ordering, intermolecular interactions, and sorption on brϕnsted acid sites, *Zeolites* 18 (1997): 75–81.

[85] Beerdsen, E., Dubbeldam, D., Smit, B., Vlugt, T. J. H., and Calero, S., Simulating the Effect of Nonframework Cations on the Adsorption of Alkanes in MFI-type Zeolites, *J. Phys. Chem. B* 107 (2003): 12088–12096.

[86] Fox, J. P. and Bates, S. P., Simulating the Adsorption of Binary and Ternary Mixtures of Linear, Branched, and Cyclic Alkanes in Zeolites, *J. Phys. Chem. B* 108 (2004): 17136–17142.

[87] Ndjaka, J. B., Zwanenburg, G., Smit, B., and Schenk, M., Molecular simulations of adsorption isotherms of small alkanes in FER-, TON-, MTW- and DON-type zeolites, *Microporous and Mesoporous Materials* 68 (2004): 37–43.

[88] Fox, J. P., Rooy, V., and Bates, S. P., Simulating the adsorption of linear, branched and cyclic alkanes in silicalite-1 and AlPO4-5, *Microporous and Mesoporous Materials* 69 (2004): 9–18.

[89] Heink, W. et al., Self-diffusion Measurements of n-Alkanes in Zeolite NaCaA by Pulsed-field Gradient Nuclear Magnetic Resonance, *J. Chem. Soc. Faraday Trans.* 88 (1992): 515–519.

[90] Datema, K. et al., Fourier-transform Pulsed-field-gradient Nuclear Magnetic Resonance Investigation of the Diffusion of Light *n*-Alkanes in Zeolite ZSM-5, *J. Chem. Soc. Faraday Trans.* 87 (1991): 1935–1943.
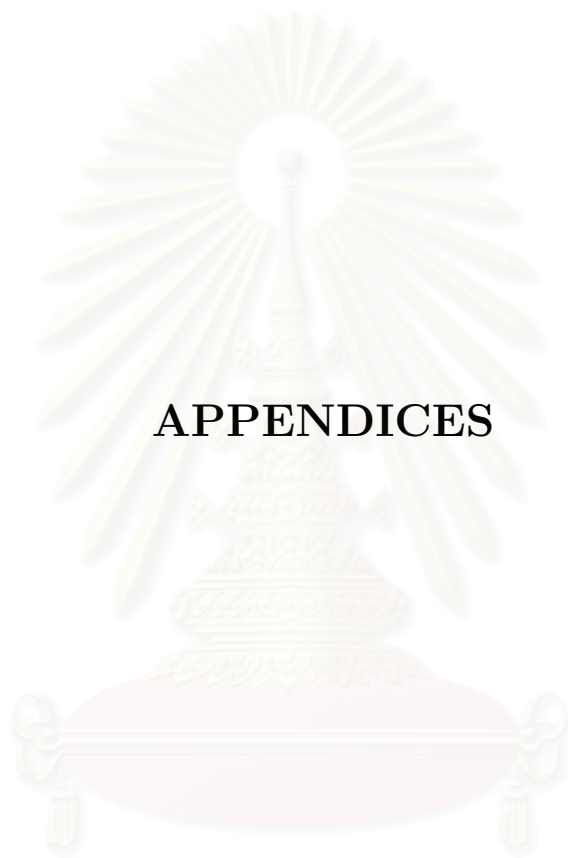
APPENDICES

Appendix A:

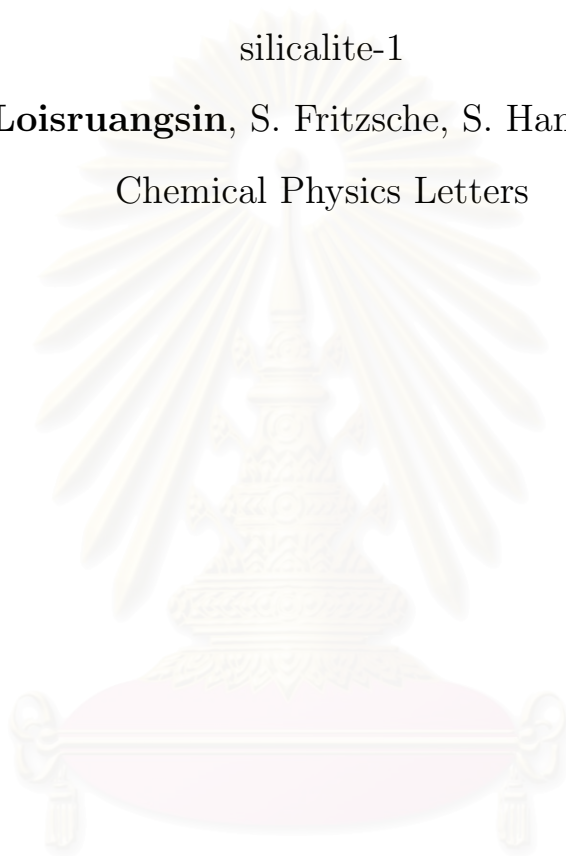Newly development of ab initio fitted potentials for n-pentane in zeolite silicalite-1

A. Loisruangsin, S. Fritzsche, S. Hannongbua

**CHEMICAL
PHYSICS
LETTERS**

Newly developed ab initio fitted potentials for molecular dynamics simulations of *n*-pentane in the zeolite silicalite-1

A. Loisruangsin [a,*], S. Fritzsche [b], S. Hannongbua [a,*]

[a] *Computational Chemistry Unit Cell, Department of Chemistry, Faculty of Science, Chulalongkorn University,
Phyathai Road, Pathumwan, Bangkok 10330, Thailand*
[b] *Institute for Theoretical Physics, University Leipzig, Augustusplatz 9-11, D-04109, Leipzig, Germany*

Abstract

Ab initio fitted potentials representing *n*-pentane/*n*-pentane and *n*-pentane/silicalite-1 interactions were newly developed at the second-order Møller-Plesset perturbation (MP2) level with the 6-31G* basis set. Characteristics of the functions were illustrated in comparison with available force field models. They were, then, applied for the molecular dynamics simulation of *n*-pentane in silicalite-1. The diffusion coefficients are in satisfactory agreement with the results of PFG-NMR experiments. The effect of the box size was also examined. It was found that the components of the diffusion tensor are very sensitive to this parameter. The structure of the *n*-pentane in the silicalite-1 pore was analyzed in terms of radial distribution functions. The first peak at 4.1 Å indicates the optimal diffusion route of the *n*-pentane along the central line of the channel of the silicalite-1.
© 2004 Published by Elsevier B.V.

1. Introduction

Alkanes in zeolites play an important role in many industrial applications [1] because the effectivity of the technical processes is usually limited by the slow migration of guest molecules through the channels and cavities of the zeolites. Numerous investigations of the diffusive properties of alkanes in zeolites have been reported using both experimental and theoretical approaches. Overviews can be found in [2–8]. Such studies are also a challenge to fundamental research because discrepancies between results obtained from different experimental methods [2,5,8,9] are not yet understood. Molecular dynamics (MD) simulations [10,11] have become a powerful tool to investigate such phenomena [2–8]. They provide deep insight into details of the diffusion mechanisms. However, it is known that the sim-

ulation results depend strongly on the quality of the potential functions used (see e.g. [12]).

In our earlier works, the water/silicalite-1 and methane/silicalite-1 intermolecular pair potentials were developed using ab initio data. These potentials were then used in the MD simulations [13–15]. The obtained diffusion coefficients are in reasonable agreement with those from PFG-NMR experiments [15–17]. A great advantage of the ab initio fitted potentials is their ability to predict the structural property of the simulated system. The results provide detailed structure and distribution of the guest molecules in the channels. It was the first time that changes of the methane structure as a function of loading were described, theoretically.

In this study, *n*-pentane in silicalite-1 was examined. The guest/guest and guest/host pair potentials were derived from ab initio data points. *n*-pentane/*n*-pentane parameters from the literature [18–20] were also considered and compared. Then, the diffusive behavior was examined in terms of the components D_x, D_y, and D_z of the diffusion tensor, their average D, and the memory factor, β.

---

[*] Corresponding authors. Fax: +1-22-187-603.
  E-mail addresses: arthorn@atc.atccu.chula.ac.th (A. Loisruangsin), siegfried.fritzsche@uni-leipzig.de (S. Fritzsche), supot@atc.atccu.chula.ac.th (S. Hannongbua).

2. Calculation details

2.1. The ab initio fitted potentials

Silicalite-1 is a cation-free zeolite of the structure type ZSM–5 which contains a network of interconnected channels. The symmetry group of silicalite-1 is *Pnma* with cell parameters $a = 20.07$ Å, $b = 19.92$ Å and $c = 13.42$ Å [21]. A three-dimensional network structure of the channels in silicalite-1 contains straight and zig-zag channels (Fig. 1a). The cross-section radii of both of the channel types are about 4 Å.

To develop the *n*-pentane/silicalite-1 potential, it is not possible to perform quantum chemical calculation of a complete unit cell. Therefore, a fragment of the 10-oxygen membered ring consisting of 10 oxygen and 10 silicon atoms (Fig. 1b) has been used to represent the silicalite-1. The selected fragment was, then, completed by adding hydrogen atoms. The *n*-pentane molecule was positioned at the center of the fragment in the configuration shown in Fig. 2a. Then, about 100 configurations of the dimer were generated by varying coordinates of *n*-pentane in terms of molecular translation and rotation along the three axes with steps of 0.2 Å and 20°, respectively.
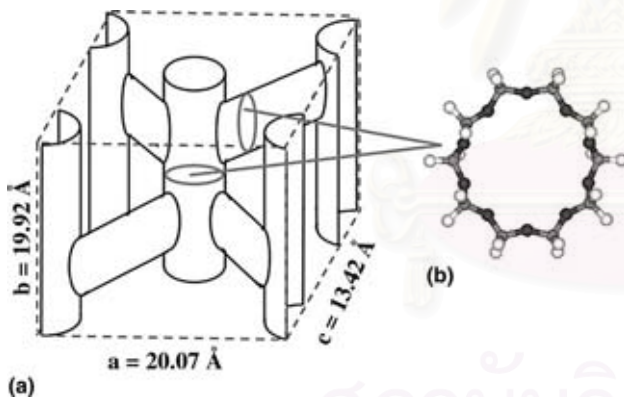

Fig. 1. Schematic views of: (a) the channel system within one unit cell of silicalite-1; (b) a 10-oxygen membered ring-fragment of silicalite-1.
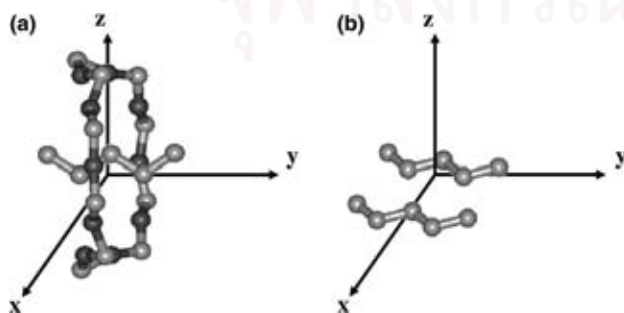

Fig. 2. Starting configurations of: (a) *n*-pentane/silicalite-1; (b) *n*-pentane/*n*-pentane which were used to develop the pair potential.

For the ab initio fitted *n*-pentane/*n*-pentane pair potential, 1300 configurations of the *n*-pentane dimer have been generated systematically. The center of mass of the first *n*-pentane was at the origin and that of the second one was at 3 Å on the *x*-axis (Fig. 2b). Positions and orientations of the second *n*-pentane were varied in terms of its translation and rotation along the three axes. The distance between the two molecules was extended until the interaction approaches zero. In addition, flexibility of the *n*-pentane was also taken into account by varying all C–C–C–C torsional angles of both molecules.

All quantum chemical calculations were performed for the above generated *n*-pentane/*n*-pentane and *n*-pentane/silicalite-1 configurations at the MP2 level with 6-31G* basis set. The basis set superposition error (BSSE) is also taken into account. The MP2 energies, $\Delta E(r)$, representing *n*-pentane/*n*-pentane and *n*-pentane/silicalite-1 interactions were fitted separately to analytical functions of the type

$$\Delta E(r) = \sum_i \sum_j \left\{ \frac{A_{ij}}{r_{ij}^6} + \frac{B_{ij}}{r_{ij}^{12}} + \frac{C_{ij}}{r_{ij}^4} \right\}, \qquad (1)$$

where A_{ij}, B_{ij}, and C_{ij} are fitting parameters and r_{ij} is the distance between atoms *i* and *j*, belonging to different molecules. Note that, the highly repulsive configurations were excluded from the fitting procedure due to the negligible likeliness of occurrence. The *n*-pentane molecule is represented by a united atom model [22], in which interaction sites of CH_2 or CH_3 groups are positioned at the carbon atoms. In addition, only oxygen atoms of the fragment were included in the *n*-pentane/silicalite-1 fitted potential as it is done in most of the MD simulations for guest/zeolite systems while the quantum calculations include, of course, also the silicon atoms.

2.2. Molecular dynamics simulations

The simulations were performed using the *velocity Verlet* algorithm with a time step of 0.5 fs. The concentration of *n*-pentane in silicalite-1 was equivalent to the experimental density of 4 molecules per unit cell. The effect of the box size was examined by performing simulations containing 2 and 16 unit cells of silicalite-1. While the lattice was kept rigid for all MD runs, *n*-pentane was modeled to be flexible with a dihedral potential according to [23]. Furthermore a harmonic potential [24] and a Morse potential [25] were introduced to model the bond bending elasticity and the stretching elasticity. The average temperature of the run was adjusted to 330 K for 50 ps by the choice of the total energy as described in [26]. Then, no further thermalization was necessary and the evaluation of the quantities of interest (e.g. diffusion coefficients, radial distribution functions) could take place with unperturbed trajecto-

ries of an MD simulation in the microcanonical ensemble with the predefined value of the temperature.

3. Results and discussion

3.1. The ab initio fitted potentials

For the functional form of the interaction energies shown in Eq. (1), the fitting parameters have been optimized. The final values are summarized in Tables 1 and 2 for the n-pentane/silicalite-1 and n-pentane/n-pentane, respectively.

Some comments could be made concerning the quality of the ab initio data points and the functional form used. In order to take into account the dispersive interaction which is very important in the alkane/silicalite-1 system, the second-order Møller-Plesset perturbation (MP2) level with the extended 6-31G* basis sets which is known to represent such interaction [27] was applied. The basis set superposition error was applied to all data points in order to diminish an artifact due to an unbalance of the basis set.

In Eq. (1) no coulombic term is presented. One reason to neglect it is the use of the united atom model in which the total charge of each united atom of type CH_2 or CH_3 is almost zero. Another argument to leave out this term is that the proposed model with the effective parameters employed in this study already yields very good agreement between the predicted (by the potential function) and the observed (by the ab initio calculation) interaction energies. In addition, an approach of the sorbate molecules to the Si atom on the silicalite-1 surface is prevented by surrounding oxygens.

To visualize the quality of the guest/host fitted potentials, energies (ΔE) yielded from the ab initio calculations are compared with ΔE values calculated using the analytical pair potentials. ΔE here means the contribution of the n-pentane/silicalite-1 interactions to the total potential energy. The comparison is shown in Fig. 3 for numerous configurations where a point on the symmetry line would mean an 1:1 agreement of model and ab initio calculations for the configuration represented by that point. The plot shows that the n-pentane/silcialite-1 potential reproduces the ab initio data very well, especially for configurations that frequently appear during MD simulations.

A comparison between the ab initio calculated energies and those from the model for the n-pentane/silicalite-1 potential energy for configurations where the n-pentane molecule lies at the center of the fragment (Fig. 2b) and moves along the $\pm x$ direction approaching the inner surface of the wall is shown in Fig. 4, where the $\pm$ distances correspond to those along $\pm x$ axes. Good agreement between the two curves confirms the reliability and quality of the fitted potential. Rapid increase of the interaction energy indicates strong repulsion between n-pentane and the inner wall of the silicalite-1.
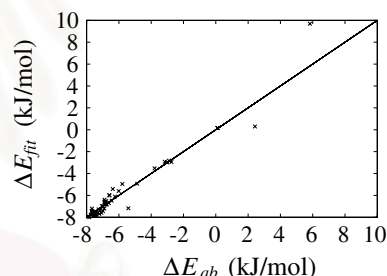

Fig. 3. The correlation between potential energy values arising from the n-pentane/silicalite-1 interaction calculated from ab initio method (ΔE_{ab}) compared to those yielded from Eq. (1) with the optimal parameters shown in Table 1 (ΔE_{fit}).

Table 1
Ab initio fitted potential parameters for the n-pentane/silicalite-1 intermolecular potential shown in Eq. (1)

Sort	Parameters		
	A (kJ Å^6/mol)	B (kJ Å^{12}/mol)	C (kJ Å^4/mol)
O–CH$_3$	−21112.16104	37738020.53015	421.23788
O–CH$_2$	−11489.01954	15095208.21206	521.16890

Table 2
Ab initio fitted potential parameters for the n-pentane/n-pentane intermolecular potential shown in Eq. (1)

Sort	Parameters		
	A (kJ Å^6/mol)	B (kJ Å^{12}/mol)	C (kJ Å^4/mol)
CH$_3$–CH$_3$	−5719.49861	39562056.94898	0.0
CH$_3$–CH$_2$	−9904.31665	35682342.74115	0.0
CH$_2$–CH$_2$	−3856.08455	2828267.10013	0.0
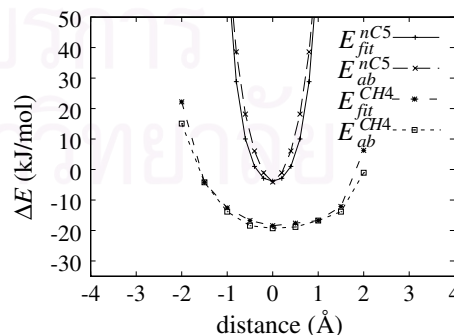
Fig. 4. Interaction potential energies (ΔE) for the n-pentane/silicalite-1 obtained from the ab initio calculations at the MP2 level with the extended 6-31G* basis sets (ΔE_{ab}^{nC5}) and from the potential functions (ΔE_{fit}^{nC5}) according to Eq. (1) where the n-pentane molecule lies in the configuration shown in Fig. 2b and moves along the $\pm x$ axes to the inner surface of the silicalite-1. (ΔE_{ab}^{CH4} and ΔE_{fit}^{CH4} were defined in a similar manner for the methane/silicalitte-1 system in [28].)

Fig. 5. The correlation between potential energy values arising from the n-pentane/n-pentane interaction calculated from ab initio method (ΔE_{ab}) compared to those (ΔE_{fit}) yielded form: (a) Eq. (1) with the optimal parameters shown in Table 1; (b) TIP potentials [23]; (c) TraPPE-UA potentials [29]; (d) PRF potentials [30].
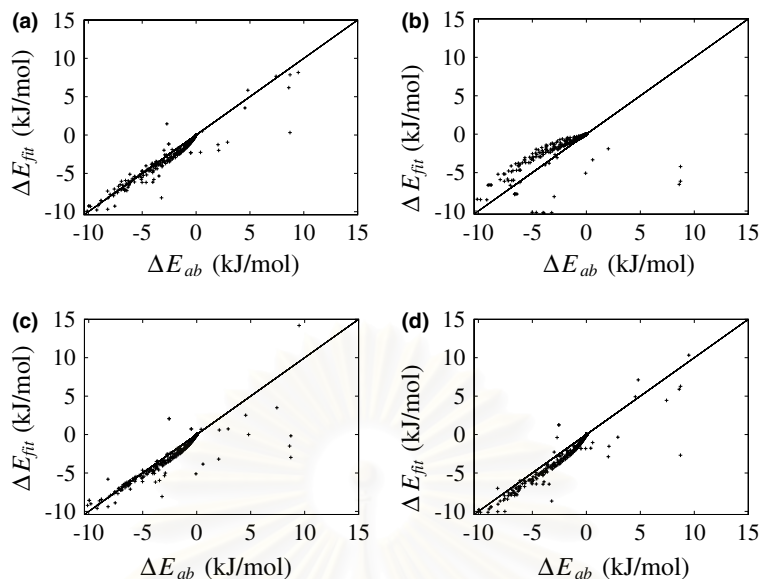
Table 3
Sum of the squares of the energy differences between (ΔE_{ab}) and (ΔE_{fit}) for the potential function presented in this Letter and those available in the literature [23,29,30]

Potential functions	$\sum(\Delta E_{fit} - \Delta E_{ab})^2$
This work	277.55
TIP [23]	4661.99
TraPPE-UA [29]	488.93
PRF [30]	644.42

This is in contrast to what takes place for water and methane molecules in the pore of silicalite-1 [13,28].

The quality of the ab initio fitted n-pentane/n-pentane function was also examined and shown in Fig. 5a. Good agreement between the two sources of the energy was yielded, especially in the attractive region ($\Delta E < 0$). Comparing to those extracted from the literature [23,29,30], (see Fig. 5b–d) our model fits better to the correlation line than the other models. A quantitative measure of the quality of the potential functions is presented in Table 3, in which the sum of the square errors between ΔE_{fit} and ΔE_{ab} was evaluated. It is clear from these data that our function shows the best correlation between the ab initio and the fitted energies among to the available potential functions.

3.2. Molecular dynamics simulations

3.2.1. Diffusion coefficients

Diffusion coefficients i.e. the single elements of the diffusion tensor D_x, D_y, and D_z corresponding to the principle axes and their arithmetical average D (the trace of the diffusion tensor divided by three) for two different MD box sizes were evaluated from the MD simulations according to the method proposed in [26]. The results, for two different evaluation times, were given in Table 4.

The following conclusions can be made: (i) the average diffusion coefficients, D obtained from the simulations using the newly developed potential are almost 4 times lower than that of the PFG-NMR experiment [31]. Taking into consideration the large variations in the available experimental diffusion coefficients for zeolites [5,9], the agreement of the simulation results with the PFG-NMR is satisfactory. One should note that the fitting was only done with respect to ab initio energies and not with respect to the experimental D values. Parameters that are corrected with respect to selected experimental D values would of course be superior in reproducing these special data. Moreover, it was shown in our previous work that the use of ab initio derived potential in molecular dynamics simulations have the power to determine a proper structure of diffusive water and methane molecules in silicalite-1 channels [13–

Table 4
Diffusion coefficients along the x-, y-, z-axes and their average values evaluated from MD simulations with two different MD box sizes (number of silicalite-1 unit cells, N), compared to that obtained from PFG-NMR measurement [31]

t (ns)	N (unit cell)	D (10^{-11} m^2/s)			Total
		x	y	z	
500	2	6.60	32.80	1.13	13.50
500	16	10.70	22.10	2.01	11.60
PFG-NMR					39.00

15,28]. (ii) The average D does not differ significantly for different box sizes while the single components of the diffusion tensor are very sensitive to this parameter (the edge length of the MD box containing 16 silicalite-1 unit cells is two times longer than the edge length for a box containing only two unit cells). Note that this was not observed for small guest molecules, such as water and methane. Therefore, a clear conclusion is that a long n-pentane molecule needs a larger simulation box. Therefore, further evaluation was carried out only for the system containing 16 unit cells of silicalite-1.

Considering the diffusion through silicalite-1 as a random walk of independent steps between the channel intersections, the components of the diffusion tensor can be shown to fulfill a relation proposed by Kärger [32]

$$\frac{a^2}{D_x} + \frac{b^2}{D_y} = \frac{c^2}{D_z}, \tag{2}$$

where a, b, c are the unit cell parameters as mentioned above. Deviations from this relation, caused by 'memory effects', can be characterized by a memory factor, β, introduced in [33].

$$\beta = \frac{c^2/D_z}{a^2/D_x + b^2/D_y}. \tag{3}$$

The value of β calculated in this study is equal to 1.6. As diffusion in z-direction can be realized in silicalite-1 only by alternating moves in x- and y-channels $\beta > 1$ indicates that exchanges of molecules between the different channel types happen not very often.

3.2.2. Radial distribution functions

To understand the structural properties of the system, several atom–atom radial distribution functions (RDF) have been examined. The RDF's are defined in the following way: $g_{xy}(r)$ is the probability density of finding a particle of type y in a distance r from a given particle of type x. For the united atoms representing the CH_2 and CH_3 groups the distance is measured from their C atom. The resulting curves for their RDF's with respect to the lattice oxygen have been displayed in Fig. 6. The CH_3–O RDF shows a pronounced first peak centered at 4.1 Å. As the channels in silicalite-1 form tubes with a diameter of approximately 8.2 Å, the first peak can be clearly assigned to molecules moving along the center of the tube. In agreement with [34], the other peaks at 5.8 and 8.3 Å can be assigned to n-pentane molecules in the 10-oxygen membered rings and in other adjacent rings on the silicalite-1 surface, respectively. The peak positions correspond to the distances from carbon atoms of the CH_3 group to the nearest oxygen atoms. These peaks are similar to those found for water and methane molecules in silicalite-1 [28,35].

The situation is different for the CH_2–O RDF, although it shows also three peaks located at almost the same positions as those of the CH_3 one. Broadening of
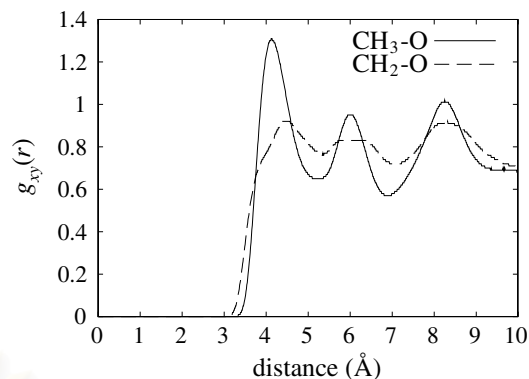

Fig. 6. Methyl–oxygen and methylene–oxygen radial distribution functions for n-pentane in silicalite-1.

the CH_2–O peaks is due consequently to the zig-zag conformation of the n-pentane molecules, i.e., when the two CH_3 ends were positioned along the central line, the CH_2 groups have to be shifted out of this line, closer to the inner surface of the wall. Note that the broad peak at 4.4 Å and the shoulder at 3.6 Å of the CH_2–O RDF are contributed by the same set of n-pentane molecules because the sum of the two distances is almost equal to the diameter of the tube. The same reason can be applied to describe the broadening of the second and the third peaks of the CH_2–O RDF in comparison to the CH_3–O one.

4. Conclusion

New potential functions for n-pentane/silicalite-1 have been successfully developed. They are in better agreement with ab initio data than any other ones found in the literature. The diffusion coefficients obtained from simulations using these potentials are in satisfactory agreement with the experiment values. The difference in single diffusion components obtained from small and large systems leads to a decision of applying MD box of 16 unit cells for further studies. The resulting potential curves, memory factor and radial distribution functions suggest that the n-pentane molecule moves preferentially around the central lines of the channels and hardly changes to diffuse to different channel types.

References

[1] Proceedings of the second FEZA conference, Giardini Naxos, 2002, Studies in Surface Science and Catalysis, Elsevier, Amsterdam, vol. 142, 2002.

[2] J. Kärger, D.M. Ruthven, Diffusion in Zeolites and Other Microporous Solids, Wiley, New York, 1992.

[3] D.N. Theodorou, R. Snurr, A.T. Bell, Molecular dynamics and diffusion in microporous materials, in: Comprehensive Supermolecular Chemistry, vol. 7, Pergamon Press, Oxford, 1996.

[4] P. Demontis, G.B. Suffritti, Chem. Rev. 97 (1997) 2845.

[5] J. Kärger, Molecular transport in zeolites (miracles, insights and practical issues), in: Proceedings of the 13th International Zeolite Conference, Materials Research Society, Warrendale, 1999, Baltimore, 1998.

[6] S.M. Auerbach, F. Jousse, D.P. Vercauteren, Dynamics of sorbed molecule, Computer Modelling of Microporous and Mesoporous Materials, 2001.

[7] R. Haberlandt, S. Fritzsche, H.L. Vörtler, Simulation of microporous systems: confined fluids in equilibrium and diffusion in zeolites, in: Handbook of Surfaces and Interfaces of Materials, vol. 5, Academic Press, San Diego, London, Boston, New York, Sydney, Tokyo, Toronto, 2001.

[8] J. Kärger, S. Vasenkov, S.M. Auerbach, Diffusion in zeolites, Handbook of Zeolite Science and Technology, Marcel Dekker Inc., New York, 2003.

[9] J. Kärger, Adsorption 9 (2003) 29.

[10] M.P. Allen, D. Tildesley, Computer Simulation of Liquids, Clarendon Press, Oxford, 1989.

[11] R. Haberlandt, S. Fritzsche, G. Peinel, K. Heinzinger, Molekulardynamik – Grundagen und Anwendungen, Vieweg-Verlag, Wiesbden, 1995.

[12] S. Fritzsche, R. Haberlandt, J. Kärger, H. Pfeifer, K. Heinzinger, Chem. Phys. 174 (1993) 229.

[13] C. Bussai, S. Hannongbua, R. Haberlandt, J. Phys. Chem. B 105 (2001) 3409.

[14] C. Bussai, S. Hannongbua, S. Fritzsche, R. Haberlandt, Chem. Phys. Lett. 354 (2002) 310.

[15] C. Bussai, S. Vasenkov, H. Liu, W. Böhlmann, S. Fritzsche, S. Hannongbua, R. Haberlandt, J. Kärger, Appl. Catal. A 232 (2002) 59.

[16] J. Caro, M. Bülow, W. Schirmer, J. Kärger, H. Pfeifer, S. Ždanov, J. Chem. Soc., Faraday Trans. I 81 (1985) 2541.

[17] J. Caro, S. Hocevar, J. Kärger, L. Riekert, Zeolites 6 (1986) 213.

[18] R.L. June, A.T. Bell, D.N. Theodorou, J. Phys. Chem. 96 (1992) 1051.

[19] B. Smit, J. Phys. Chem. 98 (1994) 8442.

[20] T.J.H. Vlugt, R. Krishna, B. Smit, J. Phys. Chem. B 103 (1999) 1102.

[21] C. Baerlocher, W.M. Meier, D.H. Olson, Atlas of Zeolite Framework Types, Elsevier, Amsterdam, 2001.

[22] J.P. Ryckaert, A. Bellemans, Faraday Discuss. Chem. Soc. 66 (1978) 95.

[23] W.L. Jorgensen, J.D. Madura, C.J. Swenson, J. Am. Chem. Soc. 106 (1984) 6638.

[24] B. Smit, J. Chem. Phys. 99 (1995) 5597.

[25] P. Demontis, G.B. Suffritti, A. Tilocca, J. Chem. Phys. 105 (1996) 5586.

[26] S. Frtizsche, M. Wolfsberg, R. Haberlandt, Chem. Phys. 289 (2003) 321.

[27] D. Cremer, in: Møller-Plesset Perturbation Theory, Encyclopedia of Computational Chemistry, vol. 3, Wiley, Chichester, 1998.

[28] C. Bussai, S. Fritzsche, R. Haberlandt, S. Hannongbua, A novel Møller-Plesset perturbation based potential to determine structural and dynamical properties of methane in silicalite-1: a molecular dynamics study, J. Phys. Chem. (submitted).

[29] M.G. Martin, J.I. Siepmann, J. Phys. Chem. B 103 (1999) 4508.

[30] A. Poncela, A. Rubio, J. Freire, Mol. Phys. 91 (1997) 189.

[31] W. Heink, J. Kärger, H. Pfeifer, K. Datema, A. Nowak, J. Chem. Soc., Faraday Trans. 88 (1992) 3505.

[32] J. Kärger, J. Phys. Chem. 95 (1991) 5558.

[33] E.J. Maginn, A.T. Bell, D.N. Theodorou, J. Phys. Chem. 100 (1996) 7155.

[34] P. Demontis, E. Fois, G. Suffritti, S. Quartieri, J. Phys. Chem. 96 (1992) 1482.

[35] C. Bussai, S. Fritzsche, R. Haberlandt, S. Hannongbua, J. Phys. Chem. B 107 (2003) 12444.

Appendix B:

Energy Barrier of Water and Methane Molecules due to the Silanol Groups on the (010) Surface of Silicalite-1 as studied by Quantum Chemical Calculations

O. Saengsawang, T. Remsungnen, **A. Loisruangsin**, S. Fritzsche, R. Haberlandt and S. Hannongbua
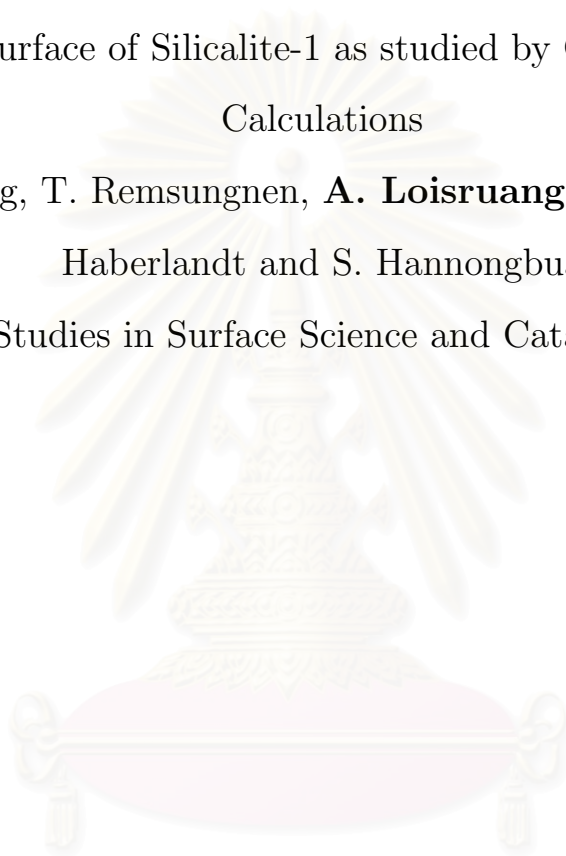
Studies in Surface Science and Catalysis

Energy barrier of water and methane molecules due to the silanol groups on the (010) surface of silicalite-1 as studied by quantum chemical calculations

O. Saengsawang[a], T. Remsungnen[b], A. Loisruangsin[a], S. Fritzsche[c], R. Haberlandt[c] and S. Hannongbua[a,*]

[a]Department of Chemistry, Faculty of Science, Chulalongkorn University, Bangkok 10330, Thailand

[b]Department of Mathematic, Faculty of Science, Khon Kaen University, Khon Kaen 40002, Thailand

[c]Department of Molecular Dynamics/Computer Simulation, Faculty of Physics and Geoscience, Institute for Theoretical Physics (ITP), University of Leipzig, Germany

Quantum mechanical calculations at different levels, HF/6-31G(d,p), B3LYP/6-31G(d,p), HF/6-31++G(d,p), and B3LYP/6-31++G(d,p), have been applied to investigate the interaction between guest molecules, water and methane, and the external surface of silicalite-1. The (010) surface which is perpendicular to the straight channel was selected and the silanol groups on the surface were generated by adding hydrogen atoms to the broken O-Si bonds. The complex geometries were fully optimized. The optimal B3LYP/6-31++G(d,p) binding energies on the external (010) surface of -13.84 kcal/mol and -0.26 kcal/mol were yielded for water and methane molecule, respectively. With the same method, the binding energy in the channel was -4.76 kcal/mol for water and -3.87 kcal/mol for methane binding. This leads to the estimated energy barrier to enter the straight channel via binding with the silanol group on the (010) surface of silicalite-1 of 9.08 kcal/mol for water while this process is barrier free for methane molecules.

1. INTRODUCTION

Zeolites are aluminosilicate materials which have high porosity and well-defined structures consisting of cavities and channels so, that molecules of suitable size and shape can readily diffuse. It is known that the surfaces of most of the zeolitic and amorphous silica materials are covered by silanol groups. However, before the activities in the pore of zeolite take place, guest molecules have to interact with the external surface, then, they diffuse into the pore opening of the zeolite. The key elements determining the adsorption or diffusion of guest molecules on the external surfaces as well as in the channels are interactions between guest molecules and the silanol groups on the zeolite surface. This can lead to an energy barrier

preventing guest molecules to penetrate through the zeolite surface into the channel. Moreover, the efficiency of the technical processes can be limited by this barrier in some cases, while the barrier is the crucial element in other applications, e. g., separation processes.

Silicalite-1 is a pure silica analogue of zeolite ZSM-5 which is an MFI type material comprising two types of channels: straight channels (5.3×5.6 Å^2) and sinusoidal (zigzag) channels (5.1×5.5 Å^2) [1]. The (010) surface of silicalite-1 is perpendicular to the straight channel. Silicalite-1 is widely used to separate paraffin or aromatics from water or other polar solvents as well as to sieve the molecules having different shapes [2-4].

In this study, the interaction between the silanol groups on the external surface of silicalite-1 and guest molecules, water and methane, were investigated using quantum chemical calculations. The energy barriers of guest molecules to enter into the silicalite-1 channels were, then, estimated.

2. CALCULATION DETAILS

2.1. Binding energies between guest molecules and the external surface of the silicalite-1

The (010) external surface of silicalite-1 (Fig. 1) which is perpendicular to the straight channels, was selected and cut from the idealized infinite MFI crystal lattice. The silanol groups on the silicalite-1 surface were represented by cluster models taken from different parts of the surface and named, for simplicity, as Single, Double-near and Double-far (see also Fig. 1), respectively. Then, the broken bonds were closed by hydrogen atoms. The three clusters, were, respectively, used to model interactions with the isolated (single) silanol and two possible configurations of the two (double) contacted silanols on the (010) surface. All O-H bond lengths and Si-O-H angles as well as the rotation of isolated silanol groups around the Si-O bond were optimized, using different levels of quantum chemical calculations. The chemical compositions of the selected Single, Double-near and Double-far fragments, after filling up the remaining valence orbitals of the oxygen atoms by hydrogen atoms, are $Si_4O_{13}H_{10}$, $Si_7O_{22}H_{16}$ and $Si_9O_{27}H_{18}$, respectively.

Several possible configurations of water molecules were assigned to bind to single and double silanol groups as shown in Fig. 2. Three mono-hydrated (Fig. 2a-2c) and one di-hydrated (Fig. 2d) configurations are considered for single silanol groups. For the Double-near silanol, the three mono-hydrated configurations were shown in Fig. 2e-2g, while for the Double-far, one mono-hydrated (Fig. 2h) and another bridged di-hydrate (Fig. 2i) were chosen. Note that the distance between the two silanols in the Double-far system is too large to form hydrogen bonds with one water molecule as in the configurations shown in Fig. 2f and 2g.

For the complexes, interactions between the surface and methane molecules were evaluated in the two configurations. Single and Double-near, shown in Fig. 3a-3b. For the same reason as in the case of water molecules, the interaction between methane and the silicalite-1 surface in the Double-far configuration (see Fig. 2h-2i) was not taken into consideration.
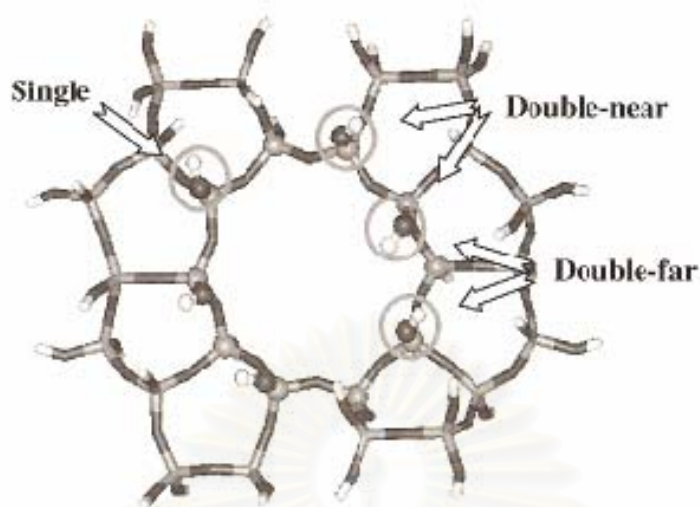
Fig. 1. The (010) surface of the silicalite-1 where three groups of silanols are defined: Single, Double-near and Double-far.

Fig. 2. Several possible configurations of water molecules were assigned to bind to single (a-d), Double-near (e-g) and Double-far (h-i) silanol groups on the (010) surface of the silicalite-1. The corresponding binding energy was obtained when the complex geometry was optimized using the B3LYP/6-31++G(d,p) method with the BSSE correction.

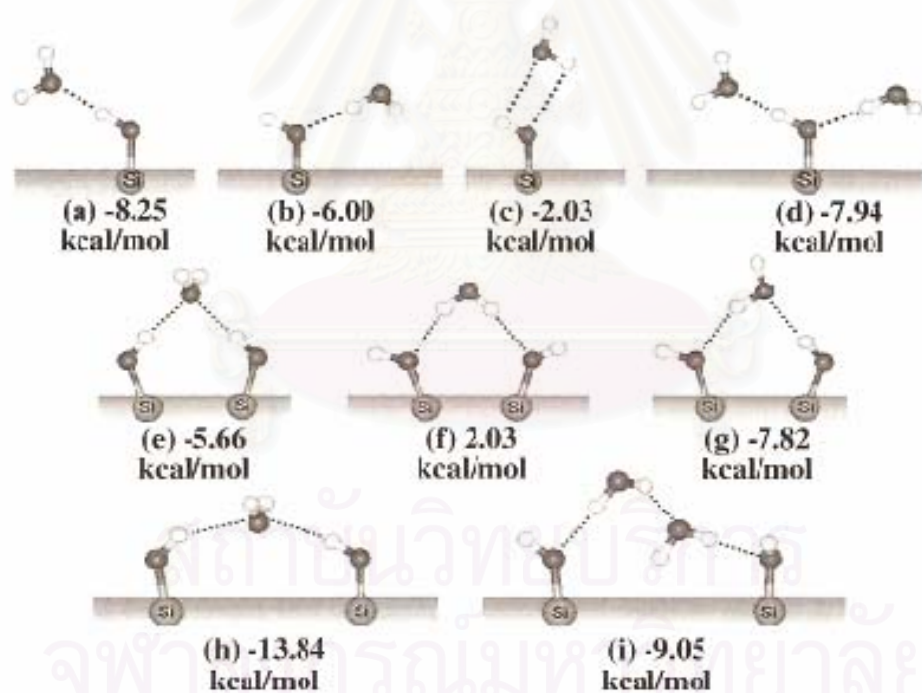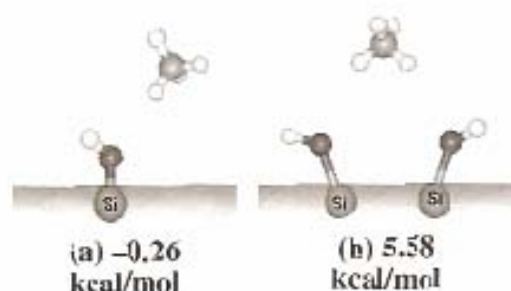Fig. 3. Investigated conformations representing interaction between a methane molecule and the Single (a) and Double (b) silanol groups on the silicalite-1's surface. The corresponding binding energy was obtained when the complex geometry was optimized using the B3LYP/6-31++G(d,p) method with the BSSE correction.

The geometries of the above mentioned complexes were, then, fully optimized. Precisely, the intramolecular geometry of the water molecule (O-H bonds and H-O-H angle), of the methane molecule (C-H bonds and H-C-H angles) and of the silanol group (O-H bond) as well as the intermolecular parameters (distances and orientation of water and methane molecules relative to the silanol group) were fully optimized. Different levels of the quantum chemical calculations, HF/6-31G(d,p), B3LYP/6-31G(d,p), HF/6-31++G(d,p), and B3LYP/6-31++G(d,p), were applied in order to seek for the appropriate method. To correct an error due to an unbalance of the basis set, the basis set superposition error (BSSE), was also taken into account. All of the calculations are calculated by the GAUSSIAN03 package [5].

2.2. Energy barrier estimation

To estimate the energy barrier, $\Delta E_{barrier}$, for guest molecules to enter into the zeolite's pore, a detailed schematic representation was shown in Fig. 4. The optimal binding energy for the guest molecule at the center of the 10-oxygen membered ring (shown in Fig. 1) was calculated; the guest molecule was put at the center of the fragment as shown in the insets a and b of Fig. 4 for water and methane molecules, respectively, then, their orientations were fully optimized. When the guest molecules are located inside the straight channel of the silicalite-1, the obtained data were used as the optimal binding energies, $\Delta E_{bind-in}$. In addition, the optimal binding energy outside the channel, $\Delta E_{bind-out}$, was represented by that obtained from the binding energy between guest molecules and external silanol groups (Fig. 2 and 3). With these criteria, the $\Delta E_{barrier}$ for a guest molecule to enter the straight channel via the adsorption due to the silanol groups on the (010) surface of the silicalite-1 can be estimated from the energetic difference ($\Delta\Delta E$) between the $\Delta E_{bind-in}$ and the $\Delta E_{bind-out}$ as defined in Fig. 4.
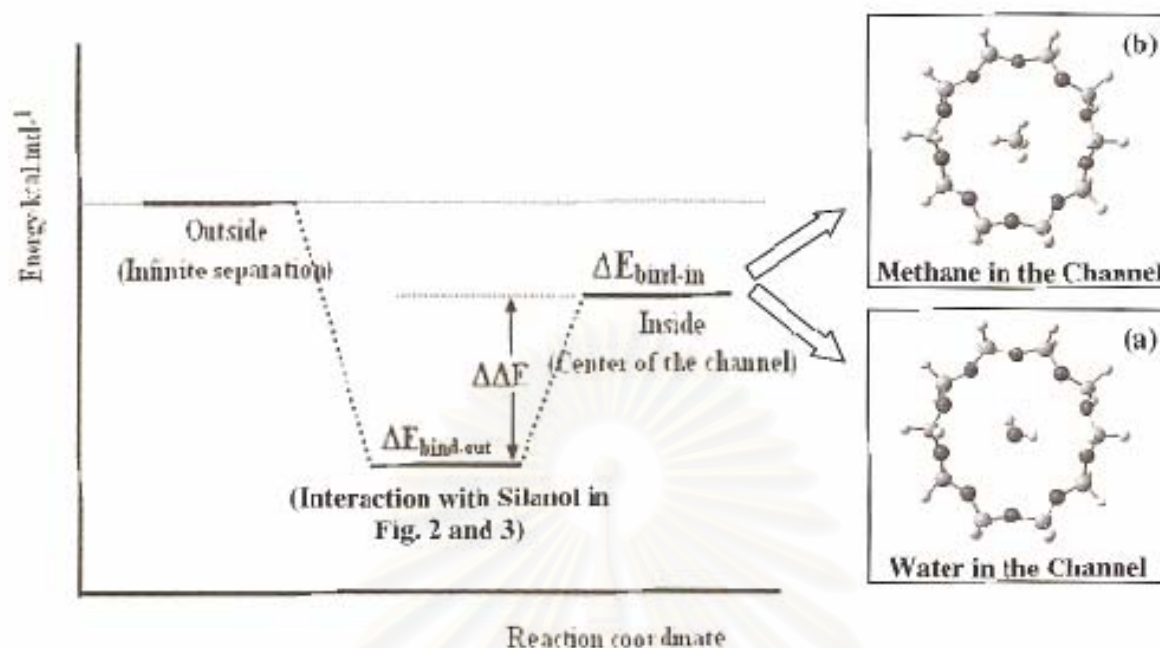
Fig. 4. Binding energies when the guest molecule coordinates to the silanol group outside the channel ($\Delta E_{bind\text{-}out}$) and at the center of the channel ($\Delta E_{bind\text{-}in}$) as well as their differences ($\Delta\Delta E$) which were used to estimate the energy barriers ($\Delta E_{barrier} = \Delta\Delta E$) for guest molecules to enter into the straight channel of the silicalite-1 via the (010) surface (see the text for more details).

3. RESULT AND DISCUSSION

In order to find an optimum between the time required for computation and reliability of the method used, the following two calculation steps were applied in the quantum chemical calculations. First, optimize the geometry of the complex using the Hartree-Fock method with the 3-21G* basis set, HF/3-21G*, then, perform the single point calculation using different levels of accuracy, HF/6-31G(d,p), HF/6-31++G(d,p), B3LYP/6-31G(d,p) and B3LYP/6-31++G(d,p), to get the energy of the complexes. Note that BSSE was taken into consideration for all data points.

With the four selected configurations and the two calculation steps for a single silanol (Fig. 2a-2d), the interactions between a water molecule and a single silanol group were summarized in Table 1. Here, the following conclusions could be made: *(i)* With the same basis set, the binding energies obtained from the B3LYP method are significantly slower than those resulting from the HF approach. *(ii)* Among the three configurations complexed with one water molecule, all calculations predict the configuration shown in Fig. 2a as the most stable conformation i.e., the water molecule points its O atom so that it forms a linear hydrogen bond with the H atom of the silanol. But, the other configurations have still a nonvanishing probability measured by their Boltzmann weight. *(iii)* With the same method, the 6-31++G(d,p) basis set gives the binding energy higher than those given by 6-31G(d,p).

952

Table 1

The birding energies (kcal/mol) between water and single silanol groups in the configurations shown in Fig. 2a-2d where the complex geometry was optimized using the HF/3-21G* while the energy was calculated using different levels of accuracy.

Configurations in Fig	HF/6-31G(d,p)	HF/6-31++G(d,p)	B3LYP/ 6-31G(d,p)	B3LYP/ 6-31++G(d,p)
2a	-5.01	-4.04	-7.01	-5.85
2b	-1.73	-1.38	-3.80	-3.12
2c	0.23	0.13	-0.54	-0.68
2d	-6.44	-5.01	-11.34	-9.83

Variations of the binding energy due to the method and the basis set used were clearly found in the Table 1. The reason for the discrepancy can be due to the fact that the optimal geometry of the surface yielding from the HF/3-21G* and used for the single point calculation, is not the optimal form for the higher levels calculations. This means that the two-step procedure, optimize molecular geometry using the cheaper method and perform single point calculation to compute the energy of the system using the more reliable one, which is normally applied for the big molecular systems in order to reduce the computation time, is not appropriate for the investigated system. Therefore, the B3LYP method with the 6-31++G(d,p) basis set was decided to be used for both steps, geometry optimization and single point calculation, for all complexes. The obtained binding energies for 9 and 2 complex geometries of water and methane molecules are given in Fig. 2 and 3, respectively. Here, the optimal B3LYP/6-31++G(d,p) binding energy for the water molecule on the external (010) surface of the silicalite-1 is -13.84 kcal/mol. The corresponding value for the methane molecule is -0.26 kcal/mol. These two data were defined as the binding energy outside the channel ($\Delta E_{bind-out}$).

With the calculation details given above, the optimal binding energies inside the pore ($\Delta E_{bind-in}$) for water and methane molecules are -4.76 kcal/mol and -3.87 kcal/mol respectively. With the schematic shown in Fig. 4, the energy barrier ($\Delta E_{barrier}$) can be estimated from the $\Delta\Delta E$. The energy data were summarized in Table 2 and represented in Fig. 5.

Table 2

Optimal binding energies (kcal/mol) on the surface ($\Delta E_{bind-out}$), optimal binding energy inside the pore ($\Delta E_{bind-in}$), ($\Delta\Delta E$) and the estimated energy barrier ($\Delta E_{barrier}$) for H_2O and CH_4 molecules to enter into the straight channel via the (010) surface of the silicalite-1.

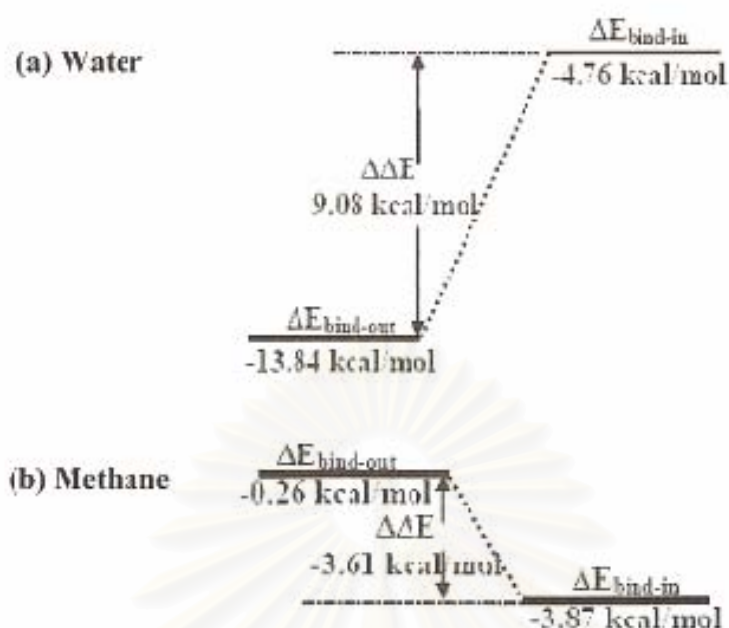| Guest molecule	$\Delta E_{bind-out}$	$\Delta E_{bind-in}$	$\Delta\Delta E$	$\Delta E_{barrier}$
H_2O	-13.84	-4.76	9.08	9.08
CH_4	-0.26	-3.87	-3.61	0.00 (barrier free)

Fig. 5. The estimated energy barrier ($\Delta E_{barrier}$), yielded from the B3LYP/6-31++G(d,p) calculations for (a) water and (b) methane molecules.

It can be seen that the strong silanol/water binding leads to a high barrier of 9.08 kcal/mol for water molecules to enter into the straight channel via the (010) surface. In contrast, the methane molecule moves from the higher energy state (-0.26 kcal/mol) on the (010) surface to the lower energy one (-3.87 kcal/mol) inside the pore. Therefore, the entering process for methane molecules is barrier free.

Experimentally, an external force has to be activated by keeping the sample under high vacuum at 473 K for 20 hours in order to bring water molecules into the pore of silicalite-1 [6]. This fact supports our observation of an energy barrier, due to the silanol/water binding on the (010) surface, of 9.08 kcal/mol.

ACKNOWLEDGEMENTS

954

REFERENCES

[1] Ch. Baerlocher, W.M. Meier, D.H. Olson. Atlas of zeolite framework types. Fifth edition, Elsevier, Amsterdam 2001.

[2] E. Jolimaitre, M. Tayakout-Fayolle, C. Jallut, K. Ragil, Ind. Eng. Chem. Res., 40 (2001) 914.

[3] T. Sano, S. Ejiri, K. Yamada, Y. Kawakami, H. Yanagishita, J. Membr. Sci., 123 (1997) 225.

[4] T. Sano, M. Hasegawa, Y. Kawakami, H. Yanagishita, J. Membr. Sci., 107 (1995) 193.

[5] Gaussian 03, Revision C.02, M. J. Frisch, G. W. Trucks, H. B. Schlegel, G. E. Scuseria, M. A. Robb, J. R. Cheeseman, Jr. J. A. Montgomery, T. Vreven, K. N. Kudin, J. C. Burant, J. M. Millam, S. S. Iyengar, J. Tomasi, V. Barone, B. Mennucci, M. Cossi, G. Scalmani, N. Rega, G. A. Petersson, H. Nakatsuji, M. Hada, M. Ehara, K. Toyota, R. Fukuda, J. Hasegawa, M. Ishida, T. Nakajima, Y. Honda, O. Kitao, H. Nakai, M. Klene, X. Li, J. E. Knox, H. P. Hratchian, J. B. Cross, V. Bakken, C. Adamo, J. Jaramillo, R. Gomperts, R. E. Stratmann, O. Yazyev, A. J. Austin, R. Cammi, C. Pomelli, J. W. Ochterski, P. Y. Ayala, K. Morokuma, G. A. Voth, P Salvador, J. J. Dannenberg, V. G. Zakrzewski, S. Dapprich, A. D. Daniels, M. C. Strain, O. Farkas, D. K. Malick, A. D. Rabuck, K. Raghavachari, J. B. Foresman, J. V. Ortiz, Q. Cui, A. G. Baboul, S. Clifford, J. Cioslowski, B. B Stefanov, G. Liu, A. Liashenko, P. Piskorz, I. Komaromi, R. L. Martin, D. J. Fox, T. Keith, M. A. Al-Laham, C. Y. Peng, A. Nanayakkara, M. Challacombe, P. M. W. Gill, B. Johnson, W. Chen, M. W. Wong, C. Gonzalez and J. A. Pople, Gaussian, Inc., Wallingford CT, 2004.

[6] C. Bussai, H. Liu, S. Vasenkov, S Hannongbua, S. Fritzsche, R. Haberlandt, J. Kaerger, Appl. Catal. A, 232 (2002) 59.

Appendix C:

Optimal Binding Site of a Methane Molecule on the Silanol Covered (010)
Surface of Silicalite-1:ONIOM Calculations

T. Remsungnen, V. Kormiltes, **A. Loisruangsin**, A. Schring, S. Fritzsche

R. and Haberlandt, S

J. Phys. Chem. B
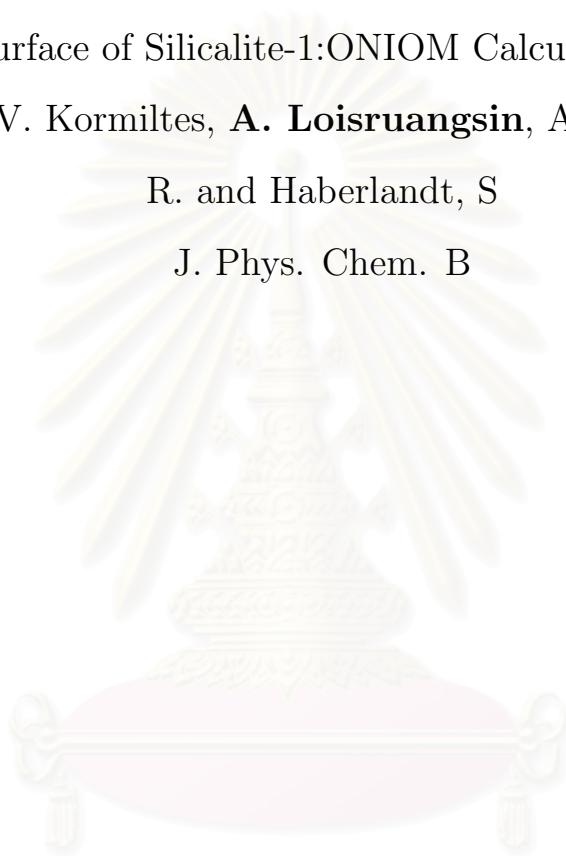
Optimal Binding Site of a Methane Molecule on the Silanol Covered (010) Surface of Silicalite-1: ONIOM Calculations

T. Remsungnen,*,† V. Kormilets,‡ A. Loisruangsin,§ A. Schüring,‡ S. Fritzsche,‡ R. Haberlandt,‡ and S. Hannongbua*,§

Department of Mathematics, Faculty of Science, Khon Kaen University, Khon Kaen 40002, Thailand, Department of Molecular Dynamics/Computer Simulation, Faculty of Physics and Geosciences, Institute for Theoretical Physics (ITP), University of Leipzig, Augustusplatz 10-11, 04109 Leipzig, Germany, and Department of Chemistry, Faculty of Science, Chulalongkorn University, Bangkok 10330, Thailand

The binding energies and the corresponding structures of a methane molecule on the silanol covered (010) surface of silicalite-1 have been investigated using ab initio methods. Different levels of calculations, HF/6-31G(d), MP2/6-31G(d) and ONIOM (MP2/6-31G(d):HF/6-31G(d)) including the correction of an error due to an unbalance of the basis set, known as basis set super position error (BSSE), as well as the size of the cluster representing the silicalite-1 surface, were systematically examined to validate the model used. The ONIOM method with the BSSE correction was found to be a compromise between accuracy and computer time required. The optimal binding site on the silicalite-1 surface was observed at the configuration where the methane molecule points one H atom toward the O atom of the silanol group. The corresponding binding energy is -1.71 kJ/mol. This value is significantly higher than that of -5.65 kJ/mol when the methane molecule approaches the center of the straight channel. At this configuration, the C atom of methane was observed to locate exactly at the center of the channel. This leads to the conclusion that the methane molecule will relatively seldom be adsorbed on the silanol covered (010) surface of silicalite-1. Instead, the adsorption process will take place directly at the center of the straight channel.

1. Introduction

During the past decades the economical as well as the scientific interest in zeolites increased rapidly. These alumino-silicates contain a regular system of nanosize pores and/or channels and in many cases they also contain exchangeable cations. Therefore, zeolites are used in industries as molecular sieves, catalysts and adsorbents. However, in any one of these applications guest molecules have to enter the zeolite crystallites before diffusing within the pore system. They have to move through the pore opening; i.e., they have to interact with the external surface of the zeolite.

Only recently[1–15] has the behavior of guest molecules on the zeolite surface been studied. It is known that the surface of most of the zeolitic and amorphous silica materials is covered by silanol groups. Therefore, the interaction with the silanol covered surface is crucial for all applications using the adsorption and diffusion of guest molecules in zeolites.

Most of the information on the characteristics of silanol on the external surface of zeolites arises from FTIR experiments.[16–24] It was observed that the O−H bond of silanol groups is softened when interacting with nitriles,[17–20] alcohols,[21] water,[22,23,25] pyridine and even with aliphatic and aromatic hydrocarbons.[19]

In IR measurements, it has been found that methane molecules are adsorbed at the surface OH groups of a silica surface in remarkable amount only at low temperatures.[26] This leads to

the assumption that these OH groups form adsorption centers of low adsorption energy on a silica surface. A weak interaction of methane with OH surface groups has also been found in numerical simulations of methane on silicalite.[27] These simulations have been carried out using empirical classical potentials. To our knowledge such measurements for the silicalite surfaces or examinations of this system using ab initio calculations are not available. Therefore, this is one of the aims of the present paper.

Noncationic zeolites, in particular silicalite-1, are widely used in the separation of mixtures between light hydrocarbons and water or other polar solvents because of the hydrophobic nature of the internal surface, whereas its external surface is hydrophilic. The latter property can be attributed to terminal silanol groups that are able to interact with guest molecules. However, most of the experimental and theoretical works focus on the internal surface, the pore or channel, whereas much less is known about the details of the external surface. Recently, the interaction between water molecules and the silanol covered surface of the silicalite-1 was, theoretically, studied.[28] Optimal binding sites, binding energies and orientations of water molecules were investigated and discussed in comparison with the experimental data.

In this investigation, the structure and the interaction between methane molecules and the silanol groups on the external surface of silicalite-1 was examined. The energetic and geometric optimizations have been performed using quantum chemical calculations at the HF and MP2 level. A combination of both methods, known as ONIOM (MP2:HF), was also examined to seek an appropriate technique for the investigated system.

---

* Corresponding authors. E-mail: Supot.h@chula.ac.th (S.H.); rtawun@kku.ac.th (T.R.).
† Khon Kaen University.
‡ University of Leipzig.
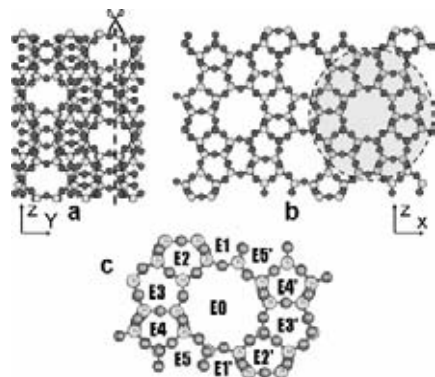§ Chulalongkorn University.

Figure 1. Side-view of the silicalite-1 lattice (a) where the (010) surface was cut along the dashed line and circles. The obtained top-view of the (010) surface can be seen in (b) and (c). The straight channel in (c) was labeled as E0 and the adjacent channels are named as Ei and Ei' where $i = i' = 1-5$.

2. Details of the Calculations

2.1. Surface Model of Silicalite-1. The idealized lattice of the MFI framework was obtained from the IZA database.[29] The lattice was cut along the dashed line in Figure 1a. The obtained (010) surface (Figure 1b), which is perpendicular to the straight channels, was, again, cut by the circle. The resulting fragment shown in Figure 1c was used for this study. Hydrogen atoms were added to the broken −Si−O− bonds. The Si−OH and Si−H bonds were optimized using quantum chemical calculation at the HF/6-31G(d) level. The obtained Si−OH groups were assumed to represent the silanols on the (010) surface of the silicalite-1. For simplicity, an area perpendicular to the straight channel, the 10 oxygen membered ring, was named as an E0 ring and the adjacent channels were labeled as Ei and Ei' where $i = i' = 1-5$ (see Figure 1c).

2.2. Test of the ONIOM Method. The high accuracy level, correlated method (MP2) that had been proven to be a feasible method for the calculation of van der Waals complexes[30,31] and was successfully used in our previous works[28,32,33] was again applied in this study. On one hand, the system fragment in Figure 1c is still too large to take into account all atoms in the MP2 calculations. On the other hand, use of each single E0−E5 ring will be too small to represent the silicalite-1 (010) surface. Seeking for an optimal compromise between fragment size vs the required computer time, MP2/6-31G(d) and ONIOM-(MP2/6-31G(d):HF/6-31G(d)) calculations were examined. For the quantum MP2/6-31G(d) calculations, the surface was represented by the fragment given in Figure 2a (which is half of the fragment shown in Figure 1c). Then, the methane molecule was located above the centers of the E3 rings and oriented in the configurations where one H atom points away from the center of the ring. The distance between the C atom of methane and the center of the ring was optimized. The binding energy including the basis set superposition error (BSSE) correction was calculated and analyzed.

For the ONIOM calculations, the model part (Figure 2b), which is a subset of the real part and covers the reaction area, the more accurate MP2/6-31G(d) method was applied. However, the real part that covers the whole fragment shown in Figure 2a (including the real part in Figure 2b) was treated by a low level method, HF/6-31G(d). The ONIOM interaction energy of the system, E_{ONIOM}, is derived as

$$E_{\mathrm{ONIOM}} = E_{\mathrm{real,low}} + E_{\mathrm{model,high}} - E_{\mathrm{model,low}} \quad (1)$$

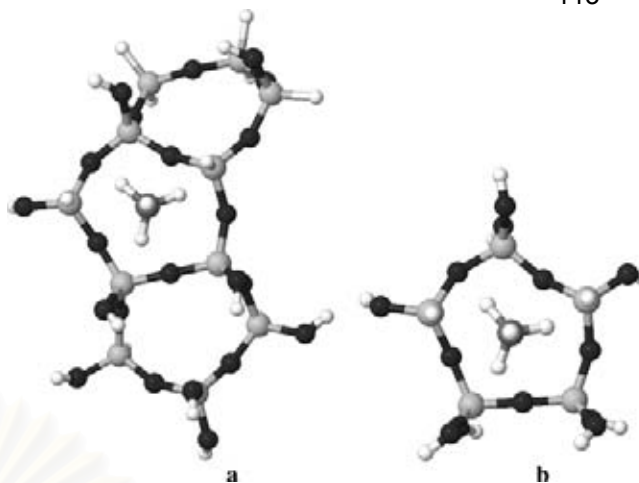where $E_{\mathrm{real,low}}$ is the total energy of the real system using the

Figure 2. Real (a) and the model (b) parts used for examining the ONIOM method.

low level method and $E_{\mathrm{model,high}}$ and $E_{\mathrm{model,low}}$ define the total energies of the model part calculated with high and low level methods, respectively.

2.3. Optimal Methane-Surface Binding Energy. To reduce the scope of the calculation, the E1−E5 rings are, respectively, assumed to be identical to the E1′−E5′ ones. With this approximation, the methane molecule was assigned to approach the surface only in the first half of the surface shown in Figure 2a. Therefore, the calculations were focused only on the complex structure in the E1−E5 and center of the E0 rings. The methane molecule in the two orientations (H-in and H-out in Figure 3b) was positioned at several points (labeled as 1−10 in Figure 3a), 2.25 Å above the silanol covered surface. The distance from the C atom of the methane molecule to point i, where $i = 1-10$ labeled in Figure 3a, was optimized in the path perpendicular to the surface. The center of mass of all Si atoms of each ring is defined to be the origin of the coordinate frame for the potential calculations on paths 7−10.

The binding energy, ΔE_{bind}, is defined according to the supermolecular approach, as shown in

$$\Delta E_{\mathrm{bind}} = E_{\mathrm{cpx}} - E_{\mathrm{met}} - E_{\mathrm{sur}} \quad (2)$$

where E_{cpx} is the total energy of the complex calculated by the ONIOM method and E_{met} and E_{sur} are the total energies of the methane molecule and of the fragment surface, respectively. All calculations were performed using the GAUSSIAN03 program.[34]
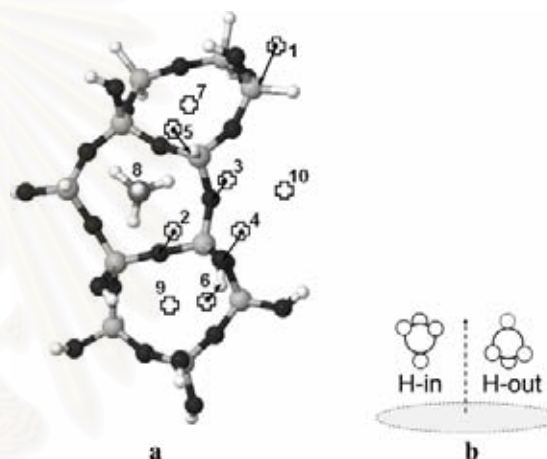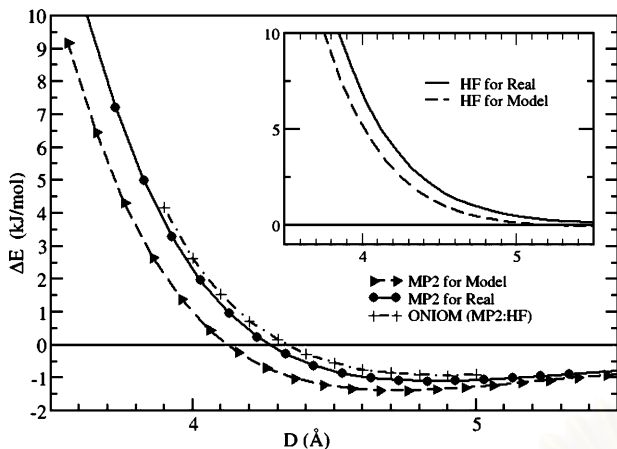

Figure 3. Methane molecule initially located at 2.5 Å above and perpendicular to the points labeled by 1−10 (a) in the two configurations, H-in and H-out (b).

Figure 4. Binding energy including BSSE corrections for the real and model systems (see Figure 2) calculated using MP2 and ONIOM method when the methane molecule is in the configuration H-in (see Figure 3b) and moves perpendicular to the center of the E3 ring (see Figure 3a), where D denotes the distance from the C atom of methane to the center of the E3 ring. The HF calculation is also depicted for comparison.

3. Results and Discussions

3.1. Validity of the Method. According to the calculation details mentioned above where the HF, MP2 and ONIOM interaction energies were evaluated using the partition shown in Figure 2 and the methane molecule was located and moved perpendicular to the E3 rings in the configuration H-in, the results were plotted and compared in Figure 4. Note that the BSSE corrections were taken into account for all data points. From the plots, the following conclusions can be made: (i) The interaction energies (dashed lines in an inset of Figures 4) yielded from the small fragment size (model part, Figure 2b) differ significantly from those of the surface of bigger size (real part, Figure 2a). A clear conclusion is that the small cluster size, such as E3 in Figure 2b, is not enough to represent the calculated system. (ii) Interestingly, the ONIOM (MP2/6-31G-(d):HF/6-31G(d)) interaction energies (dotted line in Figure 4) are almost identical to those yielded from the MP2 method (solid line in Figure 4). Note that the bigger fragment in Figure 2a was used in the MP2 calculation.

Taking into account all the data and conclusions given above, the ONIOM (MP2/6-31G(d):HF/6-31G(d)) calculation with the BSSE correction was selected and used throughout to investigate the interaction between the methane molecule and the silanol covered (010) silicalite-1 surface. This is in good agreement with that reported by Sauer et al.[35] on the adsorption of the NH_3 and H_2O molecules in acidic chabazite.

3.2. Optimal Binding Site of Methane. In Table 1, the ONIOM binding energies representing the methane/surface interaction in which the surface is represented by the fragment as shown in Figures 3a (equivalent to that in Figure 2a or half of that in Figure 1c) and methane is in the configurations H-in and H-out (see Figure 3b) were summarized. The 10 trajectories are classified into 3 groups where the H-in or H-out configuration of the methane molecule is perpendicular to the atoms (Si, O or H, trajectories 1−6), the center of the small rings (E2−E4, trajectories 7−9) and the center of the 10-membered ring (path 10) of the silicalite-1 surface.

Among the trajectories where the methane molecule points one H atom toward/away from the atoms of the surface, the O atom of the silanol group (path 4 in Table 1 and Figure 3a) was found to be the most favorable binding site. The corresponding binding energy in the H-in configuration is −1.71 kJ/

TABLE 1: Optimal ONIOM Distances (D_{opt} in Å from the C Atom of the Methane Molecule to Point i, Where i = 1−10 Labeled in Figure 3a) and the Corresponding Binding Energies (ΔE_{bind} in kJ/mol) Representing the Methane/ Surface Interaction in Which the Methane Molecule Points One of the H Atoms toward (H-in) and Away from (H-out) the Surface (Figure 3b)

	relative orientation H-in		relative orientation H-out	
path i, i = 1−10 in Figure 3a	D_{opt}	ΔE_{bind}	D_{opt}	ΔE_{bind}
H of CH₄ Points toward/Away from the Atom				
1. Si	5.00	−1.36	5.00	−1.15
2. O of Si−O−Si	4.90	−1.51	4.70	−1.62
3. O on the 10-membered ring	5.30	−1.36	5.30	−0.65
4. O of H−O−Si	4.00	−1.71	4.10	−0.62
5. H of H−Si	3.90	−0.74	3.60	−0.61
6. H of H−O	4.10	−0.47	3.30	−1.31
H of CH₄ Points toward/Away from the Center of the Ring				
7. E2	5.90	−1.94	6.30	−1.24
8. E3	4.90	−1.23	4.60	−1.68
9. E4	5.40	−2.54	5.40	−2.12
H of CH₄ Points toward/Away from the Center of the 10-Membered Ring				
10. E0	0.00	−4.26	0.8	−5.75

mol with the D_{opt} distance (from the C atom of the methane to the O atom of the silanol group) of 4.00 Å. Due to a very weak interaction between the methane molecule and the hydrophilic silanol covered surface of the silicalite-1, the potential energy curve shows a very broad minimum. Examples are the MP2 and the ONIOM binding energies for the E3 ring shown in Figure 4b. Therefore, a clear conclusion, in terms of the binding energy and the optimal distance, cannot be made because the energy of binding in different trajectories and orientations lies within the range of the thermal fluctuation at room temperature. Note that kT at room temperature is about 2.5 kJ/mol where T denotes the temperature in Kelvin and k is Boltzmann's constant.

For the trajectories pointing to the centers of small size channels, E2−E4 rings, the most stable binding site is situated at the center of the E4 ring (path 9 in Table 1) in the configuration H-in. The corresponding binding energy and distance are −2.54 kJ/mol and 5.40 Å, respectively.

Considering the path E0 in which the methane molecule moves to the center of the straight channel, more details were additionally investigated and plotted in Figure 5. In the configuration H-in (solid line in Figure 5), the first minimum was detected at the D_{opt} (from C atom of methane to center of the E0 ring) of 2.90 Å. At shorter distance, repulsion between
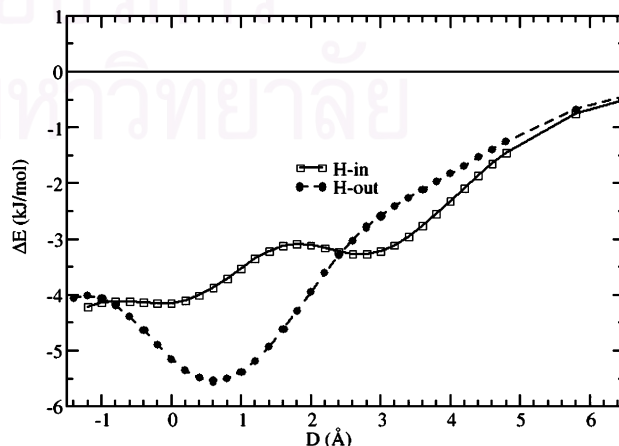

Figure 5. Binding energies ΔE_{bind} when the methane molecule is in the configurations H-in and H-out (Figure 3b) and moves perpendicular to the center of the E0 ring (Figure 3a), where D_{opt} denotes the distance from the C atom of methane to the center of the E0 ring.

D *J. Phys. Chem. B* PAGE EST: 3.9 Remsungnen et al.

115

the H atoms of methane and the atoms of the 10-oxygen membered ring leads to a slight increase of the binding energy. After a broad maximum at $D_{opt} = 1.80$ Å the binding energy, again, decreases and remains constant at −4.14 kJ/mol between $D_{opt} = 0.0$ and −1.50 Å (minus value of the D_{opt} denotes the position where the methane molecule is under the surface). Note that at $D_{opt} = 0.0$ Å in the H-in configuration, the C atom of methane is located at the center of the straight channel.

For the configuration where one H-atom of methane points away from the surface, H-out, the binding energy decreases rapidly when D_{opt} decreases. The minimum was found when the three hydrogen atoms of methane are in the E0 plane; i.e., the distance to the C atom of methane, D_{opt}, is 0.60 Å and the corresponding energy is −5.75 kJ/mol. This is the optimal binding between the methane and the silanol covered (001) surface based on the ONIOM (MP2/6-31G(d):HF/6-31G(d)) calculation with the BSSE correction. At $D_{opt} < 0.60$ Å, the energy, again, increases. The H-out configuration gives a binding energy identical to that of the H-in one, −4.15 kJ/mol, when the C atom locates below the surface $D_{opt} = -1.00$ Å and one of the H-atom lies in the silicalite-1 surface. Note, however, that in this study we examine only the influence of the external sheet of atoms of the lattice on the approach of the methane molecule. Therefore, the energies obtained from this work cannot be compared to the experimental adsorption energy because we examine the influence of the surface only. All atoms of the silicalite-1 lattice would contribute to the complete adsorption process.

The calculated energies are higher than those from refs 33 and 34 where only a small fragment was used. This can be due to the effect of the hydrogen atoms which were added to saturate the broken terminal bonds.

4. Conclusion

Quantum chemical calculations were carried out to seek for the optimal binding site and orientation as well as the binding energy of a methane molecule on the silanol covered (010) surface of silicalite-1. The ONIOM (MP2/6-31G(d):HF/6-31G-(d)) method with the correction of the basis superposition errors was found to be a compromise between the accuracy and computer time required for the investigated system. The ONIOM binding energies and distances are almost the same as those yielded from the MP2 calculations using the same fragment size as that of the real part of the ONIOM method. The optimal binding site is located at the straight channel and the binding energy is significantly lower than that of the other regions; therefore, the methane molecule was suggested to move freely above the surface and enter into the straight channel in the configuration pointing one of the H-atoms to the center of the straight channel.

References and Notes

(1) Takaba, H.; Koshita, R.; Mizukami, K.; Oumi, Y.; Ito, N.; Kubo, M.; Fahmi, A.; Miyamoto, A. *J. Membr. Sci.* **1997**, *134*, 127.

(2) Smirnov, K. S. *J. Phys. Chem. B* **2001**, *105*, 7405.

(3) Takaba, H.; Koyama, A.; Nakao, S. *J. Phys. Chem. B* **2000**, *104*, 6353.

(4) Armaroli, T.; Bevilacqua, M.; Trombetta, M.; Milella, F.; Alejandre, A. G.; Ramirez, J.; Notari, B.; Willey, R. J.; Busca, G. *Appl. Catal. A* **2001**, *216*, 59.

(5) Simon, J. M.; Decrette, A.; Bellat, J. B.; Salazar, J. M. *Mol. Simul.* **2004**, *30*, 621.

(6) Komiyama, M.; Kobayashi, M. *J. Phys. Chem. B* **1999**, *103*, 10651.

(7) Chandress, M.; Webb, E. B., III; Grest, G. S.; Martin, M. G.; Thompson, A. P.; Roth, M. W. *J. Phys. Chem. B* **2001**, *105*, 5700.

(8) Pieterse, J. A. Z.; Veefkind-Reyes, S.; Seshan, K.; Lercher, J. A. *J. Phys. Chem. B* **2000**, *104*, 5715.

(9) Tanaka, H.; Zheng, S.; Jentys, A.; Lercher, J. A. *Stud. Surf. Sci. Catal.* **2002**, *142*, 1619.

(10) Turro, N. J. *Acc. Chem. Res.* **2000**, *33*, 637.

(11) Turro, N. J.; Lei, X.; Li, W.; Liu, Z.; Ottaviani, M. F. *J. Am. Chem. Soc.* **2000**, *122*, 12571.

(12) Park, S. H.; Rhee, H. K. *Catal. Today* **2000**, *63*, 267.

(13) Klemm, E.; Scheidat, H.; Emig, G. *Chem. Eng. Sci.* **1997**, *52*, 2757.

(14) Aguilar, J.; Corma, A.; Melo, F. V.; Sastre, E. *Catal. Today* **2000**, *55*, 255.

(15) Denoyer, J. F.; Baron, G. V.; Vanbutsele, G.; Jacobs, P. A.; Martens, J. H. *Chem. Eng. Sci.* **1999**, *54*, 3553.

(16) Zecchina, A.; Bordiga, S.; Spoto, G.; Marchese, L. *J. Phys. Chem.* **1992**, *96*, 4991.

(17) Trombetta, M.; Busca, G.; Lenarda, M.; Storaro, L.; Pavan, M. *Appl. Catal. A* **1999**, *182*, 225.

(18) Armaroli, T.; Bevilacqua, M.; Trombetta, M.; Milella, F.; Alejandre, A. G.; Ramírez, J.; Notari, B.; Willey, R. J.; Busca, G. *Appl. Catal. A* **2001**, *216*, 59.

(19) Trombetta, M.; Armaroli, T.; Alejandre, A. G.; Solis, J. R.; Busca, G. *Appl. Catal. A* **2000**, *192*, 125.

(20) Armaroli, T.; Trombetta, M.; Alejandre, A. G.; Solis, J. R.; Busca, G. *Chem. Phys.* **2000**, *2*, 3341.

(21) Kawai, T.; Tsutsumi, K. *Colloid Polym. Sci.* **1998**, *276*, 992.

(22) Olson, D. H.; Haag, W. O.; Borghard, W. S. *Microporous Mesoporous Mater.* **2000**, *35*, 435.

(23) Trombetta, M.; Busca, G. J. *Catal.* **1999**, *187*, 521.

(24) Nyfeler, D.; Armbruster, T. *Am. Mineral.* **1998**, *83*, 119.

(25) Eisenberg, D.; Kauzmann, W. *The Structure and Properties of Water*; Oxford University Press: Oxford, U.K., 1969.

(26) Wu, J.; Li, S.; Li, G.; Li, C.; Xin, Q. *Appl. Surf. Sci.* **1994**, *81*, 37.

(27) Smit, B. *J. Phys. Chem.* **1995**, *99*, 5597 and references therein.

(28) Saengsawang, O.; Remsungnen, T.; Fritzsche, S.; Haberlandt, R.; Hannongbua, S. *J. Phys. Chem. B* **2005**, *109*, 5684.

(29) Baerlocher, Ch.; Meier, W. M.; Olson, D. H. *Atlas of Zeolite Framework Types*, 5th revised ed.; Elsevier: Amsterdam, 2001.

(30) Hobza, P.; Zahradnik, R. *Chem. Rev.* **1998**, *88*, 871.

(31) Sauer, J.; Ugliengo, P.; Garrone, E.; Saunders, V. R. *Chem. Rev.* **1994**, *94*, 2095.

(32) Bussai C.; Fritzsche S.; Haberlandt R.; Hannongbua S. *J. Phys. Chem B* **2004**, *108*, 13347.

(33) Bussai, C.; Fritzsche, S.; Haberlandt, R.; Hannongbua, S. *Langmuir* **2005**, *21*, 5847.

(34) Frisch, M. J.; Trucks, G. W.; Schlegel, H. B.; Scuseria, G. E.; Robb, M. A.; Cheeseman, J. R.; Montgomery, J. A., Jr.; Vreven, T.; Kudin, K. N.; Burant, J. C.; Millam, J. M.; Iyengar, S. S.; Tomasi, J.; Barone, V.; Mennucci, B.; Cossi, M.; Scalmani, G.; Rega, N.; Petersson, G. A.; Nakatsuji, H.; Hada, M.; Ehara, M.; Toyota, K.; Fukuda, R.; Hasegawa, J.; Ishida, M.; Nakajima, T.; Honda, Y.; Kitao, O.; Nakai, H.; Klene, M.; Li, X.; Knox, J. E.; Hratchian, H. P.; Cross, J. B.; Bakken, V.; Adamo, C.; Jaramillo, J.; Gomperts, R.; Stratmann, R. E.; Yazyev, O.; Austin, A. J.; Cammi, R.; Pomelli, C.; Ochterski, J. W.; Ayala, P. Y.; Morokuma, K.; Voth, G. A.; Salvador, P.; Dannenberg, J. J.; Zakrzewski, V. G.; Dapprich, S.; Daniels, A. D.; Strain, M. C.; Farkas, O.; Malick, D. K.; Rabuck, A. D.; Raghavachari, K.; Foresman, J. B.; Ortiz, J. V.; Cui, Q.; Baboul, A. G.; Clifford, S.; Cioslowski, J.; Stefanov, B. B.; Liu, G.; Liashenko, A.; Piskorz, P.; Komaromi, I.; Martin, R. L.; Fox, D. J.; Keith, T.; Al-Laham, M. A.; Peng, C. Y.; Nanayakkara, A.; Challacombe, M.; Gill, P. M. W.; Johnson, B.; Chen, W.; Wong, M. W.; Gonzalez, C.; Pople, J. A. *Gaussian 03*, revision C.02; Gaussian, Inc.: Wallingford, CT, 2004.

(35) Monfort, X. S.; Sodupe, M.; Branchadell V.; Sauer, J.; Orlando, R.; Ugliengo, P. *J. Phys. Chem. B* **2005**, *109*, 3545.

VITAE

Name: Arthorn Loisruangsin

Birth date: 5th April 1977

EDUCATION

- 2000 B. Sc. in Chemistry (Industrial Science), King Mongkut's Institute of Technology Ladkrabang, Thailand.

- 2006 Ph. D. in Chemistry (Physical Chemistry), Chulalongkorn University, Bangkok, Thailand.

PUBLICATIONS

- **A. Loisruangsin**, S. Fritzsche, and S. Hannongbua, *Newly developed ab initio Fitted Potentials for Molecular Dynamics Simulations of n-Pentane in the Zeolite Silicalite-1*, Chem. Phys. Lett. 390 (2004), 485-490.

- O. Saengsawang, T. Remsungnen, **A. Loisruangsin**, S. Fritzsche, R. Haberlandt and S. Hannongbua, *Energy Barrier of Water and Methane Molecules due to the Silanol Groups on the (010) Surface of Silicalite-1 as studied by Quantum Chemical Calculations*, Studies in Surface Science and Catalysis 158 (2005), 947-954.

- T. Remsungnen, V. Kormiltes, **A. Loisruangsin**, A. Schüring, S. Fritzsche, R. Haberlandt and S. Hannongbua, *Optimal Binding Site of a Methane Molecule on the Silanol Covered (010) Surface of Silicalite-1:ONIOM Calculations*, J. Phys. Chem. B 110 (2006), 11932-11935.